Technischen Universität München
Lehrstuhl für Metallbau

The Application of the Partial Connection Theory on Composite Beams in Fire Situations

Samuel Pfenning

Vollständiger Abdruck der von der Ingenieurfakultät Bau Geo Umwelt der Technischen Universität München zur Erlangung des akademischen Grades eines Doktor-Ingenieurs genehmigten Dissertation.

Vorsitzender:

Prof. Dr.-Ing. Oliver Fischer

Prüfer der Dissertation:

1. Prof. Dr.-Ing. Martin Mensinger
2. Prof. Dr.-Ing. Jochen Zehfuß
3. Prof. Ian Burgess, Ph.D.

Die Dissertation wurde am 06.06.2019 bei der Technischen Universität München eingereicht und durch die Ingenieurfakultät Bau Geo Umwelt am 28.11.2019 angenommen.

Danksagung

In tiefem Dank verbunden bin ich meiner Frau, welche mir mit unermüdlichem Unterstützung, fachlicher, menschlicher und finanzieller Art, zur Seite gestanden ist.

Abstract

During a fire, the elevated temperatures can create high forces within the steel section and the concrete chord of a composite beam. These forces generally are transferred by ductile shear connectors, which have a limited deformation capacity. While a reduced degree of shear connection is widely used for design at ambient conditions, designing for structural fire design requires a higher calculatory effort.

This thesis aims to provide two sets of rules for the safe application of a reduced degree of shear connection at elevated temperatures. One set of rules aims to limit the maximum slip of a composite beam in a fire situation. The second set provides rules for the calculation of the bending moment capacity at elevated temperatures.

To investigate the slip in the composite joint, four large scale experiments, parametric studies with finite element models, and analytic studies were conducted. Each large scale experiment consisted of two 9 m composite beams. With these experiments different combinations of steel sections, steel grade, fire load, and degree of shear connection where tested. For the parametric studies, detailed solid finite element models were developed using the finite element program Abaqus. These models were validated with the results of the experiments and literature. The analytic studies model the slip of a composite beam in fire and provide a linearised description of the interface slip for the first minutes in the fire. The analytic model is used to describe various influences on the slip in a fire situation.

The results of the thesis identified three dominant effects elevated temperatures have on the slip: Slip due to thermal elongation of the steel section, slip due to thermal curvature of the composite beam, and slip due to bending with decreasing stiffness at elevated temperatures. Some of the most influential parameters on the slip between the steel and concrete sections are the stiffness of the composite joint, the degree of shear connection, and the relation between the tensile capacity of the concrete chord and the shear capacity of the concrete joint. The entire list of the most influential parameters is included, along with evaluations

of each. A description of the rising degree of shear connection at elevated temperatures is presented.

Finally, practice oriented design rules and limits are given for the safe use of the partial connection theory for composite beams in fire.

Kurzfassung

Im Brandfall können in dem Stahlträger und dem Betongurt eines Verbundträgers hohe Kräfte entstehen. In der Regel werden diese Kräfte über duktile Verbundmittel mit einer begrenzen Verformungskapazität übertragen. Bei Normaltemperatur wird aufgrund der niedrigeren Kosten häufig eine reduzierte Verdübelung angewendet, dies ist im Brandfall teilweise nur mit hohem Aufwand möglich.

In dieser Arbeit werden Regeln für die sichere Anwendung der Teilverbundtheorie im Brandfall aufgestellt. Ein Teil der Regeln dient der Begrenzung der maximalen Verformungen der Verbundfuge im Brandfall. Der zweite Teil der Regeln dient der Berechung der Biegemomententragfähigkeit im Brandfall.

Zur Untersuchung des Schlupfverhaltens wurden Großbrandversuche, Parameterstudien sowie analytische Berechnungen durchgeführt. Die vier Großbrandversuche bestanden jeweils aus zwei 9 m langen Verbundträgern. In den Versuchen wurde verschiedene Kombinationen aus Stahlträger, Stahlgüte, Brandlast und Verdübelungsgrad getest. Mit Hilfe des Finite-Elemente-Programms Abaqus wurden detaillierte Volumenmodelle erstellt und mit den Ergebnissen der Brandversuche sowie mit Ergebnissen aus der Literatur validiert. Das analytische Modell liefert eine linearisierte Beschreibung des Schlupfs in den ersten Minuten der Brandbelastung. Mit diesem Modell wird der Einfluss verschiedener Faktoren auf den Schlupf im Brandfall quantifiziert.

Drei maßgebende Effekte auf den Schlupf werden beschrieben: Schlupf aufgrund der Temperaturdehnung des Stahlträgers, Schlupf augrund der Krümmung des Verbundträgers und Schlupf aufgrund reduzierten Steifigkeit bei hohen Temperaturen. Die maßgebenden Einflussfaktoren auf den maximalen Schlupf in der Verbundfuge werden genannt und bewertet. Hierzu gehören die Steifigkeit der Verbundfuge, der Verdübelungsgrad des Verbundträgers sowie das Verhältnis zwischen der Betonzugfestigkeit und der Schubtragfähigkeit der Verbundfuge. Der Anstieg des Verdübelungsgrades im Brandfall wird beschrieben.

Zum Abschluss werden praxisorientierte Bemessungsgleichungen sowie Grenzen zur sicheren Anwendung der Teilverbundtheorie bei Verbundträgern im Brandfall angegeben.

Contents

Acknowledgment

This thesis was realized during and after my time at the Chair of Metal Structures of the Technical University of Munich. The results of the thesis are mainly derived from the research project 'Mindestverdübelung von Verbundträgern im Brand' at the Technical University of Munich and the Technical University of Braunschweig. My gratitude goes to Professor Martin Mensinger for the continuous support and the valuable discussions. My gratitude also goes to my partner in the research project, Sven Brunkhorst. Professor Jochen Zehfuß shall be thanked for the valuable input during the research project and for being the second examiner of this thesis. Furthermore, I have to thank Martin Stadler for being my mentor and for providing excellent work conditions over the last month of my thesis. Various master students have contributed this thesis, namely I would like to thank Jürgen Tresch, Luca Pennisi, Rudolf Röß, Liu Yichao and Thomas Pirzer for their work. Finally I would also like to thank Claire Sembera for proofreading my thesis.

1 Introduction

Composite construction is a well-known and widely used construction method. It is characterised by a comparatively low self-weight, which makes it ideal for high rise buildings. A fast and economic construction is ensured by a high degree of prefabrication together with standardised steel connections. Headed stud shear connectors typically establish the ductile shear connection between a concrete chord and a steel beam. Under certain circumstances, it is possible to reduce the number of shear connectors by using the partial shear connection theory according to EN 1994-1-1 [1]. This is often used for construction in ambient conditions, but is not easily possible considering the conditions of a fire. According to EN 1994-1-2 [2] it is necessary to consider the variation of the longitudinal shear forces due to thermal strains for composite beams that are required to fulfil certain functions when exposed to fire. However, EN 1994-1-2 includes no further design rules to calculate the changes of longitudinal shear forces.

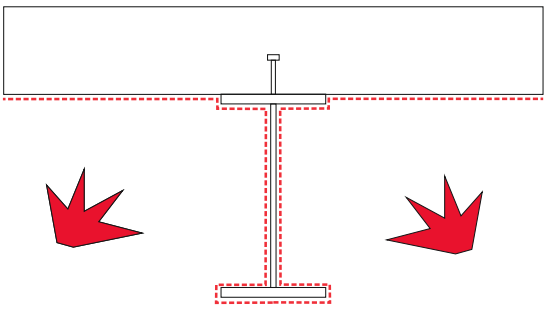

Figure 1.1: Cross-section of a typical beam considered in this thesis, flame impinged surface marked with red

The high longitudinal shear forces can effect the shear connectors in the composite joint. As it is necessary to consider the effects of elevated temperatures on the composite joint, sophisticated transient thermal calculations have to be conducted. For the calculations it is generally assumed that a composite beam in a fire situation is exposed to fire from below, as

indicated in Figure 1.1. As a result, the concrete slab is exposed to elevated temperatures from only one side and the steel section from three sides. This causes the steel section to heat significantly more than the overlying concrete slab. A change in the longitudinal shear forces therefore arises from the high temperature differences between the concrete slab and the steel section, as depicted in Figure 1.2. Due to the temperature differences and the different behaviour of steel and concrete components at elevated temperatures, high residual stresses can be expected in the composite beam. In certain situations, the effect of these stresses on the composite joint may lead to a higher slip of the composite joint than is allowed for by the maximum ductility of the headed stud shear connectors given in the EN 1994-1-1 [1]. The calculation of the longitudinal forces in a fire situation is only possible with detailed and complex calculations. Due to the complex calculations it is currently effectively impossible to use the partial connection theory for buildings with fire resistance requirements. Therefore, it is essential to establish safe and easy-to-use rules for the partial connection theory in fire situations, especially as most parts of high rise buildings are required to have some level of fire resistance.

The highly nonlinear behaviour of all components makes it very difficult to calculate the longitudinal forces. The nonlinearity is because of the highly transient temperature distribution in the composite beam. While the temperature in the composite beam ranges from ambient conditions to over 800 °C within the first 30 min of fire exposure, the composite joint reacts highly nonlinear for loading and unloading. The material properties of the concrete section vary not only due to the temperatures but also due to changing compression zones within the composite beam. Additionally, a load redistribution occurs from the steel section to the concrete chord.

These dependencies were solved by a close evaluation of four large-scale experiments and detailed numerical studies. Within certain boundaries, the dependencies were also solved within the analytic approach. The derived rules allow for easy and safe use of the partial connection theory in a fire situation.

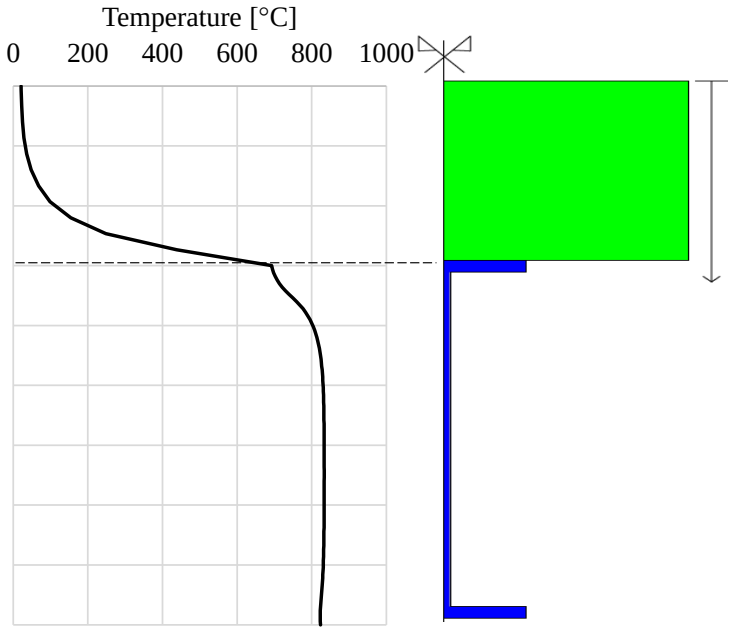

Figure 1.2: Temperature distribution in an exemplary composite beam after 30 min fire exposure

1.1 Objective

For the safe application of a reduced degree of shear connection on composite beams in a fire situation, two basic questions have to be answered:

1. Which influence does a partial shear connection have on the load carrying capacity of composite beams in a fire situation? How can the bending resistance be calculated?
2. How can the compliance of the deformation in the composite joint with the deformation capacity of the shear connectors be ensured?

Therefore, the investigations on the partial connection theory in fire situations can be split into two functional blocks: First, the investigations on the ultimate load carrying capacity and second, the investigations on the slip in the composite joint.

At ambient conditions both questions were answered in the EN 1994-1-1 [1]: The plastic resistance moment of sections with partial shear connections was calculated according to EN 1994-1-1 6.2.1.3. The compliance of the deformation of the composite joint with the

deformation capacity was ensured for certain shear connectors by limiting of the use of the partial shear connection in EN 1994-1-1 6.6.1.2.

This dissertation aims to elaborate the rules for the safe application of a partial shear connection on composite beams in fire situations, similar to the rules at ambient conditions in EN 1994-1-1.

1.2 Scope of Research

This thesis investigates the influence of an accidental fire situation on composite steel and concrete beams. The application of the outcome of this thesis is limited to building construction. A ductile shear connection with shear connectors according to EN 1994-1-1 Part 6.6 is assumed throughout the entire thesis. The thesis discusses composite beams with solid concrete slabs and profiled steel sheets. A typical example of a cross-section of a composite beam covered by this thesis is given in Figure 1.1. The boundaries of the application of a reduced degree of shear connection in EN 1994-1-1 are valid for this thesis as well. The focus was put on single span beam with a positive bending moment.

1.3 Thesis Layout

To enable the use of the partial connection theory in fire situations this thesis is split into four parts: two functional parts, the description of the conducted experiments and the built FE-model[I].

Preparatory Work

The experimental work is presented in Chapter 3. The results of the experiments are used to discuss the influence of the elevated temperatures on the slip in the composite joint in Chapter 8 and to describe the deformation behaviour in Section 5.2.

The FE-model is described in Chapter 4. The FE-model is used to analyse and describe the influences of the elevated temperatures on the slip of the composite joint in Chapter 8. In addition it is utilized for the detailed analysis of the separate effects of elevated temperatures on the composite joint in Section 6.1. Furthermore, the FE-model is employed to describe the deformation behaviour in Section 5.2. Three parametric studies are introduced in Section 4.7. The results of the parametric studies are used to investigate the influences on the slip of the composite joint.

Investigations on the Ultimate Load Carrying Capacity

Section 2.3 in Chapter 2 'State of the Art' reviews the underlying literature of the bending moment resistance of a composite beam in a fire situation. The load carrying capacity is discussed in Chapter 5.

The influence of the shear connection at elevated temperatures on the ultimate load carrying capacity is first analysed with the development of the degree of shear connection of a composite beam at elevated temperatures in Section 5.1. Section 5.2 then presents the influence of the stiffness of the composite joint on the load carrying capacity. Section 5.2

[I] Finite element model

also shows the deformation behaviour of beams with different degrees of shear connection with the results of the experiments and the FE-model.

Investigations of the Slip in the Composite Joint

Next, the slip in the composite joint is investigated. Chapter 6 'Investigations of the Slip in the Composite Joint' starts with a discussion of three effects of elevated temperatures on the composite joint in Section 6.1. Using these three effects, the development of slip in a composite joint in a fire situation is discussed in Section 6.2. The determinant load combination on the composite joint is also looked at in Section 6.2.

Chapter 7 provides an analytic approach to the description of the slip of the composite joint in a fire situation. The linearised description of the slip does not allow a highly accurate calculation of the slip in a fire situation, but it helps to understand the influence of elevated temperatures on the composite joint.

In Chapter 8, a variety of influences on the slip of the composite joint are discussed based on the parametric studies with the FE-model and the conducted experiments. Table 1.1 displays the parameters of the parametric studies.

Table 1.1: Varied parameters in the parametric studies

Parameter	**Variation**
Steel grade	S235, S355, S460
Beam span	6 m, 8 m, 10 m, 14 m
Steel section	IPE, HEA, HEM
Height steel section	300 mm, 500 mm, 600 mm, 900 mm
Degree of shear connection	20%, 40%, 70%, 100%
Thickness of concrete flange	140 mm, 170 mm, 200 mm
Load type	Single load, Distributed load
Geometry concrete chord	Solid slab, Composite slab
Protection steel section	Unprotected, Intumescent coating
Fire load	ISO 834 fire, Natural fire

All of these parameters are discussed in detail and evaluated with the help of an analytic approach, parametric studies and the experimental results. The parameters are then split

into parameters with little or no influence on the slip in Section 8.1 and parameters with a large influence in Section 8.2.

Proposal for the Safe Use of a Reduced Degree of Shear Connection in a Fire Situation

Finally, proposals are made in Chapter 9 for the safe application of a reduced degree of shear connection on composite beams in a fire situation. Two proposals for the calculation of the bending moment resistance of a composite beam in a fire situation are presented in Section 9.2, and two proposals for the assurance of the compliance of the deformation in the composite joint with the deformation capacity of the shear connectors are presented in Section 9.3.

2 State of the Art

2.1 Load Carrying Behaviour of Shear Connectors

2.1.1 Shear Connectors at Ambient Conditions

Lungershausen [3] proposed a model for the load carrying capacity of headed stud shear connectors in solid slabs and composite slabs. He divided the load-carrying behaviour of a headed stud shear connector in a solid slab into 4 load paths, cf. Fig. 2.1. Hereby Load Path A describes a compressive strut on the weld of the headed stud. Load Path B describes the plastic bending in the lower part of the headed stud due to the crushing of the concrete in the vicinity of the weld. Load Path C evolves with larger deformations of the shear connection, and it describes the tensile force in the headed stud. With rising tensile forces in the headed stud, a compressive force between the steel section and the concrete evolves, which leads to friction forces in the shear connection, named Load Path D.

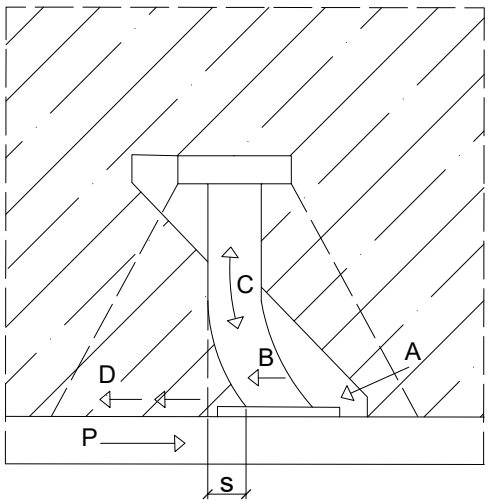

Figure 2.1: Loads paths of a headed stud shear connector in a solid slab at ambient conditions according to Lungershausen [3]

Recent developments on the rules for shear connections of composite beams at ambient conditions were done in the DISCCO-Project [4]. The research focused on the development of new rules for a partial shear connection of composite beams at ambient conditions for the revision of the EN 1994-1-1 [1]. Composite beam tests were conducted to investigate the influence of low degrees of shear connection on the bending capacity. It was found that even with low degrees of shear connection, the plasticity model of EN 1994 leads to good results. In the course of this research project, Nellinger [5] developed new rules for the calculation of the shear resistance of headed stud shear connectors in deep decking. The results of Nellinger are used in Section 4.5.5 for the development of a new design method (NL500) for the calculating the shear capacity of headed stud shear connectors in deep decking at elevated temperatures.

Further research on headed stud shear connectors in deep decking was published by Konrad [6]. Based on conducted push-out tests, Konrad proposes a revised approach for calculating of the load carrying capacity of headed stud shear connectors in solid concrete and with additional steel sheeting.

Jähring [7] proposed a mechanical model for calculating the behaviour of shear connectors in high-performance concrete. Jähring reasons that for high-performance concrete the minimum ductility of the shear connectors δ_{uk}[I] required in EN 1994-1-1 [1] is not always reached.

2.1.2 Shear Connectors at Elevated Temperatures

Various experiments on the ductility and load carrying capacity of headed stud shear connectors at elevated temperatures were conducted and reported in literature, namely Chen [8], Mirza & Uy [9], Choi [10], Zhao & Kruppa [11], and Imagawa et al. [12].

Zhao & Kruppa [11] and [13] conducted a series of push-out tests on headed stud shear connectors and experiments on composite beams subjected to ISO 834[II] fire. With this, the push-out tests were conducted in accordance with Annex 2 of EN 1994-1-1. The diameters of

[I] Characteristic value of slip capacity
[II] Temperature load according to heating curve in ISO 834-1 6.1.1 [14]

the used headed stud shear connectors were 16, 19, and 22 mm. For all headed studs in solid concrete slabs, the failure of the specimen was caused by the shearing of the headed studs at the level of the flange. Similar results were obtained for headed studs cased in composite slabs with re-entrant profiled steel sheeting. Based on this, Zhao & Kruppa proposed a force-slip relationship for headed studs cast in solid concrete slabs at elevated temperatures. They also proposed values for the slip at the maximum resistance of the connectors s_y[I]. Values for the ultimate slip of the headed stud shear connectors s_{max}[II] and the slip at the end of the linear elastic load path s_0[III] are given in Tab. 2.1.

Table 2.1: Force-slip relationship and corresponding parameters of headed studs cast in solid concrete slabs at elevated temperatures, according to Zhao & Kruppa [11] Table 1

θ °C	$\frac{P_{max}(\theta)}{P_{max}(20°C)}$	s_0 mm	s_y mm	s_{max} mm
≤ 100	1.0	0.36	5.20	11
200	1.0	0.65	5.70	12
300	1.0	0.90	6.25	13
400	0.80	1.30	6.70	14
500	0.624	1.45	7.10	15
600	0.367	1.48	7.50	16
700	0.184	1.50	7.90	17
800	0.088	1.50	8.30	18

The proposed values of Zhao & Kruppa show that there is a significant rise of ductility of the headed stud shear connectors with a rise of temperature of the shear connection. With $s_{max} \geq 11$ mm, the ductility of the shear connectors s_{max} is generally much higher than the minimum ductility of the shear connectors requested in EN 1994-1-1 [1] $\delta_{uk} = 6$ mm.

Chen [15] conducted eight push-out tests at elevated temperatures to investigate the temperature distribution, the predominant failure mechanism and the force-slip relationship of headed stud shear connectors at high temperatures. In the experiments, it was observed that

[I] Slip of a headed stud shear connector when reaching maximum load carrying capacity
[II] Slip of a headed stud shear connector at failure
[III] Slip of a headed stud shear connector at end of linear elastic load-slip path

the predominant mode of failure for the solid slab was a shear failure of the headed stud just over the weld. Both the ultimate load and stiffness decreased with increasing temperatures. The recorded load-slip relationship for solid slabs under elevated temperatures is shown in Figure 2.2. The headed studs used in the experiments of Chen had a diameter of 19 mm and a height of 100 mm. The concrete in the experiments had a cubic compressive strength of 38.5 N/mm^2. The heating of the specimens was much slower than according to ISO 834 and therefore the temperature distributions in the specimens do not match the distribution in the fire experiments described in Chapter 3.

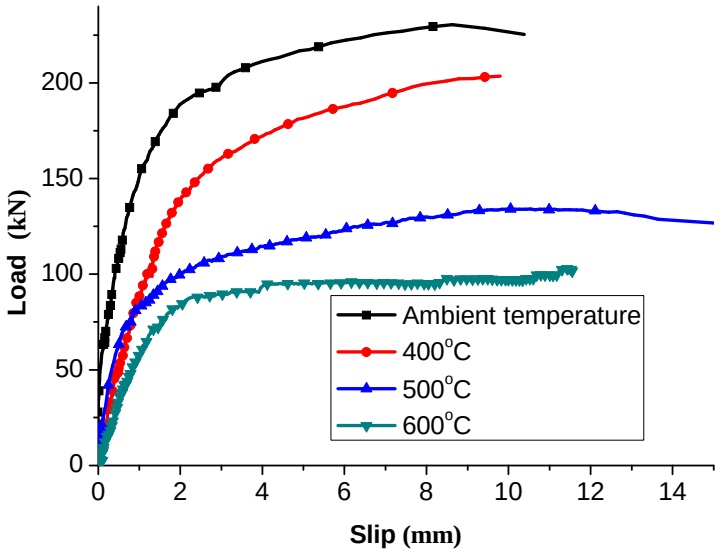

Figure 2.2: Recorded load-slip relationship of headed studs at elevated temperatures, taken from Chen [15]

It can be concluded that according to the literature there is a significant rise of ductility of headed stud shear connectors in solid concrete slabs in a fire situation. In a solid slab, the predominant mode of failure of the shear connectors is a shear failure of the stud just over the weld.

2.2 Composite Action

2.2.1 Theory of the Elastic Composite Action

Based on the sandwich theory, an horizontal elastic connection between two structural elements of a single span beam leads to slip at both ends of the beams over the supports. Among others, Möhler [16], Hoischen [17], and Schanzenbach [18] describe the theory of the elastic composite action.

Möhler [16] gives a general solution for a single span composite beam in a simplified case: the material behaviour and the behaviour of the composite joint are assumed to be ideally elastic and the moment line to be continuous. With this Möhler defines linear elastic springs with the maximum spring force being P_{max}[I] and the slip of the composite joint when reaching the maximum force being s_y.

$$C_V = \frac{P_{max}}{s_y} \tag{2.1}$$

A requisite of this solution is a continuous connection between the two structural elements. The separation of the shear connectors a and the width of the steel section b lead to the deformation resistance of the composite joint $\overline{C}$.

$$\overline{C} = \frac{C_V}{a * b} \tag{2.2}$$

$$s(x) = \frac{T(x) * a}{C_V} = \frac{\tau(x)}{\overline{C}} \tag{2.3}$$

The slip s^{II} of the composite joint at any position of a single span composite beam can be calculated with Equation 2.3 depending on the shear force *T(x)* or the shear stress $\tau(x)$ and the spring characteristics of the shear connectors C_V or $\overline{C}$.

[I] Maximum shear capacity of a headed stud shear connector at ambient conditions
[II] Slip of a composite joint

Möhler [16] also provides a closed-form expression for the differential equation of the slip for single span beams with a constant evenly distributed load. This expression is detailed in Equations 2.4-2.7.

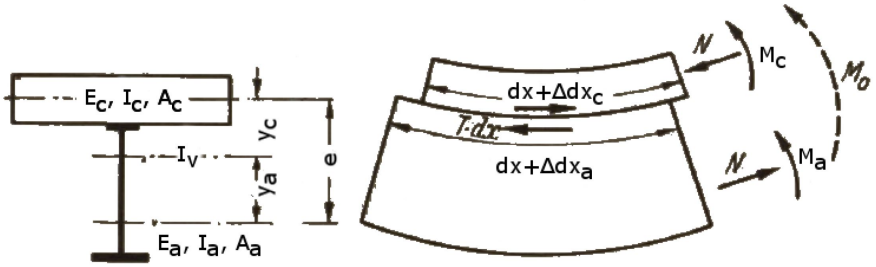

Figure 2.3: Deformation of a composite beam with elastic compound according to Hoischen [17]. Annotation similar to Möhler.

$$s(x) = \frac{q * L * e}{2\omega^2 * EI_V} * \left[1 - 2 * \frac{x}{L} - \frac{2\beta}{\omega * L} * \frac{sinh\left(\frac{\omega}{\beta} * \frac{L}{2} - x\right)}{cosh\left(\frac{\omega * L}{2 * \beta}\right)}\right] \tag{2.4}$$

with

$$\beta^2 = \frac{\sum I_i}{I_V} \tag{2.5}$$

$$\omega^2 = \frac{\overline{C} * b(1 + \frac{A_c}{nA_a})}{E_c * A_c} \tag{2.6}$$

and

$$I_V = I_c + A_c * y_c^2 + n(I_a + A_a * y_a^2) \tag{2.7}$$

I_a[I], I_c[II], y_c, and y_a are defined in Figure 2.3, n refers to the relation given in Equation 2.8.

$$n = \frac{E_a}{E_c} \tag{2.8}$$

2.2.2 Rules and Standards for a Partial Shear Connection

According to EN 1994-1-1 [1] in composite structures, headed studs commonly serve as ductile shear connectors. These transmit the longitudinal shear forces between the concrete chord and the structural steel beam. The required number of shear connectors for full shear connection n_f[III] results from the total design longitudinal shear force in the ultimate limit state. This state is calculated from the minimum of the normal force carrying capacity of the two components of the composite beam and is divided by the design resistance of a single connector P_{Rd}[IV].

n_f is described with Equation 2.9:

$$n_f = \frac{min\left\{N_{pl,a}; N_{c,max}\right\}}{P_{Rd}} \tag{2.9}$$

where

$$N_{pl,a} = A_a * f_{yd} \tag{2.10}$$

$$N_{c,max} = A_{c,eff} * 0.85 * f_{cd} \tag{2.11}$$

[I] Second moment of area of the steel section
[II] Second moment of area of the concrete chord
[III] Number of shear connectors needed for full shear connection according to EN 1994-1-1 6.6.1.2 (1)
[IV] Design value of the shear resistance of a single connector

For a solid slab $A_{c,eff}$ can be calculated as follows:

$$A_{c,eff} = b_{eff} * 0.85 * h_f \tag{2.12}$$

with b_{eff}[I] calculated using the equations provided by EN 1994-1-1 5.4.1.2.

According to EN 1994-1-1 6.6.1, within the boundaries of ductility it is possible to reduce the number of shear connectors n[II] to a value lower than n_f, the number of shear connectors needed for a full shear connection. This can reduce the degree of shear connection η[III] according to Eq. 2.13. The EN 1994-1-1 6.6.1.2 limits the use of the partial shear connection for beams in buildings. Considering the steel grade and the length of the beam, it is possible to reduce the degree of shear connection down to $\eta = 0.4$.

$$\eta = \frac{n}{n_f} \tag{2.13}$$

2.2.3 Minimum Degree of Shear Connection

The usage of the partial connection theory according to EN 1994-1-1 is based on a minimum ductility of the shear connectors u_{cr}[IV] $= 6$ mm. The ductility can either be proved by sticking to the boundary conditions of the Eurocode, or by a push test as described in Annex B of EN 1994-1-1. In both cases, the maximum slip for the design of the composite joint is assumed to be 6 mm. Therefore, certain rules were implemented into the EN 1994-1-1 to meet the maximum design slip of the shear connectors.

[I] Total effective width of flanges for shear lag
[II] Number of shear connectors, or relation between the Young's modulus of steel and concrete
[III] Degree of shear connection at ambient conditions
[IV] Deflection failure criterion

The theory of the elastic composite actions shows a direct influence of the length L^{I} and the stiffness of the shear connection $\overline{C}$ in ω on the slip over the supports of a single span beam:

$$s(L) = \frac{q * L * e}{2\omega^2 * EI_V} * \left[1 - 2 - \frac{2\beta}{\omega * L} * \frac{sinh\left(\frac{\omega}{\beta} * \frac{L}{2} - L\right)}{cosh\left(\frac{\omega * L}{2 * \beta}\right)}\right] \tag{2.14}$$

A longer beam and a lower stiffness of the shear connection lead to a larger slip at the ends of a single span beam and ultimately to a violation of the ductility criterion of the shear connectors $u_{cr} = 6$. Therefore, a dependency of the minimum degree of shear connection on the length of the beam was introduced in EN 1994-1-1 6.6.1.2 (1). With a higher yield strength f_y at a constant Young's modulus, a larger deformation of the composite beam and the shear connection is possible. Due to this relation, the dependency on f_y is also introduced into the equations to limit the use of the partial shear connection.

A different proposal on a minimum degree of shear connection was provided by Bärtschi [19]. Bärtschi suggested a deformation-based design method for the minimum degree of shear connection. The new method is especially for connector systems that differ from the commonly used welded headed stud shear connectors. The application range for the rigid-plastic design method, which is the basis for the partial connection theory according to EN 1994-1-1, was redefined by Bärtschi. Instead of limiting the use of the partial connection theory to shear connectors with $u_{cr} \geq 6$, Bärtschi recommended to use two criteria: (1) The deformation capacity u_{cr} based on the actual 'required deformation capacity for a shear connector in the beam at the chosen degree of partial shear connection' [19] and (2) the ductility of the shear connector based on 'the required ductility for a shear connector in the beam at the chosen degree of partial shear connection' [19].

[I] Span of a composite beam

2.3 Bending Resistance of Composite Beams

2.3.1 Rules and Standards for the Bending Moment Resistance

The design bending resistance can be determined by rigid plastic theory for composite cross-sections in Class 1 or Class 2 (cf. EN 1994-1-1 6.2.1. [1]). According to EN 1994-1-1 6.2.1.3, partial shear connection may be used in composite beams for buildings in regions of sagging bending. With ductile shear connectors, the bending resistance moment M_{Rd} can also be calculated by the rigid plastic theory, with the difference that a reduced value of compressive force N_{ct}[I] should be used instead of $N_{c,f}$[II]. Hereby, N_{ct} can be calculated with the degree of shear connection η: $\eta = N_{ct}/N_{c,f}$. Based on the calculated N_{ct}, the first local plastic neutral axis of the composite beam and the second local plastic axis of the steel section can be calculated. The bending resistance in fire situations can also be calculated by the plastic theory (cf. EN 1994-1-1 4.3.4.1.2).

2.3.2 Composite Beams in a Fire Situation

Important research on composite beams at elevated temperatures was done by Oven [20]. Oven developed a two-dimensional non-linear FE-model and performed a parametric study to investigate the load carrying behaviour of composite beams at elevated temperatures. All models, including the model with partial shear connection, were validated on experimental data at ambient conditions or with full shear connection. The research conducted by Oven generally suffered a lack of published data to work with. Still, the results of the parametric study show a logical response to the change of parameters such as the number of shear connectors. An important finding of Oven is that the end slip for simply supported composite beams in a fire is very small. Oven argues that this is because the direction of the thermal slip due to the fire is opposite to the mechanical slip due to the bending. He follows that 'This suggests that simply supported beams behave essentially as fully composite, even with

[I] Design value of the compressive normal force in the concrete flange
[II] Design value of the compressive normal force in the concrete flange with full shear connection

low degrees of shear connection.' [20]. Further on, he followed that the behaviour of the headed stud shear connectors does not influence the failure of a simply supported beam in a fire situation, because the dominant mode of failure is yielding of the steel. Oven proposes further research with parametric studies with three-dimensional models. He states that this could help to develop a simplified approach to modelling the behaviour of composite frames in a fire. Oven summarizes his findings as follows 'It may therefore be assumed that for practical degrees of shear connection, full-interaction is adequate for the analysis of composite beams under fire conditions.' [20]

In recent years important research on composite beams with a partial shear connection at elevated temperatures was done by Wang et al. [21], [22]. Wang conducted an experimental program with two composite beams to study the response of composite beams with partial shear connection to ISO 834 fire. One beam was built with a degree of shear connection η = 1.0 and the second beam was built with η=0.5.

An important difference to the experiments reported in Chapter 3 is the flat steel deck for the composite slab and a fire insulation coating applied to the steel section. Furthermore, the length of the composite beams tested by Wang et al. was only 5,260 mm. The failure criterion of the test specimens was set to span/30. In the experiments of Wang et al., both beams failed after nearly the same time of flame impingement. Whereas the composite beam with full shear connection failed after 51 minutes of fire, the composite beam with partial shear connection failed after 49 minutes. Wang et al. [21] concluded that 'the flexural capacities of the two test specimens are very similar, even though one specimen had only half the number of shear studs than the other.' An important conclusion of the work of Wang et al. is that in the fire experiments the two specimens with different degrees of shear connection η showed similar performance under fire exposure.

Following the experimental studies, Wang et al. [22] developed an FE-model of composite beams subjected to fire. The FE-model was validated with the results from the experiments reported in [21]. Even though the FE-model apparently did not include crucial details of the

fire experiments like the fire protection coating and the flat steel deck, the FE-model showed good agreement with the experimental results.

Based on a parametric study the author concludes that 'the shear connection ratio and height and width of the steel beam section have a significant effect on the fire behaviour of the composite beam' [22]. Wang et al. also shows that within the parametric range chosen the interface slip over the supports does rise over the critical level of 6 mm.

With the failure criterion of the computed composite beams being span/30, Wang et al. shows the influence of the degree of shear connection on the vertical deformation behaviour of composite beams in a fire situation, but he does not evaluate the influence and the consequences of a reduced degree of shear connection for the composite joint.

Further research on composite beams with reduced degrees of shear connection was conducted by Chen [23]. Chen investigated on the fire performance of composite beams with steel bar truss floor systems. He performed push out tests of headed stud shear connectors at both ambient and elevated temperatures, along with using a full numerical model to calculate the load carrying behaviour at elevated temperatures of composite beams with steel bar truss floor systems. Based on a parametric study, Chen concluded that the degree of shear connection has a negligible influence on the fire performance of a composite beam with a degree of shear connection η higher than 75 %. For lower degrees of shear connection, the limiting temperatures decrease. The results of Chen show a nonlinear increase of the vertical deflection with lower degrees of shear connection. Chen also worked with a failure criterion based on the vertical deflection of the composite beams.

3 Experimental Work

3.1 Introduction

For the examination of the joint of a composite beam in the fire, large-scale fire experiments were conducted with the Technical University of Braunschweig. In the experiments, eight beams with a length of 9 meters were tested. The beams consisted of an IPE and HEB 300 steel section and a concrete slab of 15 cm x 100 cm. A drawing of the two cross-sections can be seen in Figure 3.1.

The length of the composite beams, as well as the type of steel section, are typical for primary and secondary beams in multi-story buildings. Besides the usage of the experiments for the investigation of various effects, the results of the experiments have also been used for the validation and calibration of the numerical models, see Section 4.6.

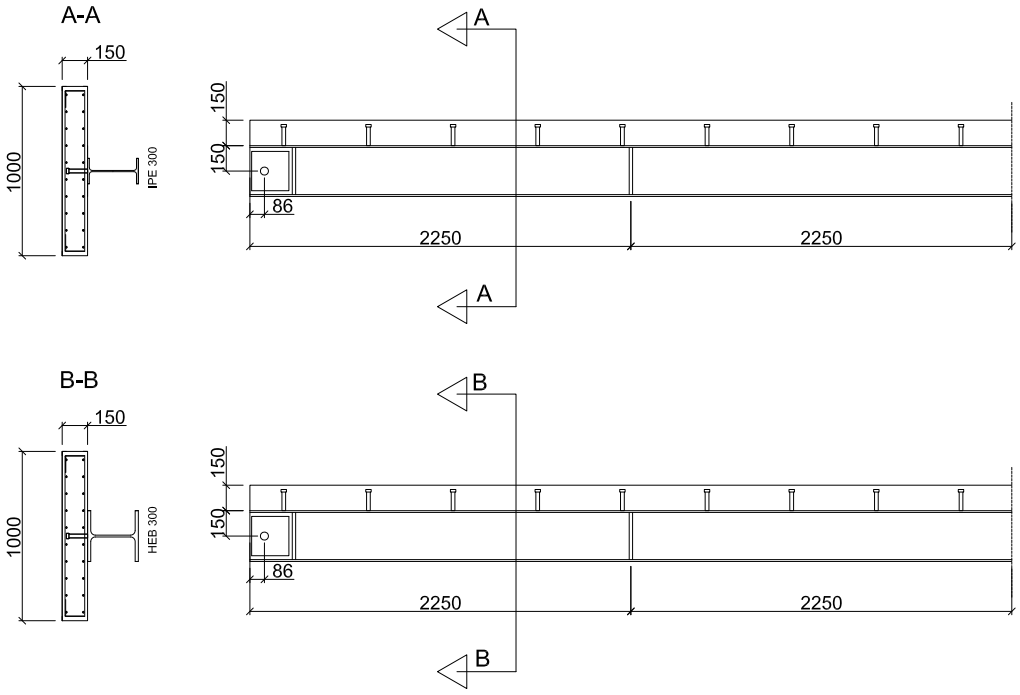

Figure 3.1: Cross sections of the tested beams. Top: IPE 300. Bottom: HEB 300. Both with secondary reinforcement

3.2 Scope of Experiments

The experiments aimed to analyse the composite action with a reduced degree of shear connection at elevated temperatures. A total of eight composite beams were tested, two in each experiment. The influence of the parameters *degree of shear connection* η, *residual stresses due to the production process*, and *different heating rates* were experimentally analysed. In the following Table 3.1, all specimens are listed with their respective parameters.

The natural fire curve used for the tests was worked out in the research project 'Mindestverdübelung von Verbundträgern im Brand' [24] by Sven Brunkhorst. 'ISO fire' refers to a fire load according to ISO 834 [14].

As different production methods of a composite beam can lead to residual stresses and different strain distributions within the beam, two different production methods have been chosen: 'propped' and 'unpropped', as referred to in Table 3.1. For the production method

Table 3.1: Varied Parameters of the Experimental set-up

Beam #	**Steel section**	**Steel grade**	**Production method**	η	**Fire load**
1	IPE 300	S460	propped	40 %	ISO fire
2	IPE 300	S460	propped	60 %	ISO fire
3	HEB 300	S355	propped	40 %	ISO fire
4	HEB 300	S355	propped	60 %	ISO fire
5	IPE 300	S355	unpropped	52 %	ISO fire
6	HEB 300	S355	unpropped	40 %	ISO fire
7	IPE 300	S355	unpropped	52 %	Natural fire
8	HEB 300	S355	unpropped	40 %	Natural fire

'propped', the concrete of the composite beam was poured with a continuous support of the steel section. With this method, the steel section is not prestressed due to the dead load of the concrete and the composite actions work for both, self-weight and variable load.

The second production method covered in this thesis 'unpropped' is widespread in building construction. While the concrete is poured, the steel section is supported at both ends and serves as a support for the scaffolding and thus as support for the concrete. This leads to imposed stresses in the steel section and potentially to an earlier plastic load carrying behaviour.

The steel profiles used, IPE 300 and HEB 300, present profiles typically used in building construction. Whereas the IPE 300 leads to a small compression zone in the concrete in the ultimate limit state, the HEB 300 leads to a compression zone which is, considering the same steel grade, larger than that of the IPE 300 by a factor of 2.8.

3.3 Fire Load

The experiments were conducted with two different fire curves, a fire curve according to ISO 834 [14] and a fire curve based on a natural fire calculated in [24]. This specific natural fire curve was chosen due to the notable difference to the ISO 834 fire before reaching a steel temperature of 600 °C. The chosen natural fire curve 'IND_2' represents an industrial building in the plastics industry with a plastics storage area. While the temperature at the

beginning of the fire is significantly lower than the temperature of the ISO 834, there is a steep increase of temperature at minute 35.

As the oil burners of the furnace are only able to produce furnace temperatures higher than 200 °C, the initial time of the natural fire curve was modified to fit the circumstances of the experiment. After the linearised preheating part, the course of the natural fire curve rises to the temperature of the ISO 834 fire.

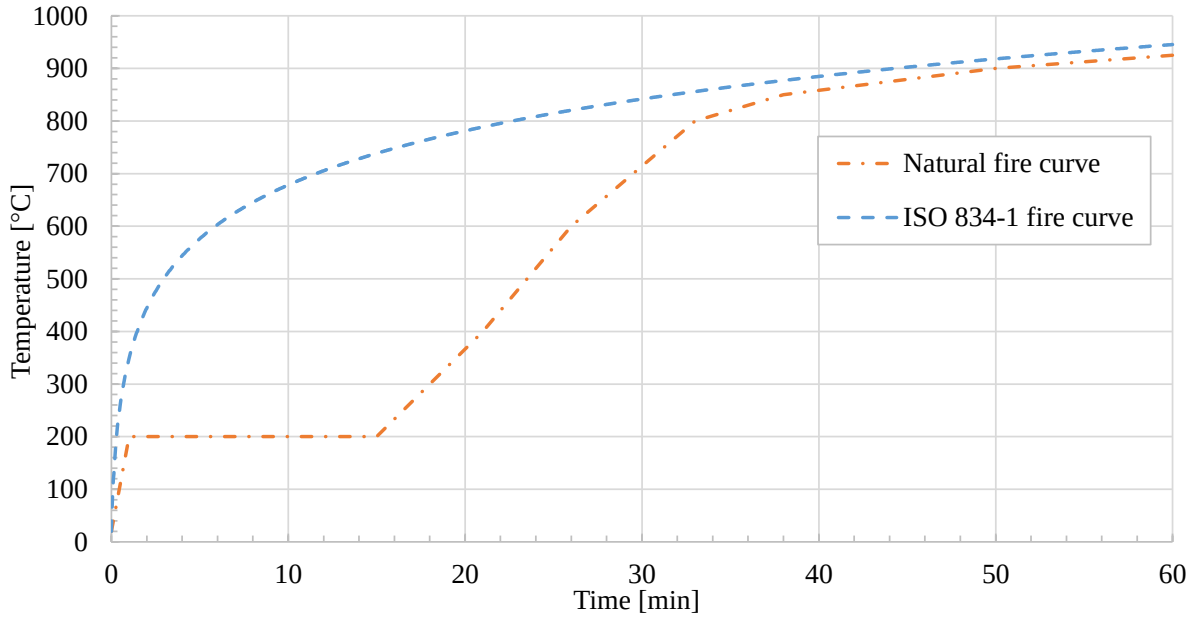

Figure 3.2: ISO 834 fire [14] and Natural fire curve chosen for Experiment 4 with Beam 7 and 8, calculated in [24]

3.4 Material and Geometrical Properties of the Specimens

The composite beams with a length of 9 m consisted of an unprotected steel section with a 1000 x 150 mm^2 concrete chord on top. The steel section and the concrete chord were connected by arc welded headed stud shear connectors type SD1 according to [25]. The diameter of the headed studs was 22 mm, the height 125 mm. 20 mm stiffeners were placed in the steel section over the supports as well as under the points of load application to prevent failure of the support construction and failure due to the stability of the steel section.

Furthermore, additional 30 mm web plates were placed on both sides of the web of the steels sections over the supports. The reinforcement of the concrete section was chosen based on the minimum reinforcement for crack control according to EN 1992-1-1 part 7.3.2 [26]. A welded wire mesh type Q335 A with a steel grade B500 A according to [27] was used; the concrete cover was 25 mm on both sides. In Figure 3.1 a cross section of the composite beam and a longitudinal cut can be seen.

The variation of the degree of shear connection was realised by alternating the spacing of the headed stud shear connectors. In the following Table 3.2 the number of the used shear connectors, the spacing, the steel section and the steel grade of the respective composite beam can be seen. The degree of shear connection η has been calculated according to EN 1994-1-1 6.6.1.1 [1], but with with the safety factor γ_V[I] set to $\gamma_V = 1.0$.

Table 3.2: Number of shear connectors used in the experiments

Beam #	**Steel section**	**Steel grade**	η	**# of headed studs**	**Spacing [mm]**
1	IPE 300	S460	40 %	18	500
2	IPE 300	S460	60 %	26	350
3	HEB 300	S355	40 %	26	350
4	HEB 300	S355	60 %	36	250
5	IPE 300	S355	52 %	18	500
6	HEB 300	S355	40 %	26	350
7	IPE 300	S355	52 %	18	500
8	HEB 300	S355	40 %	26	350

The concrete chord consists of self-compacting concrete, using portland cement CEM I 52.5 R. The concrete was designed to be of the class C40/50 according to [28]. During the placement of the concrete, four test cubes per composite beam were poured and stored for testing the concrete's strength according to [29]. The following Table 3.3 shows the results of the concrete strength tests and the respective class according to [29]. Samples have been tested after 7 days, 31 days and on the day of the experiment. Whereas the test cubes for day 7 and day 31 were stored according to the regulations, the test cubes for tests on the day of the experiment were stored outside under a plastic sheet after being 7 days in a water

[I] Partial factor for design shear resistance of a headed stud

quench. This was done to obtain concrete samples similar to the concrete in the composite beams. The age of the concrete was between 94 and 110 days on the day of the experiments.

Table 3.3: Concrete material data of the composite beam

Beam #	**7-days** $f_{\mathbf{c,cube}}\,[N/mm^2]$	**31-days** $f_{\mathbf{c,cube}}\,[N/mm^2]$	**day of exp.** $f_{\mathbf{c,cube}}\,[N/mm^2]$
1	66.2	76.0	55.0
2	66.2	76.0	55.0
3	52.1	59.6	61.1
4	52.1	59.6	61.1
5	63.8	73.5	71.6
6	60.4	72.5	66.6
7	63.8	73.5	71.6
8	60.4	72.5	66.6
Average	60.6	70.4	63.6
Class	-	C55/67	C50/60

The steel beams were of the class S460 and S355 according to [30]. From each steel section two samples were taken, one at the flange and one at the web. The exact position of the extraction is given in Figure 3.3. The tensile tests were conducted according to the EN ISO 6892-1 [31]; the shape of the samples was chosen according to [32] tensile test shape A.

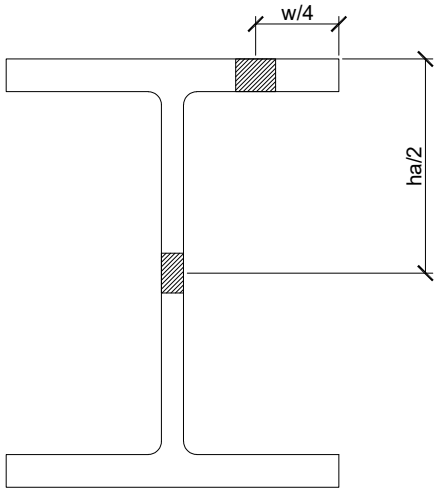

Figure 3.3: Sampling points

The results of the tensile tests are displayed in Table 3.4. All HEB 300 were of the class S355, whereas two IPE 300 with ${f_{ay}}^{\mathrm{I}} \geq 460 N/mm^2$ were correlated to the class S460 and two to class S355.

Table 3.4: Results of the tensile test

Beam #	f_{ay} **Web** $[N/mm^2]$	f_{ay} **Flange** $[N/mm^2]$
1	534	-
2	488	488
3	-	-
4	454	412
5	361	371
6	-	-
7	374	-
8	389	390

3.5 Measurement Instrumentation

3.5.1 Temperature Measurement

To be able to compare the computed temperature with the temperatures during the fire experiments, various thermocouples were installed on and in the composite beam.

NiCr-Ni thermocouples of type K were placed on the quarter points of the composite beams to measure the concrete temperature. At each quarter point, three chains of five thermocouples each ensured a constant temperature measurement over the height and the width of the section. The following figures, Figure 3.4 and Figure 3.5, show the position of the thermocouples in the concrete chord. As the thermocouples for measuring the surface temperature on the fire exposed concrete surface are not protected from radiation and convection, it can be excepted that these thermocouples measure not only the surface temperature but also the direct radiation and convection of the fire. In Figure 3.6 the measuring point in question is displayed.

[I] Nominal value for the yield strength of structural steel at ambient conditions

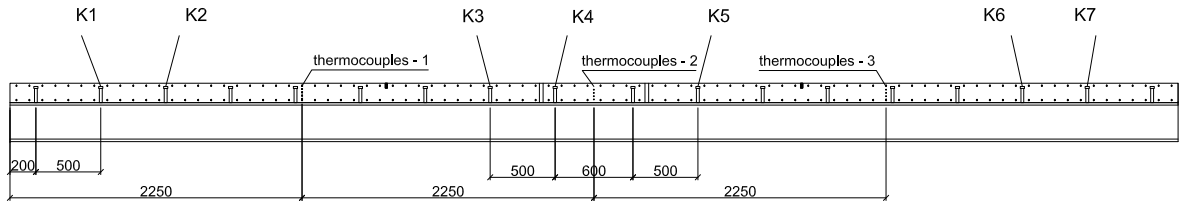

Figure 3.4: Position of the temperature measurement points on the composite beam

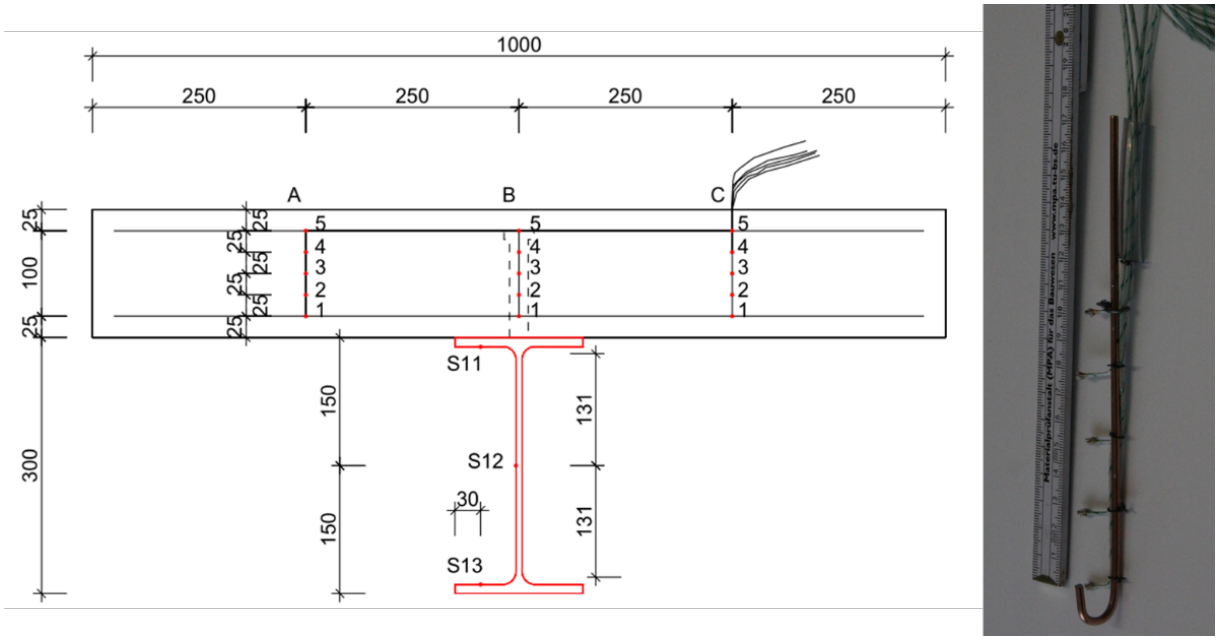

Figure 3.5: Position of the temperature measurement points on the cross section of the composite beam, taken from [24]

The steel temperature was recorded on the two flanges and the web on the quarter points of the beams. The temperature was measured by welded on thermocouples type K, class 2. The position of the measurement points can be seen in Figure 3.5, as well as in Figure 3.7.

The core temperature of the headed stud shear connectors was recorded, as it is crucial for the load slip behaviour of the composite joint. On each composite beam seven modified headed studs were used. In these headed studs a 3 mm hole was drilled with a depth of 100 mm from the head of the headed stud (see drawing in Figure 3.8). In this drill hole a thermocouple was inserted to measure the temperature 25 mm over the weld of the headed

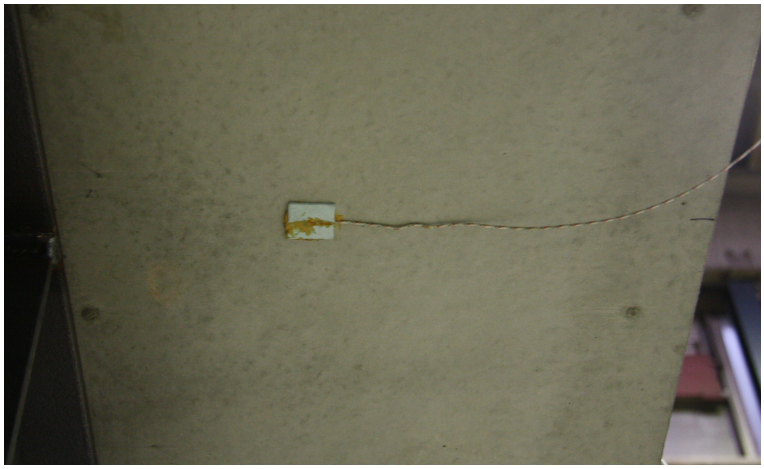

Figure 3.6: Concrete surface temperature measurement

Figure 3.7: Welded thermocouples on the steel section

stud. In Figure 3.4 the position of the modified headed studs on one test specimen can be seen.

3.5.2 Displacement measurement

The horizontal slip over the supports, named L1 - L4 in Figure 3.9, as well as the vertical deflection at midspan, named D1 - D4, were continuously measured during the experiments to evaluate the influence of the elevated temperatures on the composite joint.

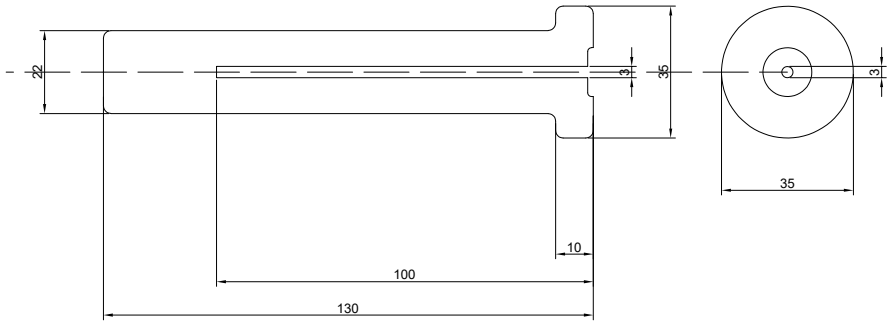

Figure 3.8: Drawing of the modified headed stud shear connectors

The vertical deflection was measured by potentiometers fixed on a reference beam outside of the furnace. Figure 3.10 displays the reference beam as well as the potentiometers.

The horizontal slip between the concrete chord and the steel section in the composite joint was recorded at both ends of the composite beam. Linear potentiometers (L1 - L4) were fixed on an extension of the steel section and measured at the end of the concrete chord. Figure 3.9 depicts the positive direction of these measurement points. Figure 3.11 shows an installed linear potentiometer.

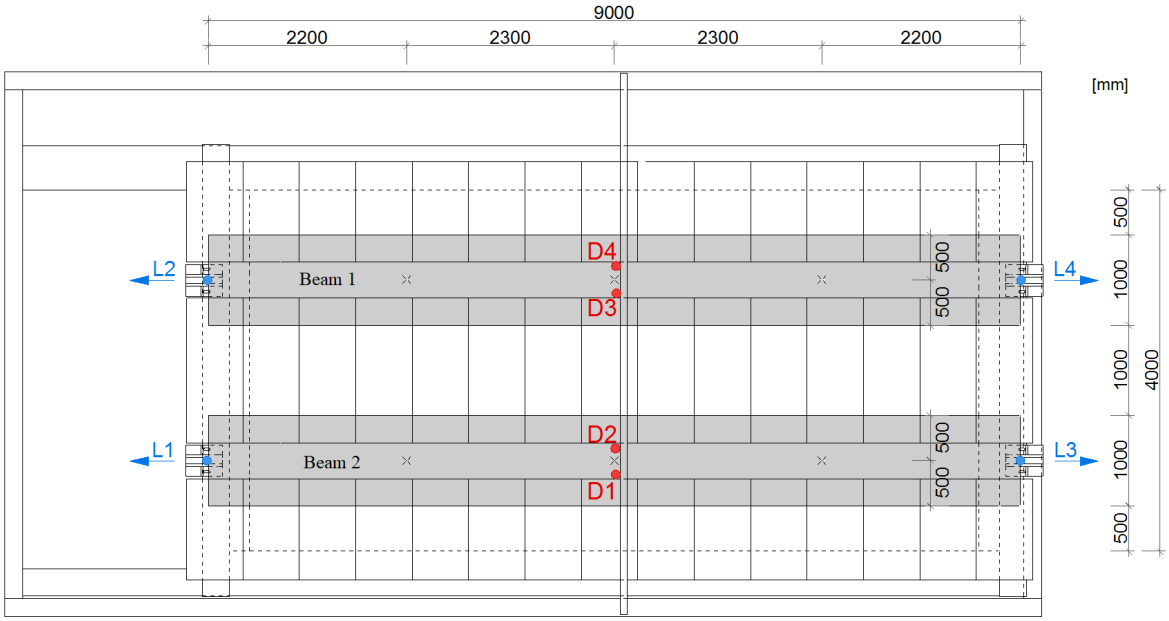

Figure 3.9: View of the test set-up and position of the deflection measurement points, from [24]

Figure 3.10: Reference beam for measuring the vertical deflection

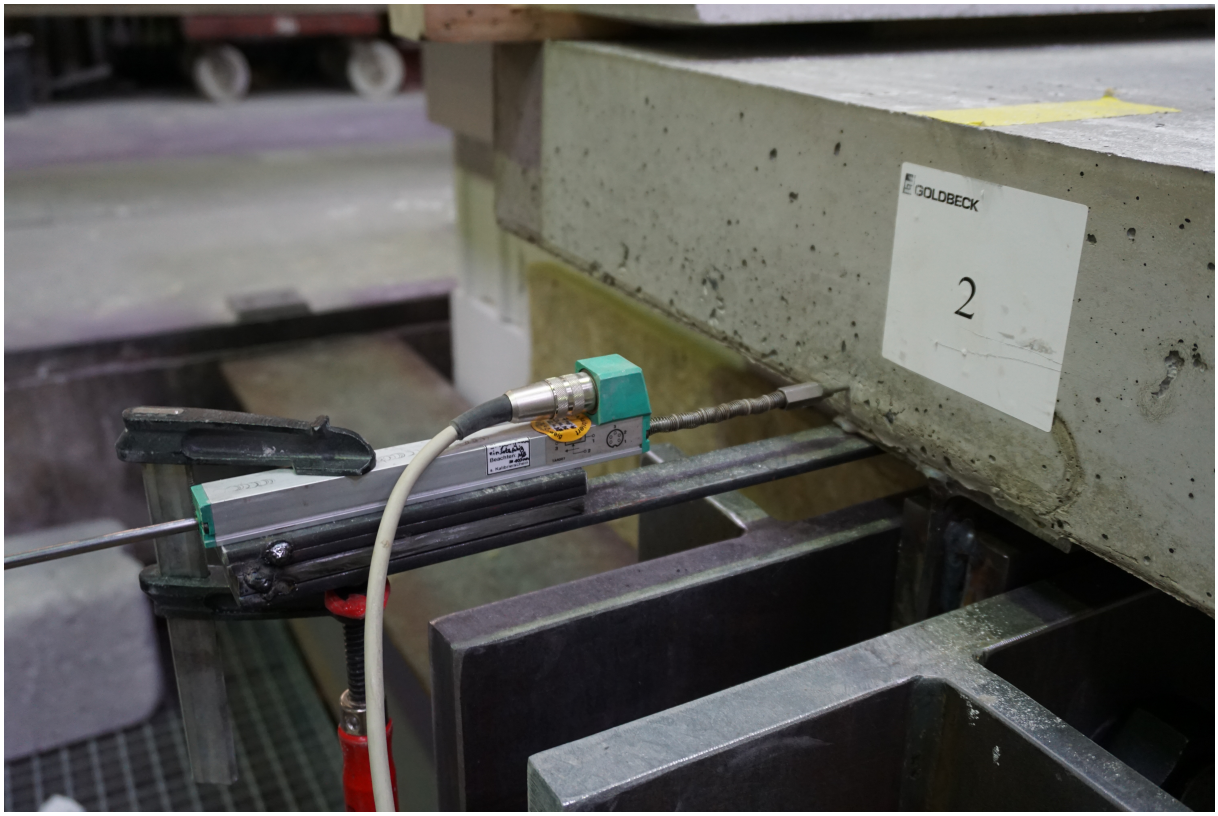

Figure 3.11: Linear potentiometer for slip measurement

3.6 Testing Frame and Loading Devices

The load application was realized by three hydraulic jacks on the quarter points of the composite beams to ensure an even load distribution. As the hydraulic jacks were controlled by oil pressure, the experiment was load controlled. The hydraulic system was coupled for all three jacks, and therefore the same load was applied to all load introduction points. In this way the bending line of the test specimen was similar to the bending line of a beam with even load distribution. The force was measured by the oil pressure of the hydraulic jacks. Figure 3.12 shows the exact location of the load application.

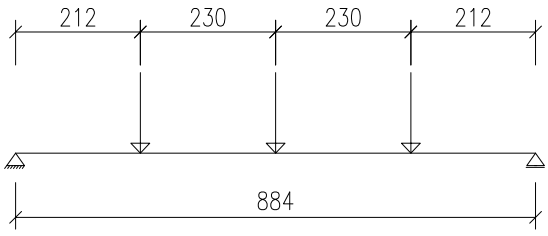

Figure 3.12: Position of the mechanical load application and static system of the composite beam

A simple support of the beams was targeted at to avoid horizontal restraints. One of the used bearings was one-valued, whereas the second bearing was two-valued. M42 bolts were used to connect the bearings with the web of the steel section to enable free rotation of the beams over the supports. The support also served as a clevis bearing due to the horizontal restraint of the web. As the walls of the furnace can only be loaded vertically, the bearings were constructed in a U-like shape to transfer the load directly onto the walls of the furnace. The bearings were constructed out of 30 mm steel sheets. Therefore, the thermal mass of the bearing, as well as additional insulation, prevented heating of the web of the steel section and the bearing itself. During the fire experiments, the temperature of the bearings was controlled regularly, staying well below 50°C. Figure 3.13 illustrates a one-valued bearing with an M42 bolt and a large rotation during an experiment.

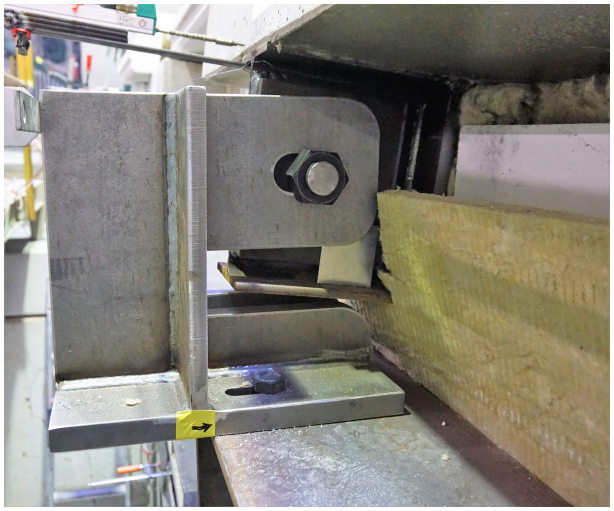

Figure 3.13: One directional bearing during an experiment

3.7 Furnace

For the fire experiment, an 8.0 m long, 4.0 m wide and about 3.0 m high furnace was used. The flame impingement was from the bottom side of the beams. The concrete slabs of the composite beams were used as the upper enclosure of the furnace. To close the gaps in the enclosure between the two tested beams, 150 mm thick and 625 mm wide aerated concrete units were put on top of the composite beams. Figure 3.14 shows a picture of the furnace from the outside during a fire experiment as well as a drawing of the furnace.

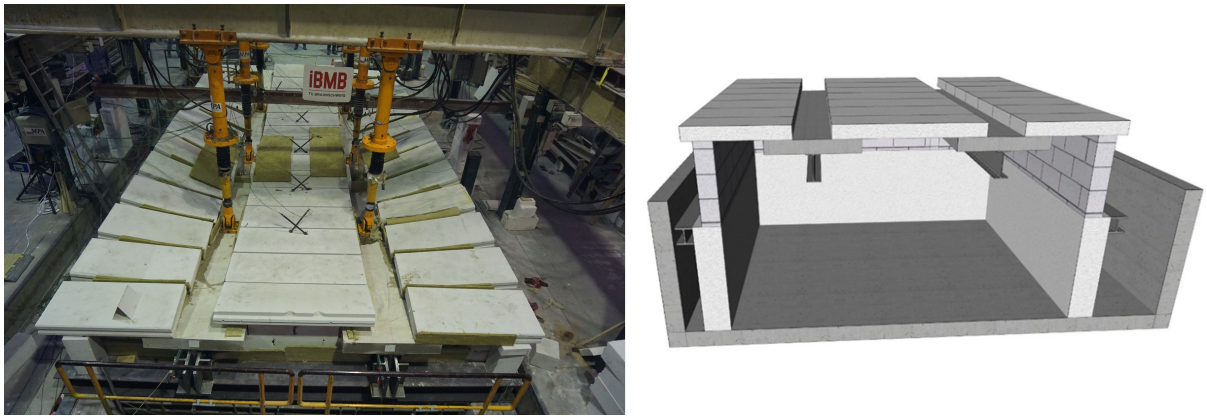

Figure 3.14: Left: Picture of the test set-up during the fire experiement
Right: Cross section of the test set-up, from [33]

3.8 Test Procedure

The experiments aimed to investigate the reaction of the composite joint to a fire in a high rise building. Therefore, a mechanical load, which represents a moderate live load, was put on the composite beam before the start of the fire for 15 min. The load was held constant during the first phase of the flame impingement. After reaching a steel temperature of 600°C, the mechanical load was increased until the abortion criterion of the experiment, a vertical deflection of 400 mm, was reached. There was a constant pre-load of the beam for the first experiment. For experiment two, three, and four, the load was applied cyclically to overcome the adhesive bond between the concrete and the steel. As the mechanical and thermal loads varied strongly during the experiments, the results of the experiments cannot be considered as a fire resistance test of composite beams.

Procedure of the experiments:

1. Preloading of the composite beam (constant for experiment 1, cyclic for experiment 2,3, and 4)
2. Holding the load for 15 minutes
3. Flame impingement until reaching a max. steel temperature of 600°C
4. Additional load until reaching a max. deformation of 400 mm

Table 3.5: Overview of the mechanical and thermal loads due to the procedure of the experiments

Beam #	**Preload [kN]**	**Cyclic load [kN]**	**Fire [min]**	**Total load [kN]**
1	110	-	15	209
2	110	-	15	209
3	290	600	22	394
4	290	600	22	394
5	110	249	16	110
6	110	600	23	277
7	110	249	35	110
8	110	600	40	251

During the flame impingement the resistance of the steel section decreases with the rising temperatures. At a steel temperature of approximately 500°C the resistance of the shear connection generally becomes greater than the resistance of the steel section. A failure of the composite joint is only possible as long as the resistance of the composite joint is lower than the respective resistance of the steel or the concrete section, i.e., when the degree of shear connection is lower than $\eta \leq 1.0$. Consequently, when the mechanical load is increased at a steel temperature of 600 °C, it is expected that the steel section, and not the composite joint, fails.

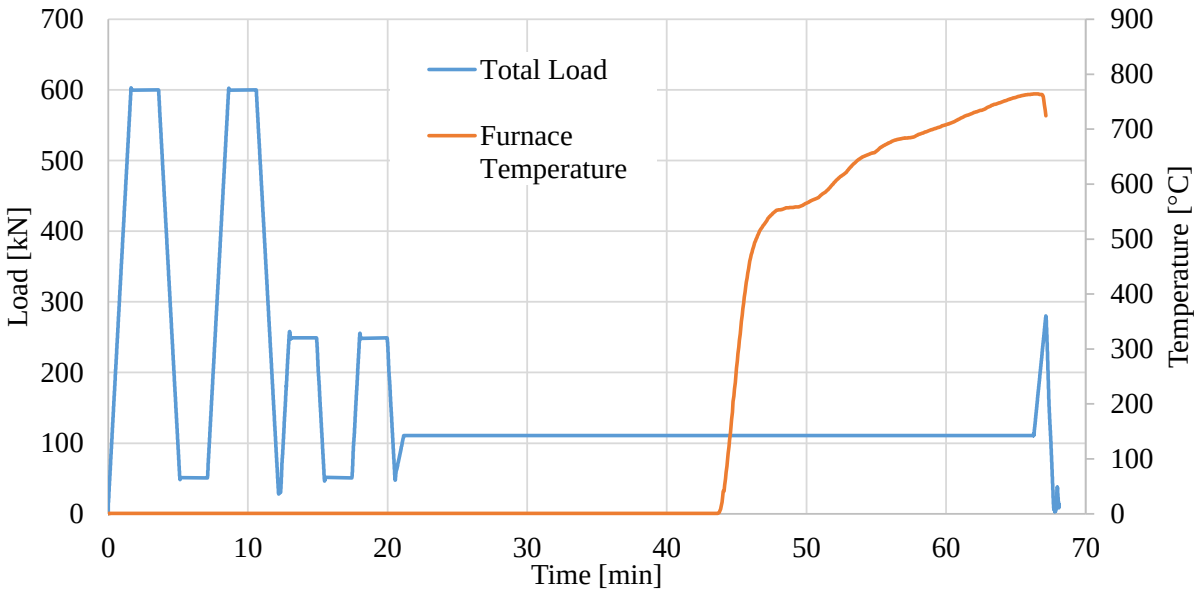

Figure 3.15: Test procedure of Beam 5 and 6, the cyclic preload of 600 kN was only applied to Beam 6

3.9 Results of the Experimental Work

In this section, a synopsis of the results of the experimental work is provided. For all temperature, slip and deformation results, only significant and descriptive values are presented and discussed. More detailed results can be found in the final report of the research project 'Mindestverdübelung im Brand' [24].

3.9.1 Temperature Development

Headed Stud Shear Connectors

An essential result of the temperature measurement is the core temperature of the modified headed stud shear connectors. Figure 3.16 depicts the measured temperatures of beams 5 and 6. During the experiment, the temperatures of the shear connectors always stayed well below 300 °C, even though the temperature of the steel section was rising to over 600 °C at the same time. The core temperature of the shear connectors continued to rise after the end of the fire impingement at minute 23.

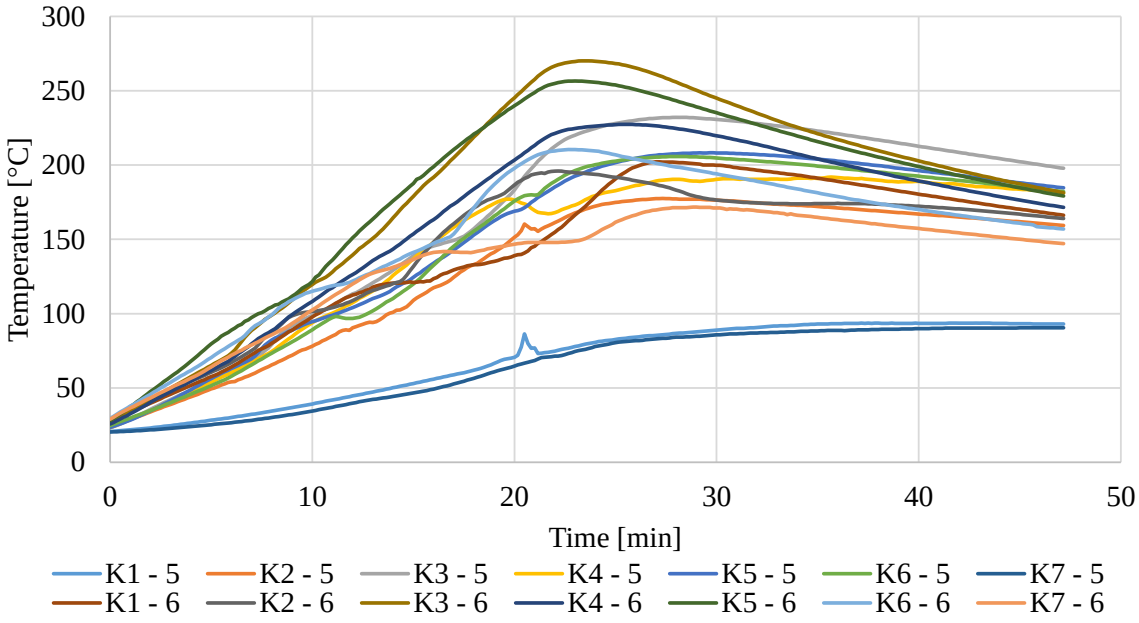

Figure 3.16: Core temperature of the headed stud shear connectors of Beams 5 and 6

A direct comparison between the core temperatures of the headed studs at midspan of Beams 5 and 6 can be seen in Figure 3.17. There was only a slight temperature difference of the headed studs, even though the average steel temperature of the IPE 300 was noticeably higher. The steel section of Beam 5 was an IPE 300, the steel section of Beam 6 was an HEB 300.

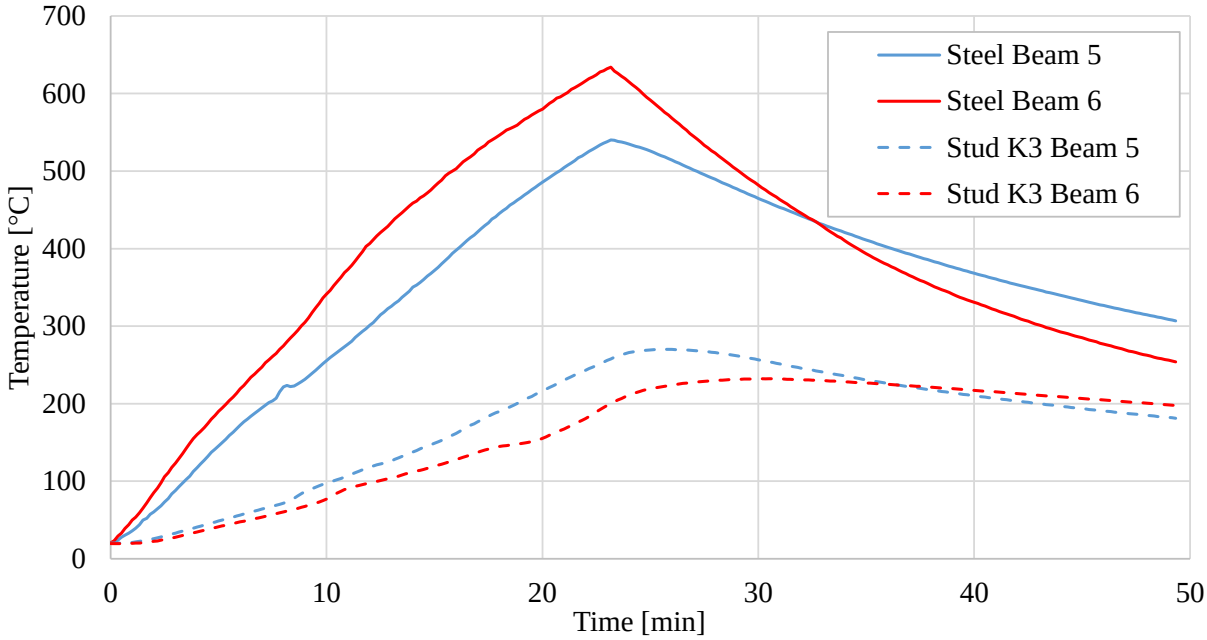

Figure 3.17: Comparison of the headed stud and steel temperature

Concrete Chord

As depicted in Figure 3.18 the concrete chord is dominated by a strong temperature gradient from 20 °C on the unexposed side to 500 °C on the exposed side. The critical temperature for the concrete of 500 °C according to EN 1992-1-2 [34] was reached on the fire-exposed surface. The temperature already dropped to 220 °C at the first measuring point after 25 mm.

Just over the steel section, the concrete chord was protected from direct influences of the fire impingement; therefore the temperature was lower than in the unprotected concrete chord. At a distance of 25 mm from the fire-exposed surface, there was a temperature of 220 °C in the unprotected chord. With the protection of the steel section, the temperature was about 92 °C. Figure 3.18 illustrates the temperature distribution of both the unprotected concrete and the protected concrete with its steel section after 26 minutes of fire exposure. The thermocouple at a depth of 25 mm was also taking the temperature of the lower reinforcement. In all experiments, including the experiment with the natural fire curve, the temperature of the reinforcement at the measuring points never exceeded a temperature of

250 °C. Nevertheless, significant concrete spalling was observed at edges of the specimens, some reaching up to the reinforcement.

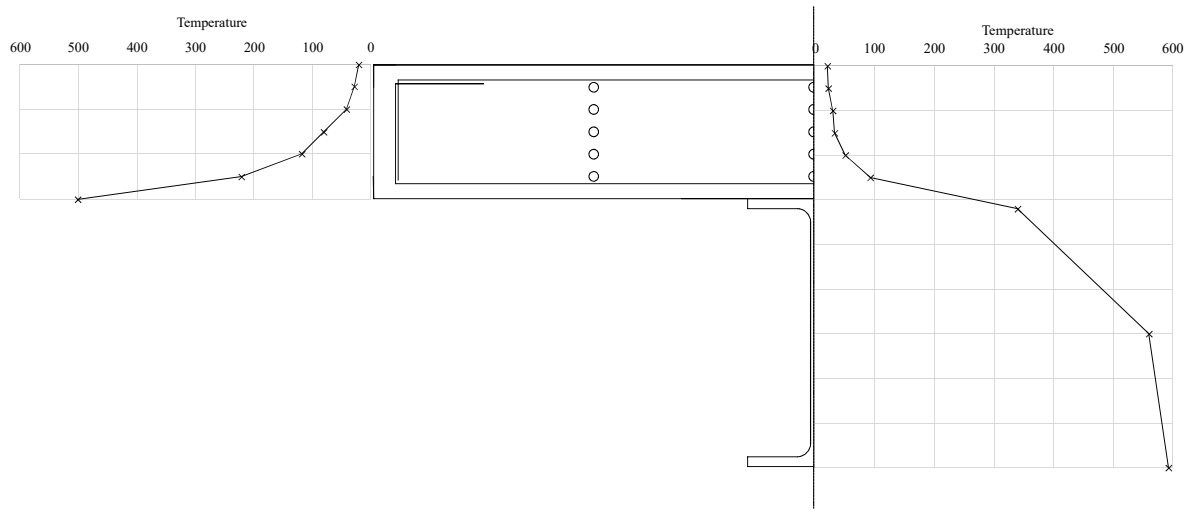

Figure 3.18: Temperature distribution in °C in composite Beam 5 at midspan after 26 minutes of fire exposure. Measuring point 'thermocouples 2' in Figure 3.4
Left: Unprotected concrete, measuring point A in Figure 3.5
Right: Temperature in middle axis of the beam, measuring point B in Figure 3.5

Steel Section

A distinct difference between the IPE 300 and the HEB 300 can be seen in the steel temperature. While the maximum average temperature for the IPE 300 was 633 °C, the maximum average temperature of the HEB 300 was 540 °C. A high temperature difference can also be noted between the upper flange and the lower flange of the steel sections. As the upper flange of the steel sections was protected from the fire from one side and was cooled by the concrete chord, the maximum temperature of the upper flange of the IPE 300 in Beam 6 rises to 480 °C, as can be seen in Figure 3.19. At the same time, the maximum temperature of the lower flange of the IPE 300, which was exposed to the fire from all four sides, rises over 700 °C. A similar temperature development can be observed in the HEB 300 steel section of Beam 5. Hereby, the temperature of the upper flange is only about 350 °C, whereas the temperatures of the lower flange and the web are over 600 °C.

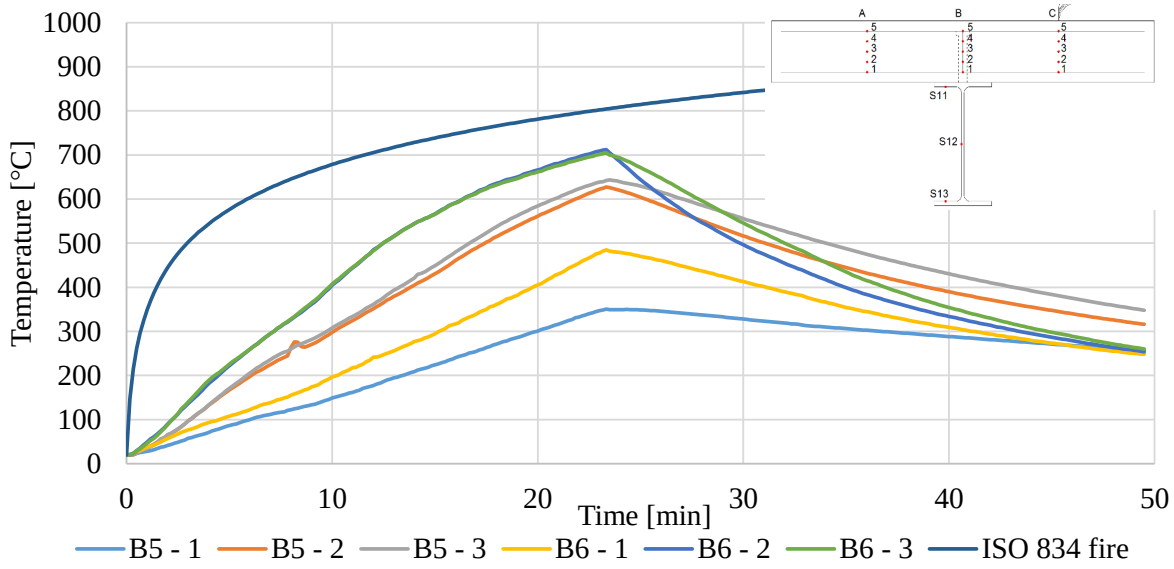

Figure 3.19: Evolution of the steel temperature in Beam 5 and 6 due to ISO 834 fire

3.9.2 Interface Slip over the Supports

For a single span composite beam, the highest slip in the composite joint is to be expected over the supports. Therefore, a focus was put on evaluating the slip at this position. For the slip it is crucial to differentiate between Beams 1-2 and Beams 3-8. Whereas Beam 1-2 only had been preloaded to μ_0[I] = 36 % and μ_0 = 32 % of their respective ultimate load carrying capacity according to EN 1993-1-2 4.2.4 [35], Beams 3-8 experienced cyclic preloading to about μ_0 = 80 % of their ultimate load carrying capacity. Due to the cyclic preload of the composite beams, the adhesive bond between the steel and concrete was released, and a larger slip was recorded.

Figure 3.21 shows the recorded slip for Beams 1 and 2, the applied mechanical load, and the measured average steel temperature.

With the application of the preload in minutes 0 to 2, positive slip arises at both ends of the beam, meaning the steel section gets shorter than the concrete chord. As Beam 1 has a lower degree of shear connection, the measured initial slip is higher than the slip of Beam 2.

[I] Degree of utilization at time t=0 according to EN 1993-1-2 4.2.4

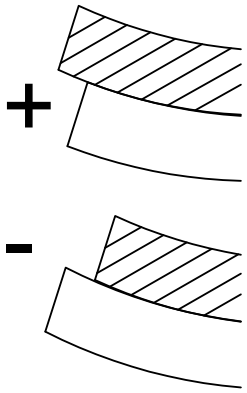

Figure 3.20: Definition of positive slip

After the preload, the mechanical load was sustained until the final second load application in minute 31. In the holding phase in minutes 2 to 17 a slight increase of the slip can be observed. It is assumed that this increase is due to short-term creep of the stressed concrete. With the fire impingement in minute 17 and the rising steel temperature, the slip over the supports fell for both Beams 1 and 2. Due to the higher degree of shear connection, the reduction of the slip of Beam 2 was not as high as in Beam 1. A high nonlinearity can be observed in the course of the decreasing slip. In the beginning, the slip is decreased rapidly, but with the steel temperature approaching 600 °C the slip effectively stopped decreasing.

In both cases, the flame impingement led to falling slip and a reduction of stresses in the composite joint. With further mechanical load in minute 31, the slip rose again.

In the following Figure 3.22 the measured slip for Beams 5 and 6 is displayed. Different from Beams 1 and 2, these beams experienced a higher cyclic preload. Due to this, the measured slip was generally much higher than in Beams 1 and 2. Whereas in Beam 1 the maximum measured slip was about 0.3 mm, the maximum measured slip in Beam 5 was over 0.9 mm. Also for Beams 5 and 6 the slip of the composite joint decreased with fire impingement. It can be observed that the decrease of slip due to the fire was larger with the lower stiffness of the composite joint due to the cyclic preloading. For Beam 6 the slip over the support dropped to under zero. This means the steel section became longer than the concrete chord, even though there was a vertical displacement at the midspan of over 400 mm. Between

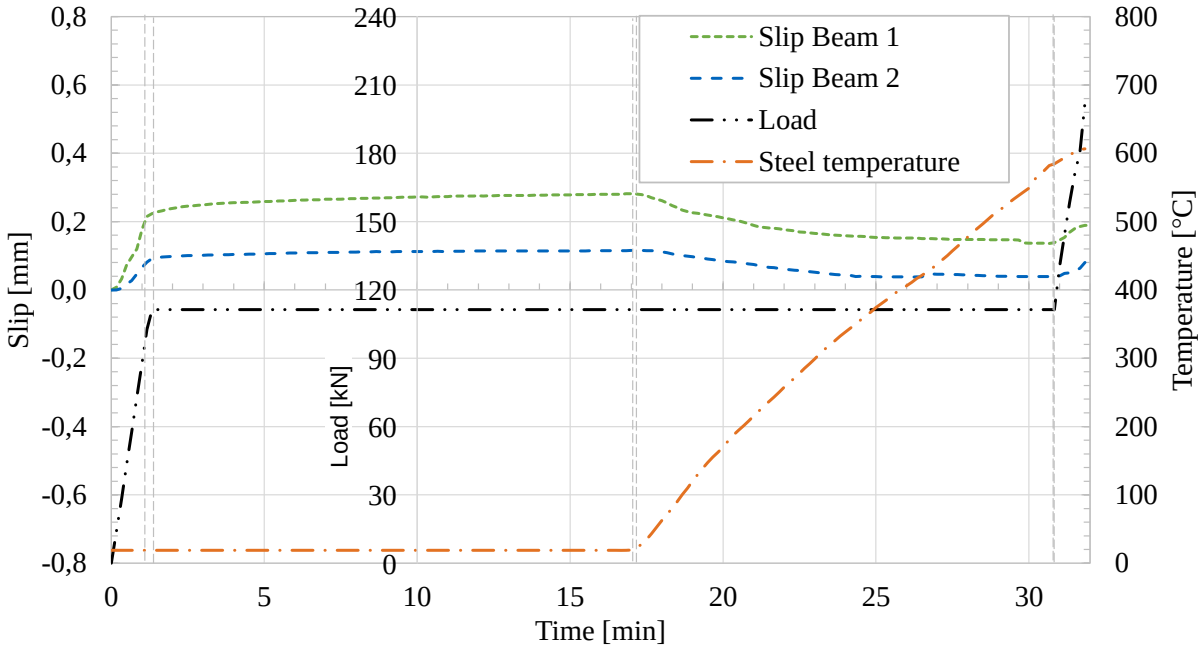

Figure 3.21: Evolution of slip of the composite joint
Beam 1: IPE 300, S460, $\eta = 0.4$
Beam 2: IPE 300, S460, $\eta = 0.6$

the first and the second load cycle of Beam 5, plastic deformation of the composite joint of Beam 5 was observed.

The test abortion criterion of a midspan deformation of 400 mm was reached by Beam 5 before the end of the fire impingement, and therefore the load increase after the fire impingement was only put on Beam 6.

Figure 3.23 depicts the recorded interface slip in Beams 7 and 8 due to the natural fire curve. For Beam 8 a significant slip of about 2.5 mm was recorded. The slip of Beam 7 did not rise as much due to the initial load, but dropped significantly to negative slip due to the fire load. Beam 8, a composite beam with an HEB 300 steel section, showed a significantly higher slip than Beam 6, which is built the same way. The interface slip of Beam 7 evolved similarly to Beam 5.

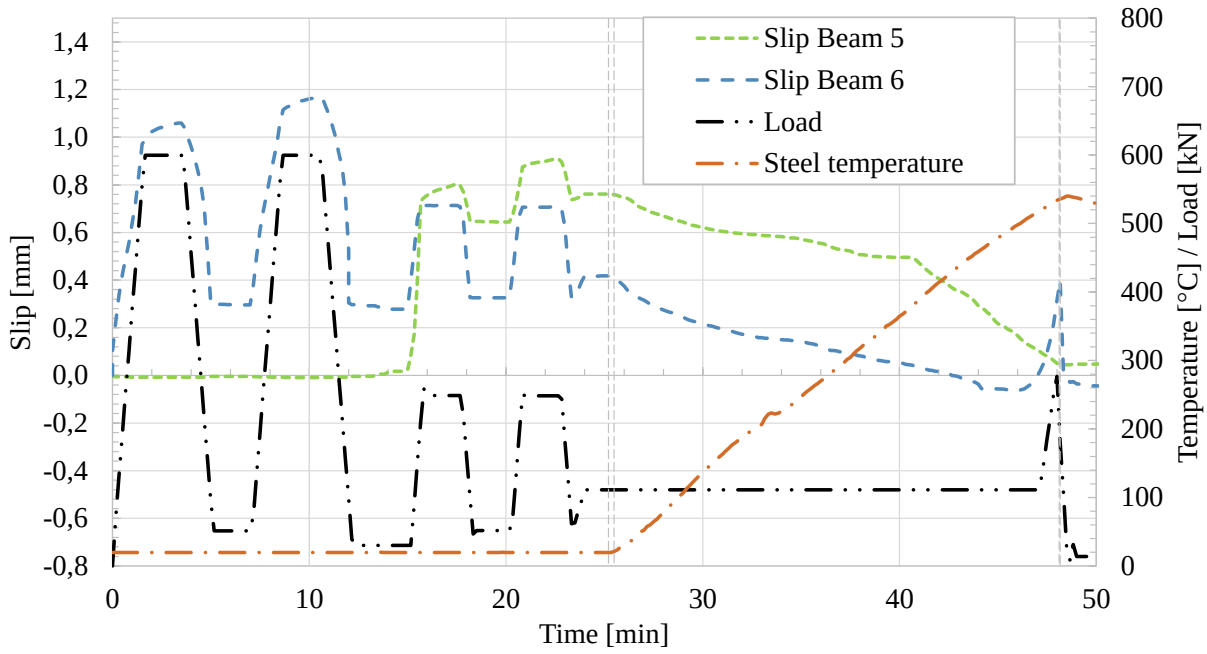

Figure 3.22: Evolution of slip in the composite joint
Beam 5: IPE 300, S355, $\eta = 0.52$
Beam 6: HEB 300, S355, $\eta = 0.4$
Average steel temperature of Beam 5

3.9.3 Vertical Deflection

The abortion criterion for all experiments was a vertical deflection of 400 mm at the midspan. For safety reasons, the deformation was stopped mechanically at 450 mm vertical deformation at the midspan. The deformation of the supports was measured and taken into account for the calculation of the deformation.

For all beams, the deformation grew with flame impingement. Even at steel temperatures below 100 °C, and therefore without any reduction of the stiffness of the steel section, a significant deformation was recorded. In the following Figure 3.24 the deformation of Beam 5 and Beam 6 at a steel temperature of up to 200 °C is shown. Only the rising temperature of the steel section led to a deformation of 23 mm for Beam 6 and 54 mm for Beam 5 at a temperature of 100 °C. For further discussion of this observation, please see Section 6.1.2.

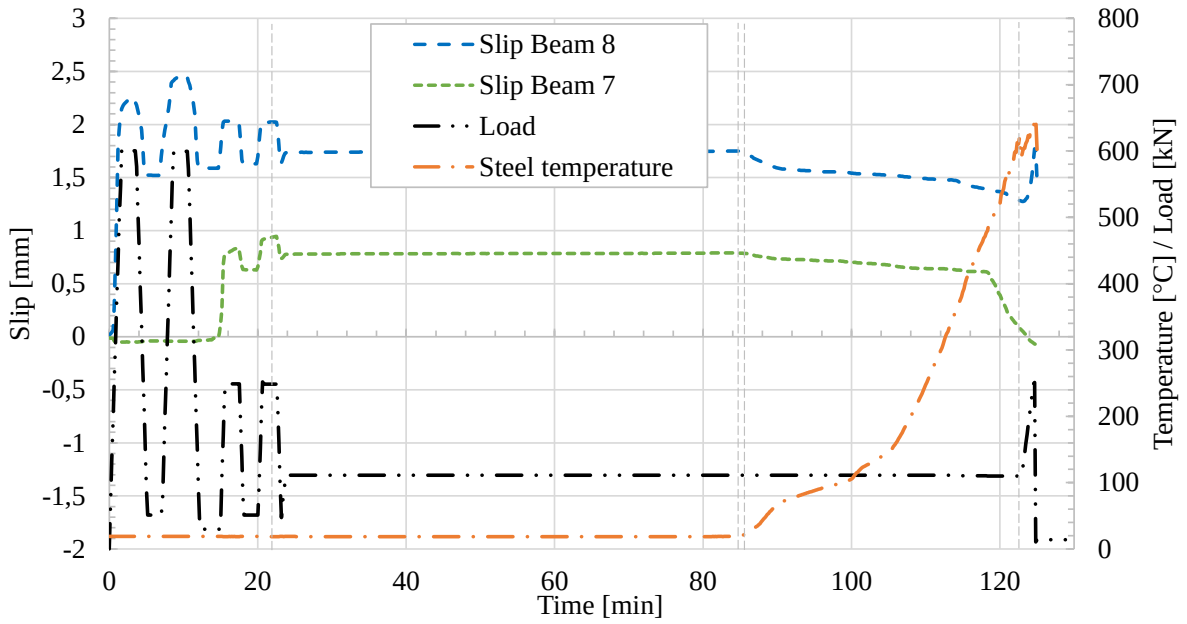

Figure 3.23: Evolution of slip of the composite joint
Beam 7: IPE 300, S355, $\eta = 0.52$
Beam 8: HEB 300, S355, $\eta = 0.4$
Average steel temperature of Beam 7

In the load-deflection curves of the experiments, a plastic deformation due to the cyclic preload can be seen for Beams 3 to 8. Figure 3.25 displays the load-deflection curve of Beams 5 and 6.

Figure 3.26 shows the vertical displacement of Beams 3 and 4. As Beam 3 had a lower degree of shear connection, the deflection due to the initial load, as well as due to the fire, was significantly larger.

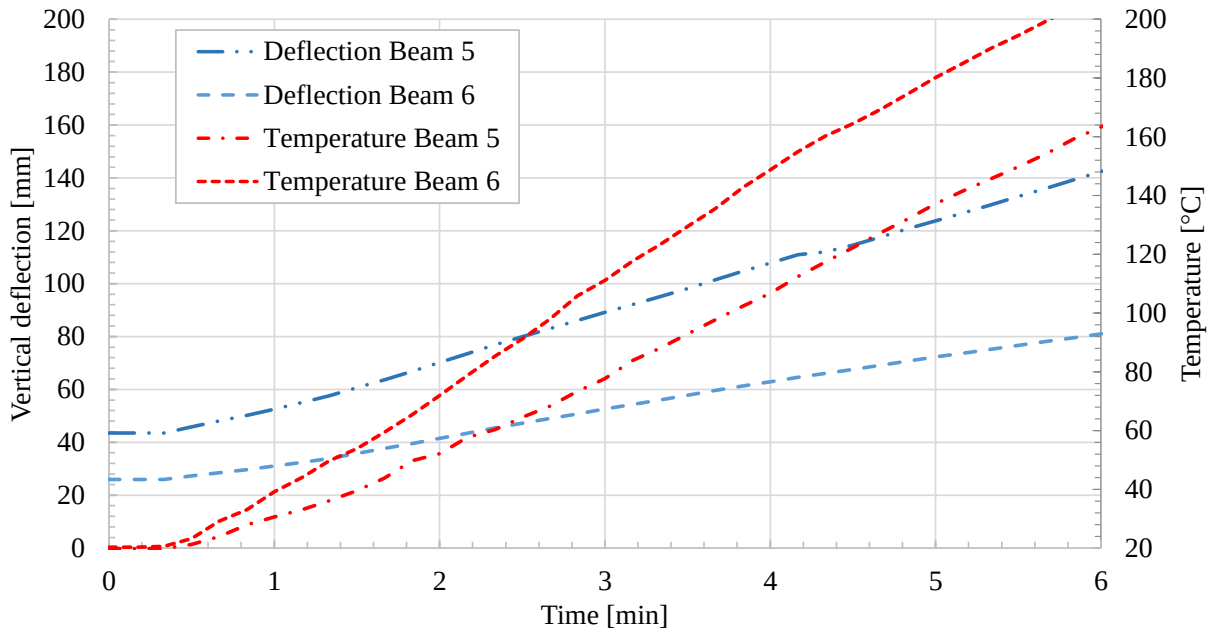

Figure 3.24: Vertical deformation of Beams 5 and 6 up to a steel temperature of 200°C

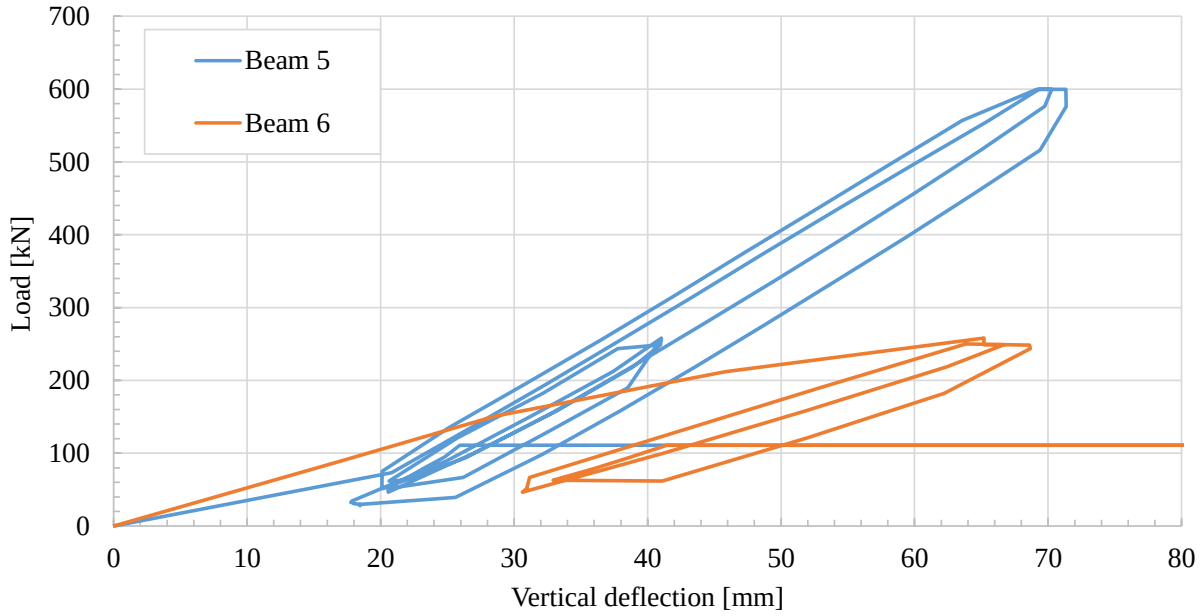

Figure 3.25: Load deflection diagram of Beams 5 and 6 during the cyclic preload

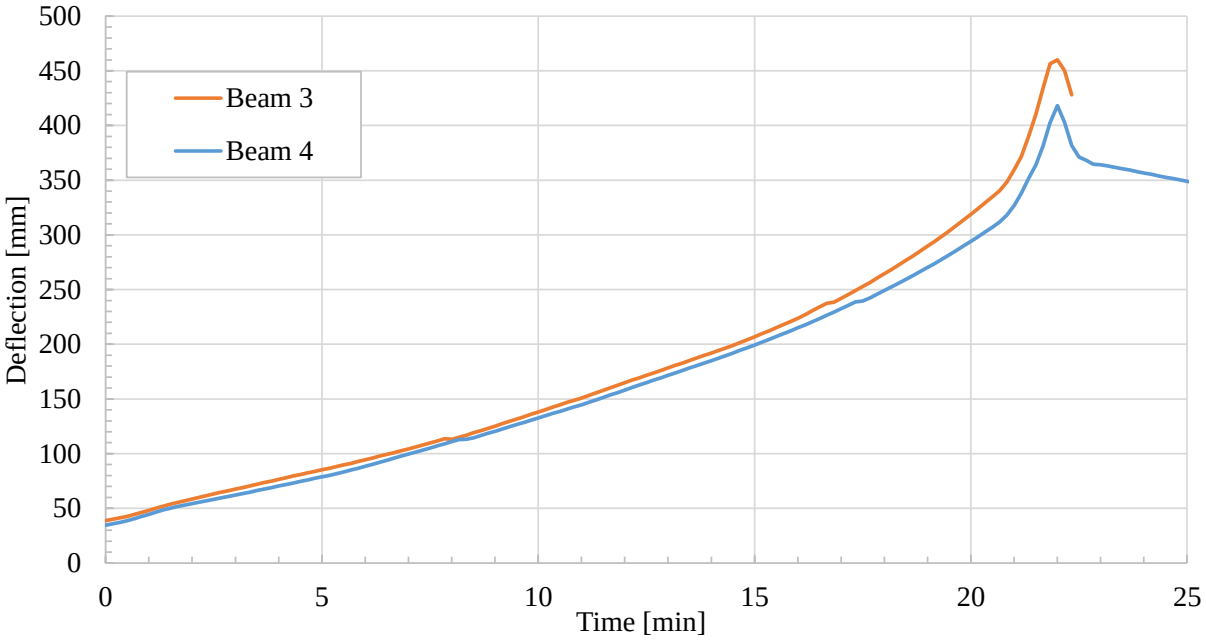

Figure 3.26: Vertical deformation of Beams 3 and 4 during fire impingement

3.10 Conclusion of the Experimental Work

The objective of the experiments was to examine the influence of rising temperatures on the composite joint.

The examination of the temperature distribution showed a high thermal gradient within the composite beam (see Figure 3.18). At the end of the experiment the temperature of the steel section was over 600°C, whereas the top of the concrete section was barely over ambient temperature. The steel sections themselves showed a relatively constant temperature distribution; the temperature of the web and the lower flange were nearly identical. The core temperature of the headed stud shear connectors did not rise above 300°C.

For all eight beams, the general course of the interface slip over the supports was similar. There was an initial positive slip due to the pre-load. During the flame impingement the slip was at first falling rapidly and then, with rising steel temperatures, slower. It was observed that the thermal load led to a slip contrary to the slip out of vertical mechanical loads. Whereas in this setup mechanical loads led to a positive slip, thermal loads led to a negative slip.

The cyclic preload of the composite beam led to much larger deformations in the composite joint.

4 Finite Element Modelling of Composite Beams in Fire

4.1 Introduction

For the numerical simulation of composite steel-concrete beams in a fire situation, two accurate three-dimensional finite element models were developed with the commercial software package Abaqus/CAE [36]. Both thermal and structural loads were included in the models. Therefore, the numerical simulation of the structure in fire was conducted in two steps:

First, there was a transient-thermal analysis of the structure with particular elements for the heat transfer analysis. Second, the results of the transient-thermal analysis were implemented in the static-structural analysis module via multiple temperature fields. The models used the temperature-dependent material properties of the EN 1994-1-2 [2]. The ISO 834 fire was used as a thermal load for the thermal analysis.

The numerical analysis of a composite beam in the fire was split into five separate models: two full models of a composite beam with a solid concrete slab, one model of the headed stud shear connectors, one model of a composite beam with deep decking, and one model with an intumescent coating.

Model I was used for the description of the effects of elevated temperatures on the composite joint (see Section 6.1) and for the investigation of the influence of a reduced degree of shear connection on the load carrying behaviour of a composite beam in a fire situation. This model was built with a high level of detail and was modified to match the results of the experiment.

Model II, a model of the headed stud shear connectors, was used to calculate the load-slip behaviour of the shear connectors at elevated temperatures. It was built to depict a standard push test according to Annex B of the EN 1994-1-1. In all other models, the headed stud shear connectors were modelled with two non-linear springs: a vertical and a horizontal spring. The properties of these springs were partially derived from *Model II*. The results of *Model II* are discussed in Section 4.5.4

Model III was generated for the examination of the mode of failure of composite beams with deep decking. The model covers various decking geometries, different degrees of shear connection, and different spans.

Model IV was built to examine the influence of intumescent coating of the steel section on the composite joint in the fire. As the three influences of elevated temperatures on the composite joint (cf. Section 6.1) are highly influenced by the temperature distribution in the composite beam, additional insulation of the steel sections leads to a change of behaviour in the composite joint. Apart from the transient thermal insulation by the intumescent coating, *Model IV* is similar to *Model I*.

Model V is a simplified version of *Model I*. It was used for the large parametric study and was therefore modelled to be a reasonable compromise between computation time and precision. Due to the number of parameters, this model was built with full parametric pre- and post-processing included.

The level of detail of the models varies, depending on their purpose. While reduced models were utilised for the large parameter study, detailed models with fine meshing were used for the validation and calculation of the three effects.

4.2 Mechanical Properties

4.2.1 Mechanical Model Steel

The material properties of the steel section at elevated temperatures were modelled according to EN 1994-1-2 [2]. The stress-strain relationship of steel was modelled in four sectors. Figure 4.1 shows an illustration of the stress-strain sectors according to EN 1994-1-2. Sector one represents the linear elastic stress-strain relationship with the stiffness of Young's modulus E_a[I]. The second sector starts at the proportional limit $\epsilon_{ap,\theta}$[II], running elliptically until the start of the third sector at the yield range $\epsilon_{ay,\theta}$[III]. The value of the strain at the beginning of the yield range $\epsilon_{ay,\theta}$ was set to 2%. The fourth sector according to EN 1994-1-2 describes the softening of the steel. Sector four was not included in the material model as the necessary strain for reaching sector four was very unlikely to be reached within the scope of this investigation. Figure 4.2 shows the stress-strain relationship of the modelled steel at ambient conditions and at elevated temperatures for sectors one and two.

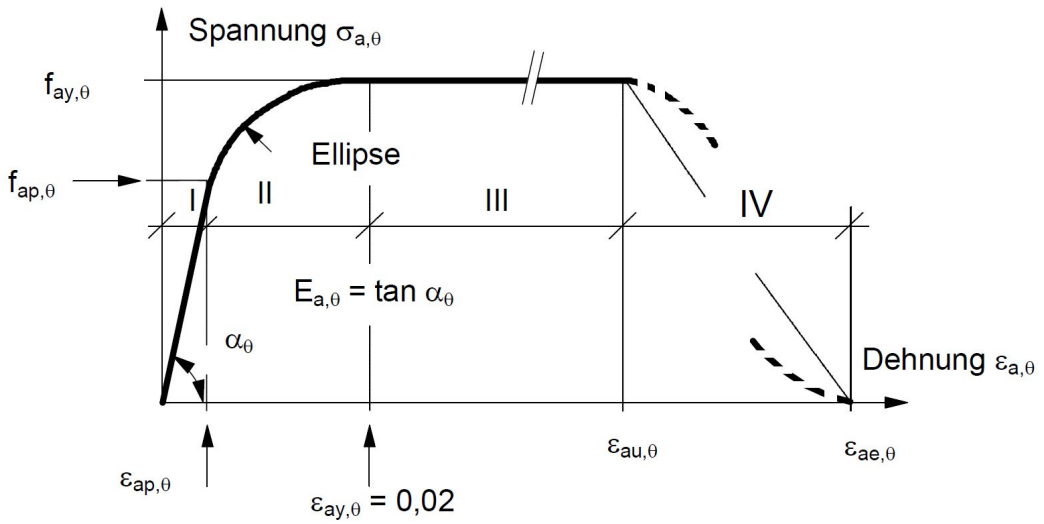

Figure 4.1: Stress-strain relationship of steel at elevated temperatures from EN 1994-1-2 Figure 3.1

[I] Characteristic value for the modulus of elasticity of structural steel at ambient conditions
[II] Strain at the proportional limit in the fire situation
[III] Yield strain in the fire situation

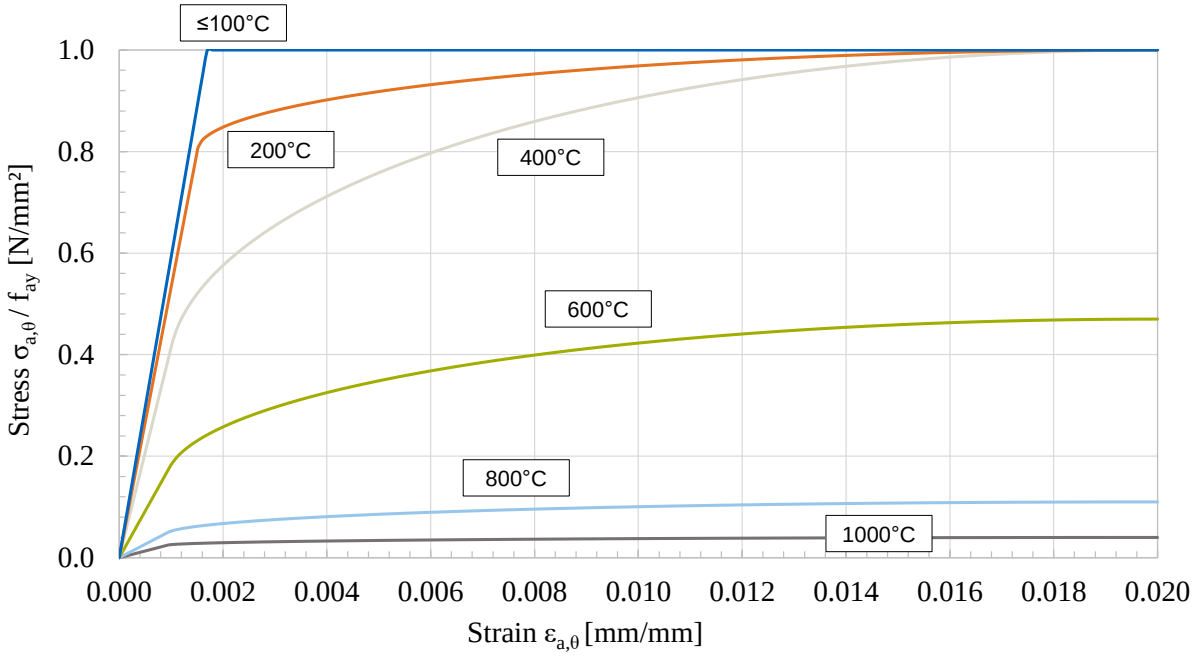

Figure 4.2: Stress-strain relationship of sectors one and two at elevated temperatures as used in the FE-model

Sector one was modelled from a temperature dependent Young's modulus $E_{a\theta}$[I] starting at $E_{a\theta} = 210000\ N/mm^2$. The Poisson's ratio ν_a[II] was held constant at $\nu_a = 0.4$ for all temperatures. The elliptic curve in sector two was approximated by multiple lines. The lines connect pairs of variates, which were calculated from elastic strain of the Young's modulus and the respective plastic strain. As there is a high limit of variate pairs in Abaqus for the material definition, the elliptic curve was approximated closely. As shown in Figure 4.2, the yield strength f_{ay} at ambient conditions stayed constant up to temperatures of 400 °C. At temperatures up to 100 °C the linearly elastic sector I connects directly with the start of the yield range $\epsilon_{ay,\theta}$, without the need for modelling the elliptic sector II. The yield strength f_{ay} of the steel section at ambient conditions was set to the values measured in Section 3.4.

[I] Characteristic value for the modulus of elasticity of structural steel in the fire situation
[II] Poisson's ratio for structural steel

According to EN 1994-1-2 [2] the concrete reinforcement steel could be modelled with the same mathematical model as the structural steel. Only the value of the maximum yield strength f_{sy}[I] was set to 500 N/mm^2 and the strain ϵ_{uk}[II] at failure was set to 25 ‰.

4.2.2 Mechanical Model Concrete

The material properties of the concrete section in the FE-model were chosen according to EN 1991-1-2 [37]. The class of the concrete modelled was C55/67. For the validation of the experiments, the compressive strength of the concrete was chosen based on the compressive strength test in Section 3.4. According to the EN 1992-1-2 [34] the density of the concrete was chosen depending on the use case of the concrete. For the structural analysis, the density was considered to be independent of the temperature, this way the self-weight of the concrete was constant during the flame impingement. Temperature dependence of the density was used for the thermal analysis. Hereby the density fell due to the vaporisation of the water in the concrete.

In ABAQUS the concrete was implemented with the material model 'concrete damage plasticity' [36]. Besides the compressive strength $f_{cm,\theta}$[III] and the tensile strength $f_{c,\theta}$[IV], there are four parameters to be defined in the concrete damage plasticity model: ε_{aba}[V], Ψ_{aba}[VI], σ_{b0}/σ_{c0}[VII] and K_c[VIII]. In the following simulations the parameters of the material model were chosen as follows:

$K_c = 0.6666,$

$\varepsilon_{aba} = 0.1,$

$\sigma_{b0}/\sigma_{c0} = 1.16,$

[I] Nominal value of the yield strength of reinforcing steel
[II] Characteristic strain of reinforcement or prestressing steel at maximum load
[III] Mean value of concrete cylinder compressive strength
[IV] Mean value of axial tensile strength of concrete, temperature dependent
[V] Eccentricity in Abaqus material model
[VI] Dilatation angle in Abaqus material model
[VII] Ratio of initial equibiaxial compressive yield stress to initial uni-axial compressive yield stress in Abaqus material model
[VIII] Ratio of the second stress invariant on the tensile meridian to that on the compressive meridian in Abaqus material model

$\Psi_{aba} = 35$.

Similar to the model of steel, the strain of the concrete model was also split into an elastic and a plastic part (cf. Abaqus/CAE Users Guide [36]).

$$\varepsilon = \varepsilon^{el} + \varepsilon^{pl} \tag{4.1}$$

Based on EN 1992-1-1 [26] the uniaxial stress-strain relationship of concrete was split into three parts, a linear elastic part, a parabolic arc between $0.4 * f_{cm,\theta}$ and $f_{cm,\theta}$ and a third part with the degradation after reaching the compressive strength of the concrete. With the strain equation given in Equation 4.1, the elastic part of the stress-strain relationship was defined by a temperature dependent Young's modulus. In the compressive part, the transition between the linear elasticity of the concrete and its compressive strength was described by Equation 4.2 and Figure 4.3, both from EN 1992-1-1. The degradation of the concrete after reaching the compressive strength $f_{cm,\theta}$ was modelled to be linear up to a remaining compressive capacity of 10 % of its initial value.

$$\sigma_c = f_{cm} * \frac{k * \eta - \eta^2}{1 + (k - 2) * \eta} \tag{4.2}$$

with

$$\eta = \frac{\varepsilon_c}{\varepsilon_{c1}} \tag{4.3}$$

$$k = 1.05 * E_{cm} * \frac{\varepsilon_{c1}}{f_{cm}} \tag{4.4}$$

The tensile capacity $f_{c,\theta}$ of the concrete was assumed to be 10 % of the compressive strength $f_{cm,\theta}$. Hereby the stress-strain relationship was modelled to be linear up to the tensile failure

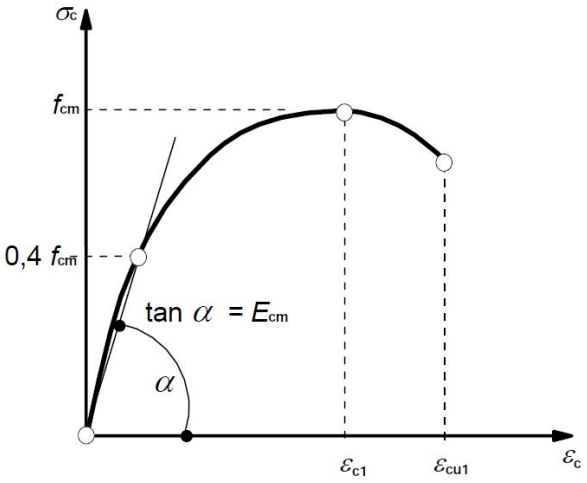

Figure 4.3: Stress-strain relationship of concrete under compression from EN 1992-1-1 Figure 3.2

of the concrete. The Young's modulus used was the same as for the compression zone, $E_{cm\theta}$[I]. For reasons of numerical stability, a linear post-failure behaviour was assumed.

Figure 4.4 shows the stress-strain relationship as implemented in the FE model. $f_{ck,\theta}$[II] and $\epsilon_{c,\theta}$[III] were taken from EN 1994-1-2.

Young's Modulus Concrete

Different to the steel, EN 1994-1-2 does not include values for the temperature dependent Young's modulus $E_{c\theta}$[IV]. Minnert and Wagenknecht [38] propose calculating the initial tangent modulus $E_{c\theta}$ from the temperature dependent values $f_{c,\theta}$[V] and $\epsilon_{c,\theta}$ from EN 1994-1-2.

$$E_{c,\theta} = 1.5 * \frac{f_{c,\theta}}{\varepsilon_{cu,\theta}} \tag{4.5}$$

As described by Bergmann [39], the initial tangent modulus was used for the calculation of composite columns rather than for the calculation of composite beams. Therefore, Equa-

[I] Secant modulus of elasticity of concrete, temperature dependent
[II] Characteristic value of the cylinder compressive strength of concrete at 28 days, temperature dependent
[III] Concrete strain in the fire situation
[IV] Tangent modulus of elasticity of concrete, temperature dependent
[V] Characteristic value for the compressive cylinder strength of concrete in the fire situation

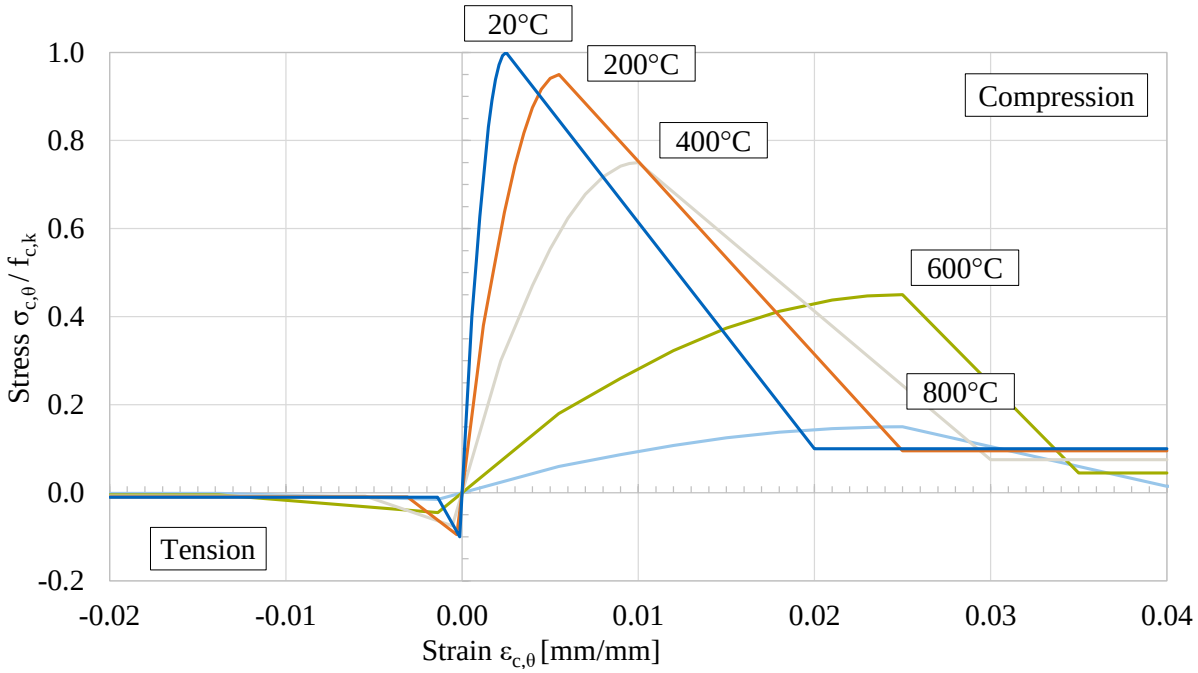

Figure 4.4: Stress-strain relationship of the concrete at elevated temperatures as used in the FE model

tion 4.5 results in values too low for the calculation of composite beams, even at ambient conditions.

For the transition of a tangent modulus to a secant modulus, Bergmann proposes the following Equation 4.6.

$$E_c = \frac{0.8}{1.35} * E_{cm} \simeq 0.6 * E_{cm} \tag{4.6}$$

The combination of Equation 4.5 and 4.6 leads to 4.7.

$$E_{cm,\theta} = \frac{1.5 * f_{c,\theta}}{0.6 * \varepsilon_{cu,\theta}} \tag{4.7}$$

Table 4.1 shows the Young's modulus at 20 °C calculated from Equation 4.7 and according to EN 1992-1-1.

Table 4.1: Comparison of the Young's modulus based on EN 1992-1-1 and Equation 4.7

	$E_{cm,20°C}[N/mm^2]$	
Strength class	EC2 Table 3.1	Equation 4.7
C 20/25	30,000	20,000
C 25/30	31,000	25,000
C 30/37	33,000	30,000
C 35/45	34,000	35,000
C 40/50	35,000	40,000
C 45/55	36,000	45,000
C 50/60	37,000	50,000

As Equation 4.7 only works well at low and high strength classes, a reduction factor for the Young's modulus at elevated temperatures $E_{c\theta}$ was introduced. With $k_{Ec,\theta}$[I] the temperature dependent reduction of the tangent modulus $E_{c\theta}$ according to Equation 4.5 can be used with values of the Young's modulus according to EN 1994-1-1.

$$E_{cm\theta} = k_{Ec,\theta} * E_{cm,20°C} \tag{4.8}$$

with

$$k_{Ec,\theta} = \frac{E_{c,\theta}}{E_{cm,20°C}} \tag{4.9}$$

A verification and comparison of the fraction $\frac{E_{c\theta}}{E_{cm,20°C}}$ was done by Mannsfeld [40]. When comparing the values of the literature, the Young's modulus according to Equation 4.5 is generally lower than the values of other research.

[I] Temperature dependent reduction factor of the tangent modulus E_{cm}

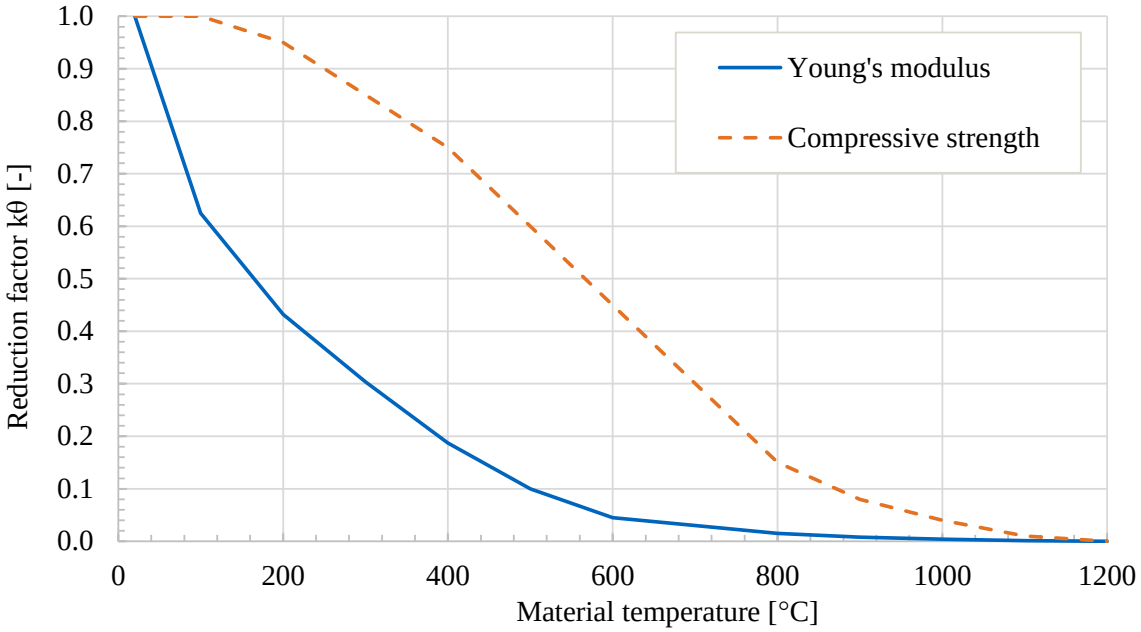

Figure 4.5: Comparsion between the reduction of the computed temperature dependent Young's modulus $E_{cm\theta}$ and the compressive strength $f_{cm,\theta}$

4.3 Thermal Properties Steel, Concrete & Intumescent Coating

The thermal properties of both steel and concrete were taken from EN 1994-1-2 and EN 1992-1-2. The following material parameters were defined at elevated temperatures: $\lambda(\theta)$[I], $\rho(\theta)$[II], α_θ[III] and $c_p(\theta)$[IV].

4.3.1 Thermal Properties of Intumescent Coating

Based on the work of Kraus [41], Tabeling [42], Sothmann [43], and Molochnikowa [44] an intumescent coating of the type SIKA UNITHERM Platinum [45] was implemented in Abaqus. Here it was assumed that the reaction of the intumescent coating starts at a

[I] Conductivity, temperature dependent
[II] Density, temperature dependent
[III] Coefficient of thermal expansion, temperature dependent
[IV] Specific heat capacity, temperature dependent

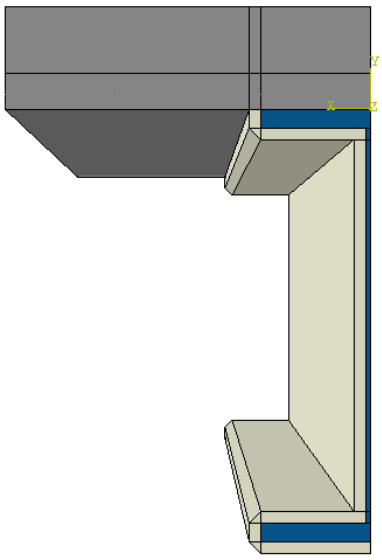

Figure 4.6: Cross section of the FE-model of a composite beam protected with intumescent coating

temperature of 300 °C. At a temperature of 530 °C the expansion reaches its maximum and the pyrolysis of the intumescent coating starts. Figure 4.7 shows the course of the expansion factor of the intumescent coating with a rising material temperature. According to Sothmann [43], the maximum expansion factor was first set to 37. During the validation of the material properties in the research project [24] it was corrected to 35.

The similarity law (cf. Sothmann [43]) was used for the transient thermal analysis of the coating in the FE program Abaqus. This way the thickness of the material in the FE-model was kept constant and only the material properties were scaled depending on the actual expansion factor given in Figure 4.7. Tabeling [42] elaborated the presented material properties. Due to the expansion of the coating with elevated temperatures, the specific heat capacity $c_p(\theta)$, the density $\rho(\theta)$, the expansion factor $\alpha_{i,(\theta)}$, and the conductivity $\lambda(\theta)$ are highly transient. The following figures, Figures 4.8 and 4.9, display the material properties as used in the FE-model. While both the specific heat capacity and the conductivity of the material were changed with the expansion of the coating, the density was not.

It was assumed that the conductivity of the intumescent coating can be split into heat transmission and thermal radiation in the pores and the transmission in the base material of the

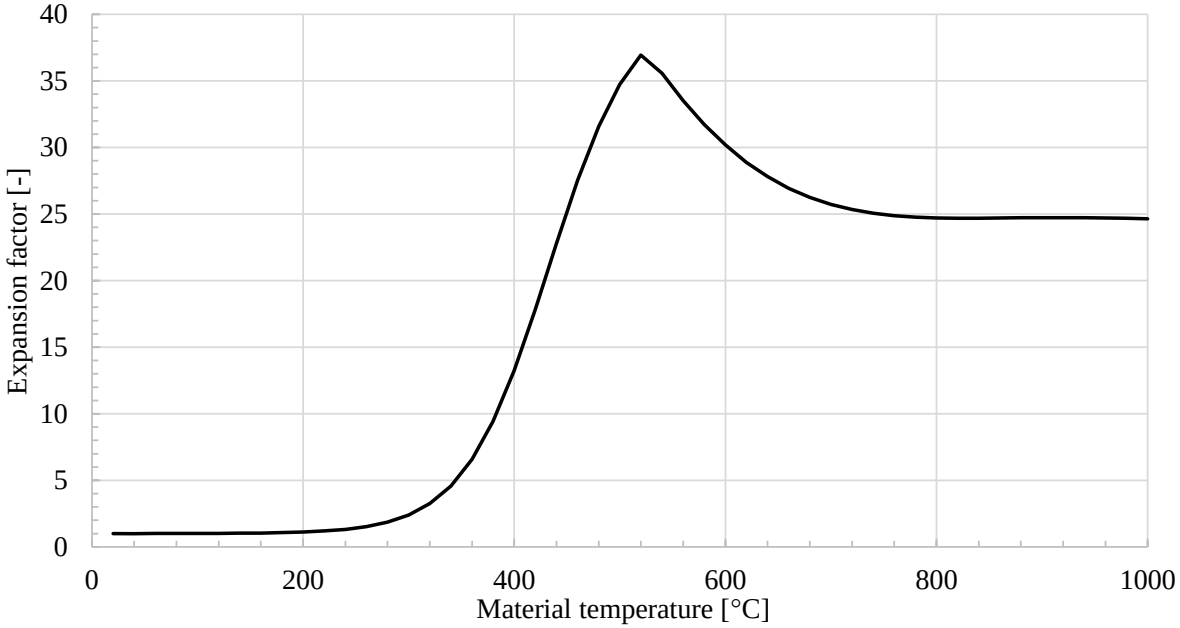

Figure 4.7: Expansion factor $\alpha_{i,(\theta)}$[I] of the intumescent coating in relation to the material temperature for a heating speed of 50 K/min according to Tabeling [42]

coating (cf. Sothmann [43]) to calculate the conductivity of the intumescent coating. Figure 4.9 displays the equivalent conductivity λ_{eq}[II] of the intumescent coating with the expansion of the material considered. Figure 4.9 also shows the effect of the intumescent coating's expansion on the conductivity. Up to the beginning of the expansion, there was no change in the conductivity, while during the expansion of the material, the conductivity dropped significantly. With the beginning of pyrolysis of the intumescent coating, the conductivity started to rise again.

[II] Equivalent conductivity intumecent coating

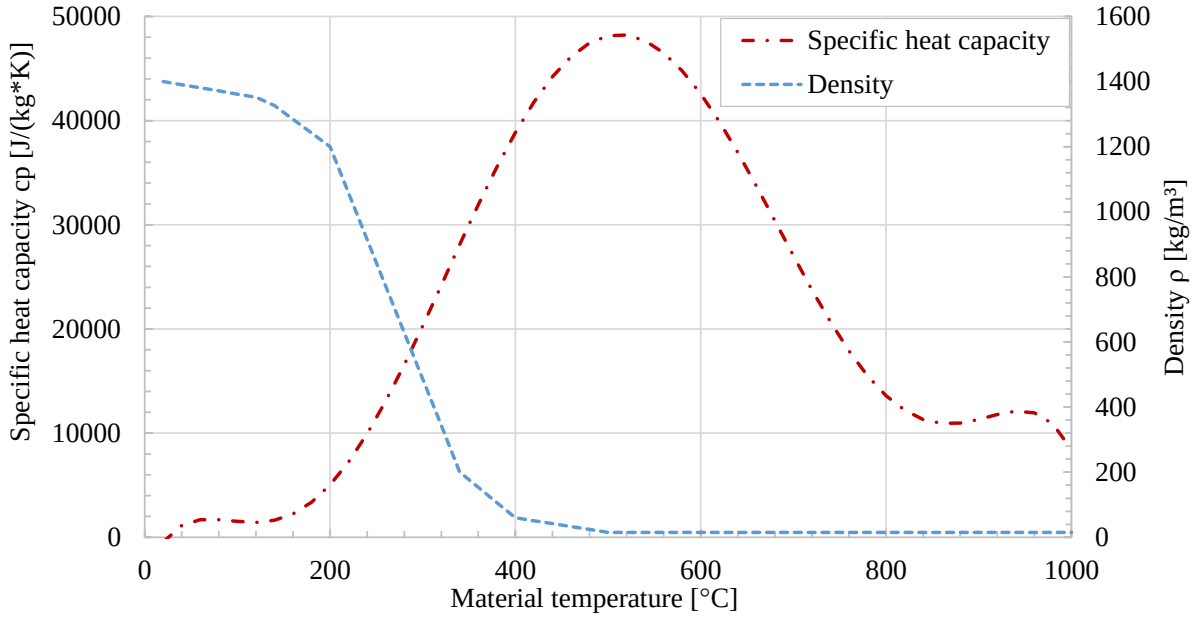

Figure 4.8: Specific heat capacity $c_p(\theta)$ and density $\rho(\theta)$ of the intumescent coating with the change of volume included, as used in the FE model

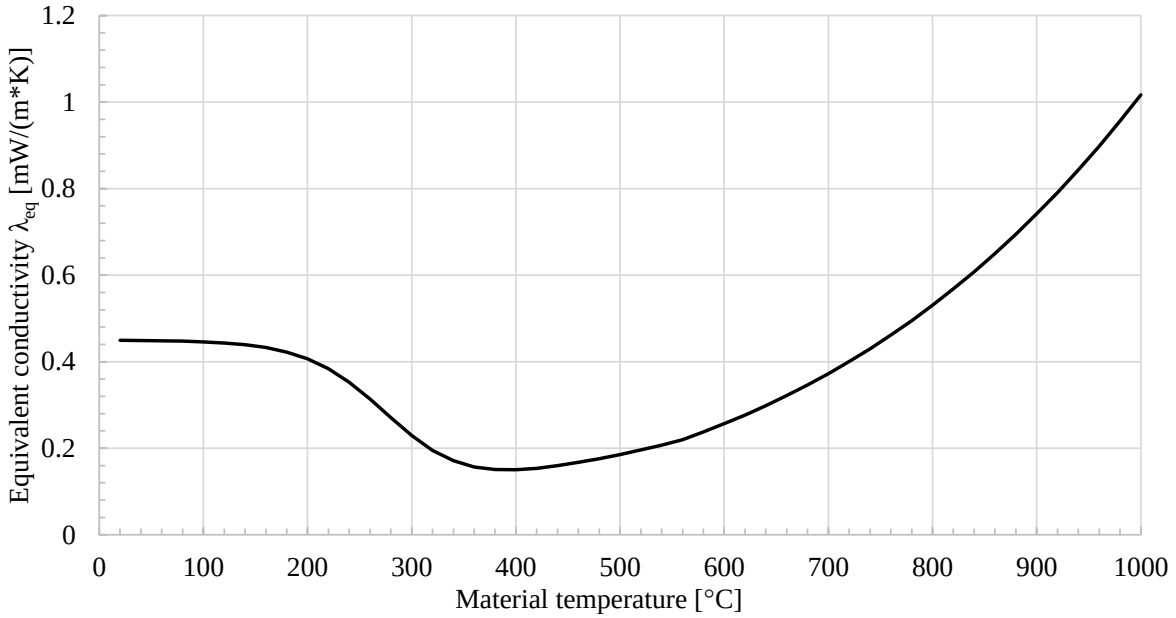

Figure 4.9: Equivalent conductivity $\lambda(\theta)$ of the intumecent coating with the expansion included

4.4 Details of the Modelling

4.4.1 Modelling of the Contact Areas

The contact between the steel and the concrete surface was modelled differently for the thermal and the structural analysis. For the thermal analysis, a full bound of the surfaces was implemented. In the structural analysis, the contact between the steel section and the concrete chord was established with the 'hard contact' model in Abaqus. This contact model allows a gap opening between the surfaces with separating forces and prevents penetration of the material with pressure between the surfaces. In the tangential direction, a coefficient of friction μ_{ca}[I] $= 0.3$ was modelled; this value is consistent with values of the literature (cf. Claßen [46] and Jähring [7]).

4.4.2 Modelling of the Full Beam

The steel beam was modelled with hexahedral solid elements. As the width consists of only one element, the incompatible modes, such as shear-locking or hourglassing, were deactivated. The concrete chord was also modelled with hexahedral solid elements. Reinforcement was considered with two-node truss elements and was embedded in the concrete region. For the thermal and structural analysis two different element types were used. The element type are listed in Table 4.2, as well as shown in Figure 4.10.

Table 4.2: Elements used in the Abaqus/CAE FE-model

Analysis type	Structural	Thermal
Steel beam	C3D81	DC3D8
Concrete chord	C3D8	DC3D8
Reinforcement	T3D2	DC1D2
Fasteners	CONN3D2	-

As the symmetries of the system were used, only a quarter of the structure was modelled. The deflection perpendicular to the respective symmetry planes was suppressed. For single

[I] Coefficient of friction between steel and concrete

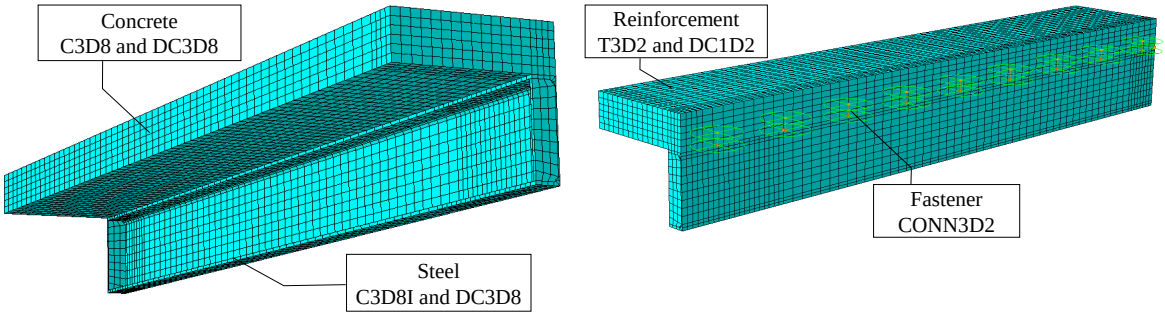

Figure 4.10: Types of elements used in the FE model

span beams, there was a vertical support at one end of the beams. In this way, a statically determinate support condition was reached. Figure 4.12 shows the two modelled symmetry regions, the position of the vertical support and the contact region between concrete and steel.

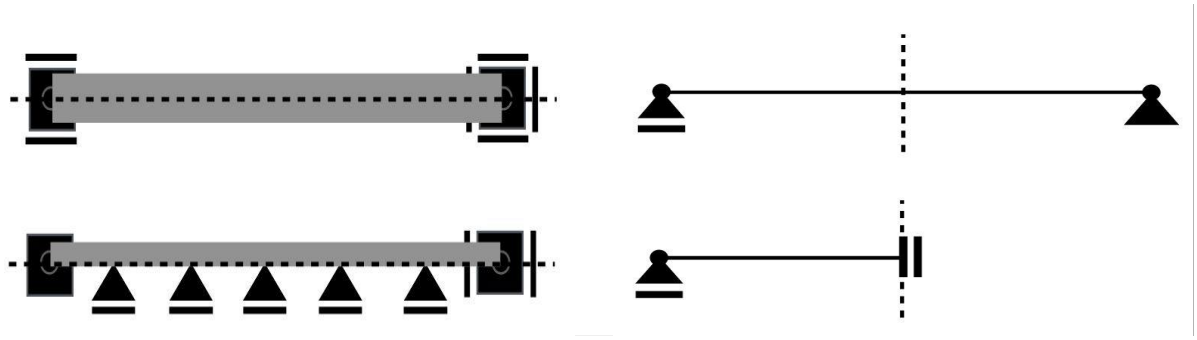

Figure 4.11: Symmetry conditions of the full model, only a quarter of the beam was modelled, from Röß [47]

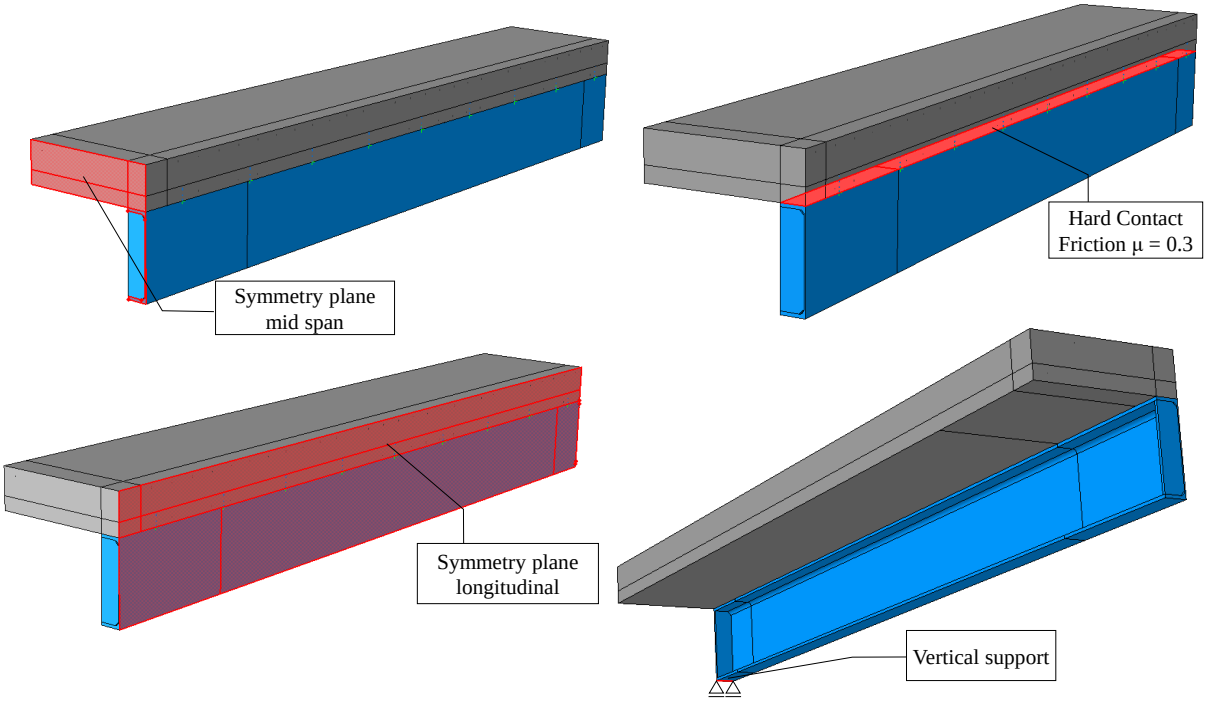

Figure 4.12: Symmetry regions of the full beam as implemented in the model

4.5 Headed Stud Shear Connectors

4.5.1 Modelling of the Headed Stud Shear Connectors

The composite action between the steel beam and the concrete chord was modelled by two springs. These springs were implemented in Abaqus with fasteners (CONN3D2) between two discrete points. The surface of origin was set on the surface of the steel section; the target surface was modelled as a surface in the concrete chord with a distance of 4 cm to the top of the steel section. The used discrete fasteners allowed the definition of an influence radius. Therefore, the fasteners could be implemented independently from the mesh of the FE model. 'Planar' fasteners were chosen, they allow for three degrees of freedom, whereas only horizontal and vertical directions were needed in the FE-model. The direction of the fasteners also stayed the same for nonlinear geometric analysis. This is according to Abaqus Users Manual [36] which states that the local coordinate system of the used fastener rotates with the global deformation of the surrounding nodes. As depicted in Figure 4.13, the load

carrying behaviour of headed stud shear connectors was therefore described by two springs: A vertical spring preventing the lift of the concrete chord, and a horizontal spring preventing the horizontal slip between steel and concrete.

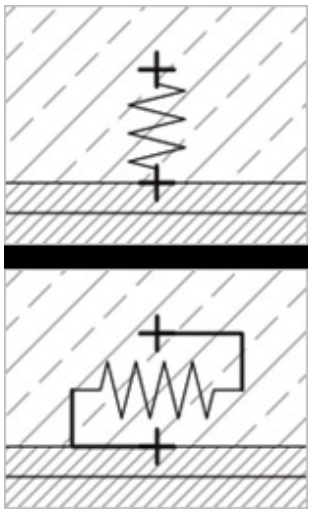

Figure 4.13: Implemented springs

4.5.2 Modelling of the Pushout Test

Similar to the full-scale fire experiments conducted at the Technical University of Braunschweig [24], headed stud shear connectors with a diameter of 25 mm and a height of 100 mm were used to perform the analysis of a push-out test. The concrete used was of the grade C40/50. For reasons of reproducibility a standard push-out test according to EN 1994-1-1, Annex B [1] was simulated. For faster calculation, only one-quarter of the standard push-out test was modelled. Figure 4.14 illustrates the modelled push-out test. A fine tetrahedral mesh was built around the headed stud to meet the stress peaks around the headed stud. The rest of the model was built with hexahedral solid elements.

Due to the concrete crushing around the bottom weld of the headed stud shear connector and the plastic behaviour of the stud itself, a high non-linearity of the model occurred. An implicit dynamic analysis with direct integration and over one thousand time steps was used to meet this non-linearity.

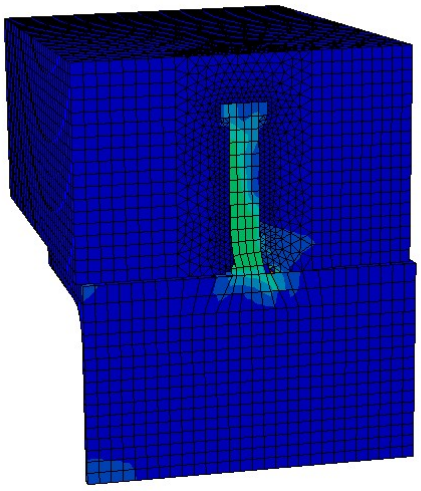

Figure 4.14: Illustration of the model used in the pushout test

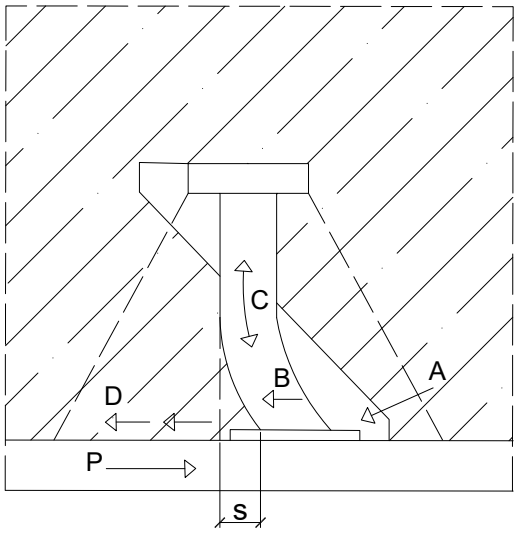

Figure 4.15: Modes of failure at ambient conditions according to [3]

4.5.3 Load-Slip Behaviour of Headed Stud Shear Connectors at Ambient Conditions

The vertical load carrying behaviour of a headed stud shear connector in a concrete slab was dominated by the tensile resistance of the stud (cf. load path C in Figure 4.15). With the high strength concrete used in the experiments and in the simulations a concrete failure is unlikely. Therefore, the linear stiffness of the shear connector on tension equals the linear tension stiffness of the headed stud c_{sc}[I], calculated from the cross section A_{sc}[II], the height h_{sc}[III] and the Young's modulus E_a of the headed stud:

$$c_{sc} = \frac{E_a * A_{sc}}{h_{sc}} \tag{4.10}$$

For the used headed stud shear connectors SD 22 x 125 mm according to [25] a stiffness of $c_{sc} = 638.6$ MN/m can be calculated.

[I] Stiffness of the headed stud shear connection on tension
[II] Cross-sectional area of headed stud shear connector
[III] Nominal height of a stud connector

Lungershausen [3] describes the tangential stiffness of headed stud shear connectors as mainly the load path A and B in Figure 4.15. Hereby, load path A describes the concrete compression strut on the weld of the headed stud shear connector, and load path B describes the shear force which is transferred in the steel stud just over the weld. With a higher concrete strength, a failure of load path B becomes more and more dominant. Becker [48] proposed the following non-linear load-slip curve for the numerical simulation of headed stud shear connectors at ambient conditions:

$$P(s) = P_{max} * \frac{12 * \frac{s}{s_y} - (\frac{s}{s_y})^{1.6}}{1 + 10 * \frac{s}{s_y}} \tag{4.11}$$

P_{max} was set to 145.8 kN for the headed stud shear connectors used in the experiments and the numerical study. s_y was set to 2.5 mm. The values were obtained in the push-out test with a similar concrete strength as used in the experiments. The load slip curve was assumed to be horizontal after a deformation of s_y to avoid numerical problems. As the minimum ductility δ_{uk} of headed stud shear connectors according to EN 1994-1-1 is 6 mm, the maximum transversal slip of the springs used in the FE model was set to 10 mm.

4.5.4 Load-Slip Behaviour of Headed Stud Shear Connectors at Elevated Temperature

The load slip behaviour of headed stud shear connectors at elevated temperatures was dominated by the non-uniform heating of the composite cross-section. As presented in Section 3.9, the temperature of the steel section and the headed stud shear connectors rose steeply with the beginning of the fire impingement, whereas the temperature of the concrete did not rise as fast. This results in a fast decay of the shear capacity of the headed stud just over the weld, named load path B in Figure 4.15. At the same time, the load carrying capacity of the compressive strut, load path A, did not decrease as much.

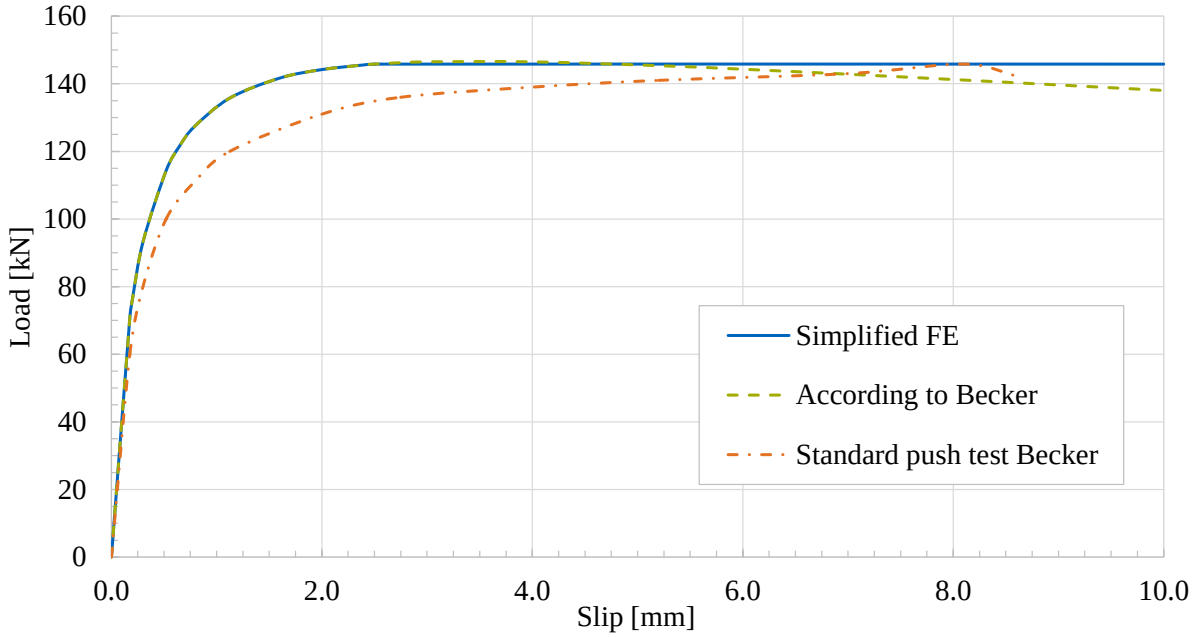

Figure 4.16: Load-slip curve of a headed stud shear connector ⊘ 22 mm according to Becker [48]

Therefore, the shear capacity of the headed stud just above the weld controlled the behaviour the shear capacity of the entire headed stud shear connector. For the numerical investigations, the load carrying capacity of the shear connectors was elaborated in two ways, which both resulted in similar values.

First, the temperature dependent equation for the load carrying capacity of headed stud shear connectors at ambient conditions of EN 1994-1-1 Paragraph 6.6.3.1 was used. For this calculation, the exact temperature of the surrounding concrete $\theta_{sc,c}$[I] and the headed stud $\theta_{sc,a}$[II] just over the weld was taken from the FE model at the positions given in Figure 4.17.

$$P_{RD,b}(\theta) = \frac{0.8 * f_u(\theta_{sc,a}) * \pi * d^2/4}{\gamma_v} \tag{4.12}$$

$$P_{RD,a}(\theta) = \frac{0.8 * f_u(\theta_{sc,c}) * \pi * d^2/4}{\gamma_v} \tag{4.13}$$

[I] Temperature of the concrete around the weld of a headed stud shear connector in fire situation
[II] Temperature of a headed stud over the weld in fire situation

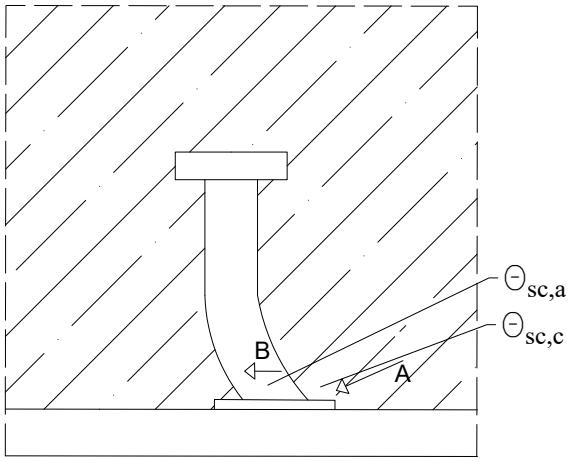

Figure 4.17: Temperature measurement points for the calculation of the load carrying capacity of headed stud shear connectors at elevated temperatures based on EN 1994-1-1

Second, a detailed FE model of a headed stud shear connector in a standard push test according to EN 1994-1-1 Annex B was built and validated against the results of push out tests at an elevated temperature out of the literature (cf. Section 4.6.2). This FE model is referred to as *Model II*.

Figure 4.18 shows the reduction factor of the considered headed studs for average steel temperatures of 20 °C, 300 °C, 500 °C and 700 °C for both calculation methods and for the experimental values of Imagawa [12]. It can be seen that there is only little reduction of the shear capacity up to a steel temperature of 500 °C. This temperature was recorded in the experiments after 12 minutes of standard fire according to ISO 834 (cf. Figure 3.17). At a steel temperature of 500 °C, the proportional limit of steel $f_{ap,\theta}$[I] according to EN 1994-1-2 is already reduced to 36 % of its initial strength f_{ap}[II].

For these simulations, it is therefore sufficient not to consider a temperature dependency of the headed stud shear connectors. With a steel temperature of over 500 °C, there is a full shear connection and the decay of the steel section dominates the behaviour of the shear connection (see *Effect III* in Chapter 6.1). Furthermore, the results of the experimental

[I] Nominal value for the proportional limit of structural steel in fire situations
[II] Nominal value for the proportional limit of structural steel at ambient conditions

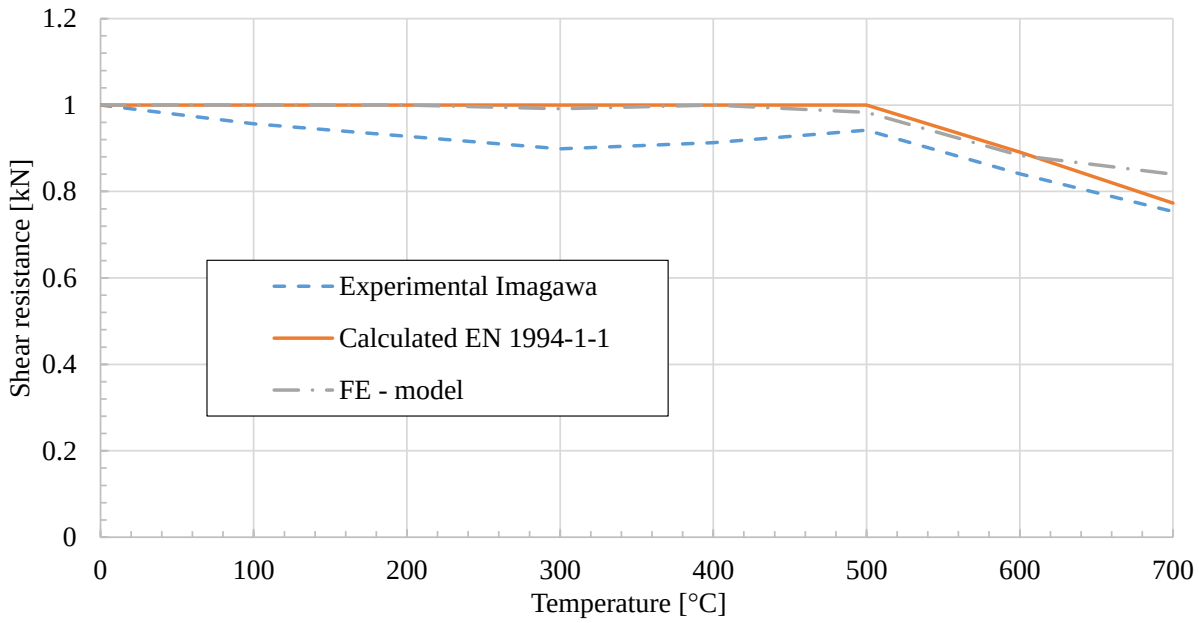

Figure 4.18: Reduction factor of the shear capacity after EN 1994-1-1, own simulations, and experiments of Imagawa [12] in relation to the temperature of the steel section

work show, that the most significant change of slip happens at the beginning of the flame impingement when the temperature of the composite joint was still at ambient conditions.

To conclude, within the scope of this simulations the behaviour of the composite joint at elevated temperatures was assumed to be similar to the behaviour at ambient conditions. As this assumption is only not met at steel temperatures of over 500 °C and with a degree of shear connection $\eta \geq 1.0$ (cf. Chapter 5.1), the margin of error is considered to be low. The results of the validation in Section 4.6 support this assumption.

4.5.5 Behaviour of Headed Studs in Deep Decking

A new design method (NL500) for the shear capacity of headed stud shear connectors was developed for this parametric study. It aims to provide more precise values for the shear capacity in case of fire (cf. [49] and [47]). The model for the shear capacity at ambient conditions as elaborated on by Nellinger [5] and the 500 °C isotherm method from Annex B of EN 1992-1-2 [34] were taken as the basis for a new model. The model presumes that the

concrete retains its full load-bearing capacity of up to 500 °C; above 500 °C the load-bearing capacity is assumed to be zero. The break-out area of the Nellinger model (cf. Figure 4.19) is reduced, but not the concrete strength.

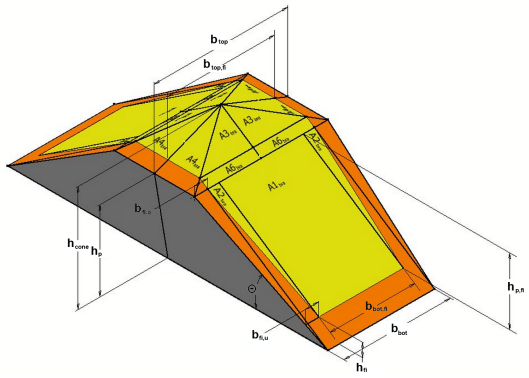

Figure 4.19: Reduced breakout area with the NL500 method, from [49]

In deep steel decking, the location of failure of the headed stud shifts from the weld of the headed stud to the transition between the concrete rib and the solid slab. Nellinger describes the load-bearing behaviour at ambient conditions. The break-out area of the concrete cone depends on the concrete strut angle, the sheet geometry and the stud height. The load-bearing capacity of cracked concrete depends on the depth of the stud's embedment in the concrete above the concrete rib. For this reason, the stud fails either with one yield hinge with a shallow stud embedment or with two yield hinges with a greater stud embedment.

With the NL500 [49] concept, a new method was created to determine the load-bearing capacity of headed stud shear connectors in a fire situation using three reduction factors. These determine the break-out area (Figure 4.19) by adapting the height of the concrete ribs, the width at the top of the cone and the width at the bottom.

The shear resistance of the stud was reduced with temperature-dependent reduction factors. Hereby the temperature was taken at the height of 10 mm over the weld of the headed stud. Equation 4.14 defines the shear capacity of a headed stud in a fire situation using the NL 500 method. The values α_{c1}[I], $f_{c,\theta}$, f_u[II], and $k_{u,\theta}$[III] correspond to the values of the EN 1994-

[I] Factor for long-term concrete strength
[II] Specified ultimate tensile strength
[III] Reduction factor for the yield strength of structural steel at elevated temperature

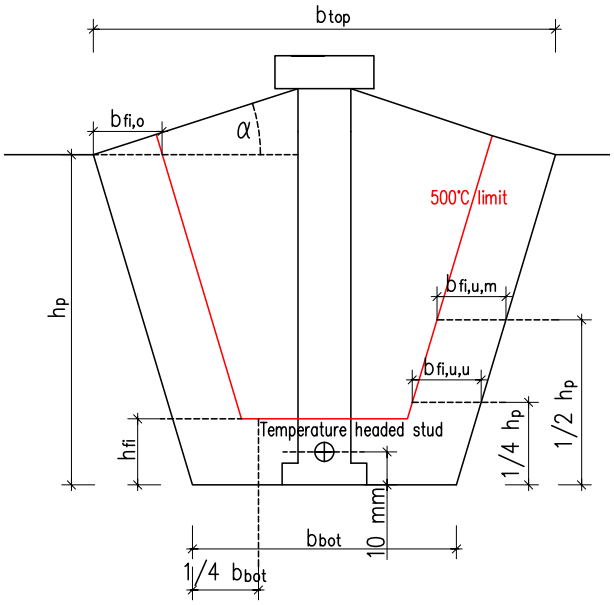

Figure 4.20: Calculation parameters of the NL500 method

1-2. The value n_y[I] relates to the number of possible yield hinges in the headed stud. $I_{y,fi}$[II] correlates to the second moment of area of the concrete cone, as used by Nellinger. h_s[III] is calculated by the height of the centroidal axis of the concrete breakout area over the steel section, as calculated in Equation 4.17. Without the temperature dependent reduction, the equation can also be used at ambient conditions.

$$P_{Rd,c,fi} = \left[\left(\frac{a_{cc} * f_{ctm}}{cos(\alpha)} + \frac{0.1 * k_{u,\theta} * f_u * \pi * \frac{d_{sc}^2}{4}}{A_{fi}} \right) * \frac{2 * I_{y,fi}}{b_{top,fi}} \right] * \frac{1}{h_p + s_2} + \frac{n_y * k_{u,\theta} * f_u * \frac{d_{sc}^3}{6}}{h_{s,fi} - \frac{d_{sc}}{2}} \tag{4.14}$$

with

$$s_2 = (h_{cone} - h_p) * \left(1 - \frac{b_{top,fi}}{b_{top}}\right) \tag{4.15}$$

[I] Number of possible yield hinges in the headed stud
[II] Second moment of area of the concrete cone
[III] Height of the centroidal axis of the concrete failure surface over the steel section according to Equation 4.17

$$A_{fi} = \sum_{i=1}^{n} A_{i,fi} \tag{4.16}$$

$$h_s = \sum_{i=1}^{n} (A_{i,fi} * h_{s,i}) / A_{fi} \tag{4.17}$$

Röß [47] compared the results of the NL500 method with experimental results of Chen [50]. Even though the first results of the comparison were promising, further validation has to be done.

4.5.6 Consideration of the Load History

With the different mechanical and thermal loads, the composite joint experienced load in two directions. At the beginning the mechanical load lead to a positive slip of the headed stud shear connectors, while with the thermal load a strong negative slip occured. Due to the non-linear load carrying behaviour of headed stud and the concrete crushing around the stud, the load path for loading is unlike the load path for unloading. The load path described in Section 4.5.3 is only true for the initial loading of the headed stud. The cyclic load carrying behaviour was already described by Gattesco [51], Wang [22], and others. For the numerical studies, a linear elastic unloading behaviour, similar to the model of Wang in Figure 4.21, was assumed. There is only little literature about the exact stiffness of the headed studs during cyclic loading. Therefore the stiffness between point A and B in Figure 4.21 was adjusted with the results of the experiments. The following equation was proposed by Tresch [52] starting from a local coordinate system.

$$P'(s) = P_{max} - \frac{s'}{(1-\alpha) * s_{max}} * P_{max} \tag{4.18}$$

with $\alpha = 4/5$, calibrated with the experiments.

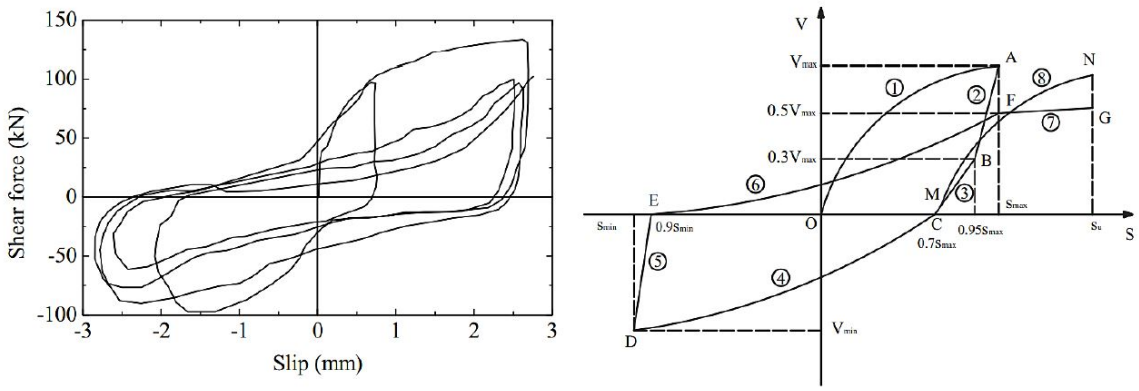

Figure 4.21: Cyclic load-slip behaviour of headed stud shear connectors, from Wang [22]

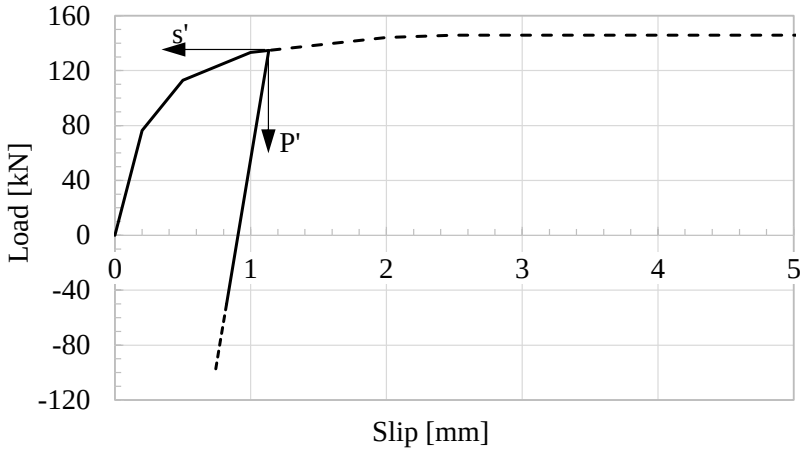

Figure 4.22: Exemplary load-slip curve with unloading starting at local coordinate system

In Abaqus the cyclic behaviour was implemented with a model for isotropic hardening. According to the Abaqus Users Guide [36] the model is defined by a linear part and a plastic part, each defined by Equation 4.19 and Equation 4.19, respectively.

$$P(s_{el}) = \frac{F_0}{s_{p1}} * s_{el} \tag{4.19}$$

$$P(s_{pl}) = F_0 + Q_{inf} * (1 - e^{-b * s_{pl}}) \tag{4.20}$$

where

s_{p1}[I] = 0.0005 m

F_0[II] + Q_{inf}[III] = P_{max}

F_0 = 0.7 * P_{max} b = 3000

Factor b is a form factor for point P2 at s_{p2}[IV] = 0.002 m. The relation between F_0 and Q_{inf} has to be adjusted depending on the used headed stud.

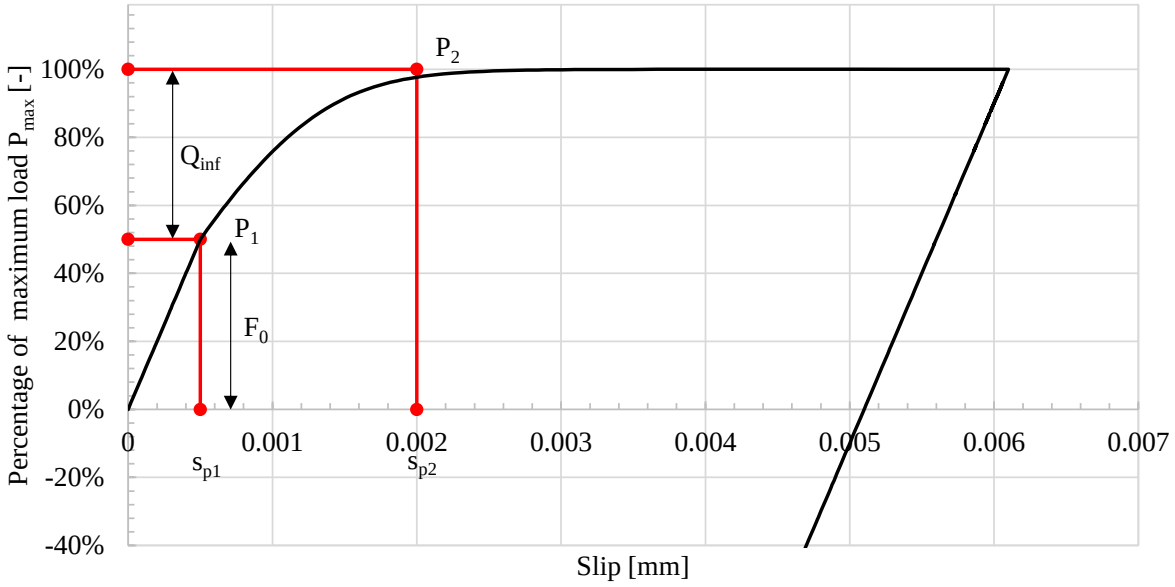

Figure 4.23: Load-slip curve of the headed stud shear connectors as implemented in Abaqus

[I] Slip of a headed stud shear connector at maximum load carrying capacity, as implemented in Abaqus, similar to s_y

[II] Load of a headed stud shear connector at end of the linear elastic load-slip path, as implemented in Abaqus

[III] Load of a headed stud shear connector between end of the linear elastic load-slip path and P_{max}, as implemented in Abaqus

[IV] Slip of a headed stud shear connector at end of the linear elastic load-slip path, as implemented in Abaqus, similar to s_0

4.6 Comparison of the Numerical Model with Experimental Data

All FE models were validated against experimental data before they were used for the parametric study. As *Model I* and *Model V* were built similarly, both were validated against the results of the full scale experiments described in Chapter 3. *Model II*, the model of the standard push test at elevated temperatures, was validated against experimental results of Imagawa [12]. *Model III* features composite beams with deep decking, and was validated against experimental results at ambient temperatures according to Nellinger [5]. The only difference between *Model IV* and *Model I* is the transient thermal calculation of the intumescent coating. Therefore, for *Model IV* only the use of the intumescent coating was first validated against the ETA[I] of the intumescent coating used, and secondly validated against experimental results of Tabeling [42].

4.6.1 Validation of Model I and V

The vertical deformation and slip over the supports of Beam 1 were calculated and compared with the experimental results for the validation of *Model I* and *Model V*. Figure 4.24 shows the recorded results for Beam 1. For more details about Beam 1, see Table 3.1 on page 34.

The graphs in Figure 4.24 illustrate the procedure of the tests and also show the temperature development of the steel beam. The temperature curves for the FE model and the experimental set-up are nearly identical. Also, there is almost no difference in the deflection at ambient temperatures. After approximately 15 minutes of exposure to ISO 834 fire, the difference of the numerical and experimental results for deflection at mid-span is approximately 2 cm. During the application of the failure load at the end of the tests, the two curves converge again. Comparing the interface slip over the supports of Beam 1 shown in Figure 4.25, there is hardly any difference between numerical and experimental results. In

[I] European Technical Approval

the beginning, there was a positive slip because of the load application at ambient temperatures. During the heating of the structure the slip decreased with constant structural load. The falling slip was mainly caused by the thermal elongation of the steel section considered as *Effect I* in Section 6.1. With the increasing load at the end of the experiment, the slip slightly increased again.

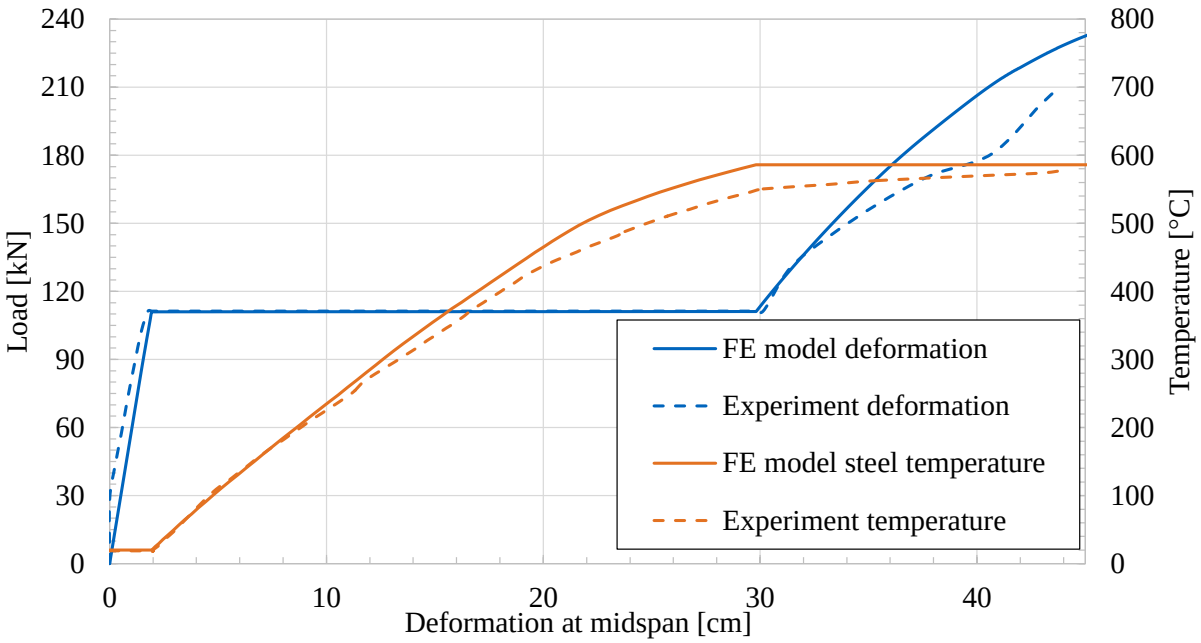

Figure 4.24: Load-deflection diagram for Beam 1

4.6.2 Validation of Model II

The standard push test of *Model II* was validated based on results of Imagawa [12] and El-Lobody [53]. Imagawa conducted push-out tests of headed studs at temperatures between 300 and 700 °C. The results of Imagawa suggest that the maximum shear resistance was only marginally affected by the heating. The size of the shear stud used in the experiments of Imagawa was similar to the shear studs used in the experiments described in Chapter 3: d_{sc}[I] = 22 mm and h_{sc} = 150 mm. The compressive strength $f_{cm,\theta}$ of the concrete was 32

[I] Diameter of headed stud shear connector

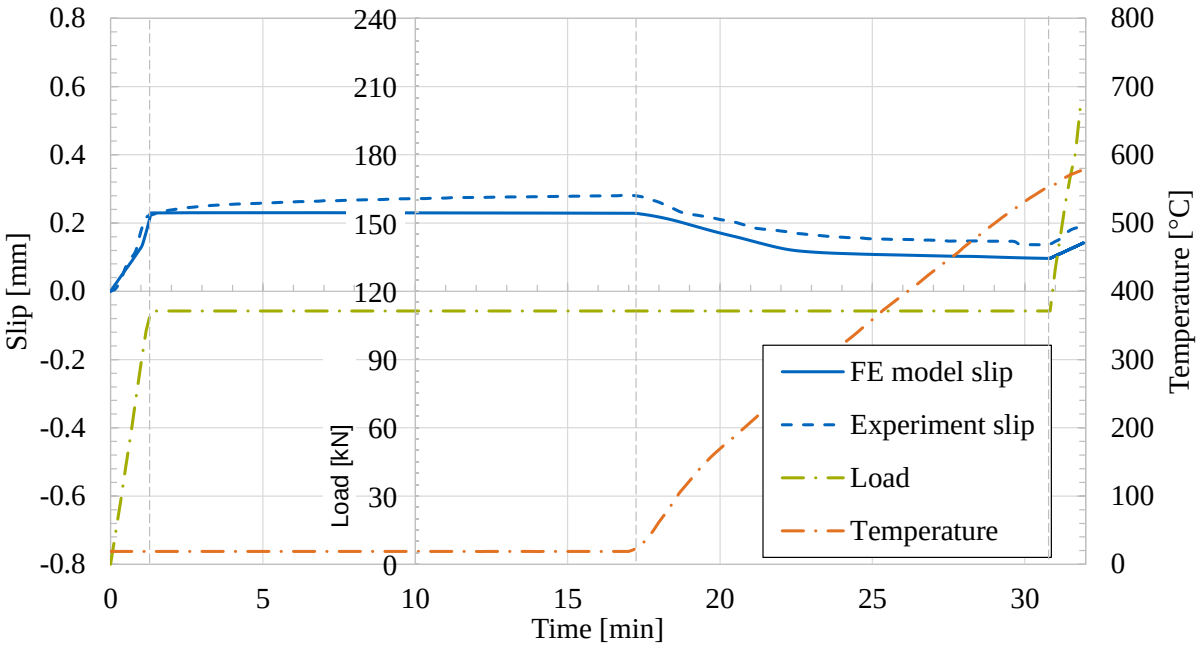

Figure 4.25: Load-deflection diagramm for Beam 1

N/mm^2, in the experiments of this study it was $f_{cm,\theta} = 50\ N/mm^2$. *Model II* was validated at temperatures of 20 °C, 300°C and 700 °C.

Figure 4.26 shows the load-slip curves of a push-out test at ambient conditions. The numerical results of this study and the the experimental results of Imagawa and El-Lobody show very similar behaviour. As the failure of the headed stud was always just over the weld of the stud, the implementation of reinforcement into the FE model did not change the load carrying behaviour of the headed stud shear connector. In Figure 4.27 the results at 300°C and 700°C are presented. Whereas at 300°C the results of the FE model and the experiment fit very well, at 700 °C the load carrying capacity is overestimated.

At ambient conditions and at 300 °C the FE model was able to depict the experiments accurately; only at a temperature of 700 °C can a deviation from the experimental values be noted. As at a steel temperature of 700°C the load carrying capacity of the steel section is already very low, this error can be accepted and the validation can be considered successful.

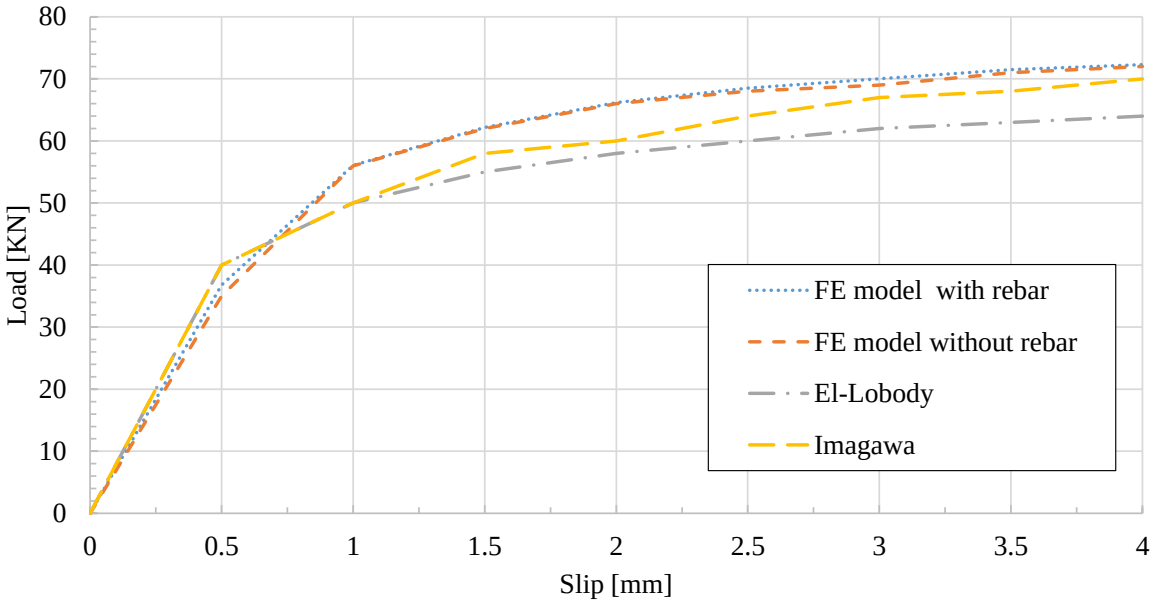

Figure 4.26: Load-displacement curves of a simulated push-out test with and without rebars at 20 °C and experimental curves of Imagawa and El-Lobody

4.6.3 Validation of Model III

The behaviour of the model of a composite beam with deep decking perpendicular to the load carrying direction was compared with the experimental results of Nellinger [5]. Nellinger conducted two composite beam tests with CF 80 decking at ambient conditions. Figure 4.28 shows the set-up of the composite beam tests. The considered beam had a degree of shear connection $\eta = 0.135$ (cf. Röß [47]). For the validation, the vertical deflection, as well as the interface slip, were compared in Figure 4.29 and Figure 4.30. Figure 4.29 shows good accordance between the computed and the measured results for the vertical deflection. Two faulty headed stud shear connectors can explain the difference in deflection in the experiment.

Figure 4.30 depicts the slip over the supports of the composite beam. Whereas the initial slip and the maximum slip of the beam are met precisely by the FE model, the plastic stiffness is first underestimated, then overestimated. As the general behaviour of the composite joint as well as the vertical deformation is described well, the FE model is considered to be valid.

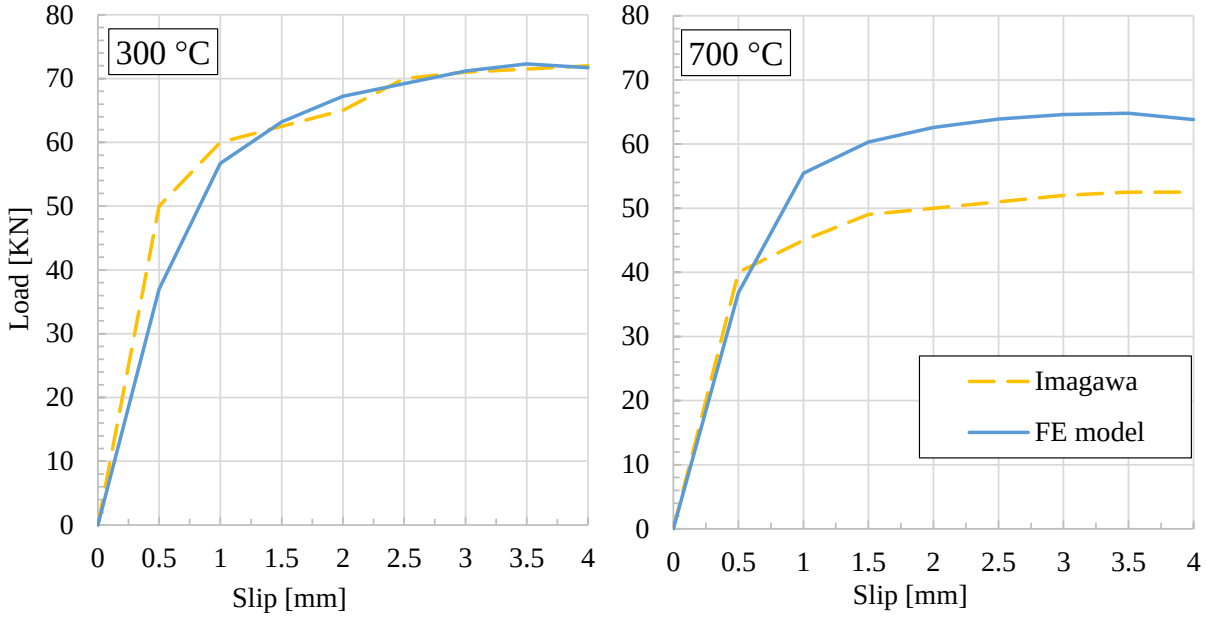

Figure 4.27: Load-displacement curves of simulated push-out tests at 300 °C and 700 °C with experimental curves of Imagawa [12]

4.6.4 Validation of Model IV

A steel sheet with a section factor of 85 m^{-1} and a coating thickness of 272 µm was modelled for the validation of the intumescent coating Sika Unitherm Platinum with its technical approval (ETA) [45]. According to the ETA, the temperature of this setup should be 450°C after 30 minutes of ISO 834 fire. Figure 4.31 shows the temperature distribution in the steel sheet and the intumescent coating. The average temperature in the steel was 449°C. Therefore it is assumed the temperature calculation with the intumescent coating is possible and the underlying assumptions are correct.

For further validation of the model, an HEB 700 profile with a coating of 674 µm and a profile factor of 83 m^{-1} was simulated. According to the ETA, the temperature after 60 minutes of ISO 834 fire should be at 500 °C. Figure 4.32 shows the calculated temperature distribution. While the temperature in the web was at over 500 °C, the temperature in the flange was lower; therefore the average temperature was at about 500 °C and the validation was successful as well.

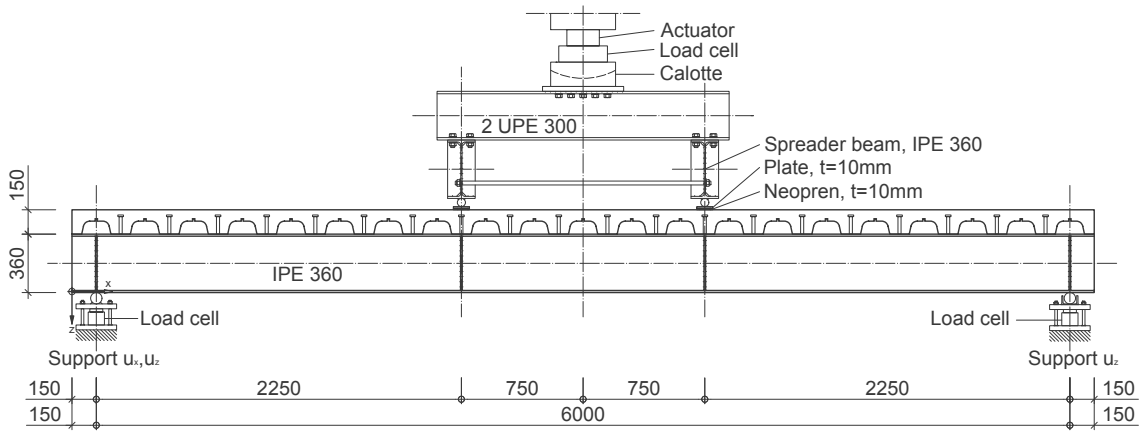

Figure 4.28: Test set-up of 6 m span composite beam tests, taken from Nellinger [5]

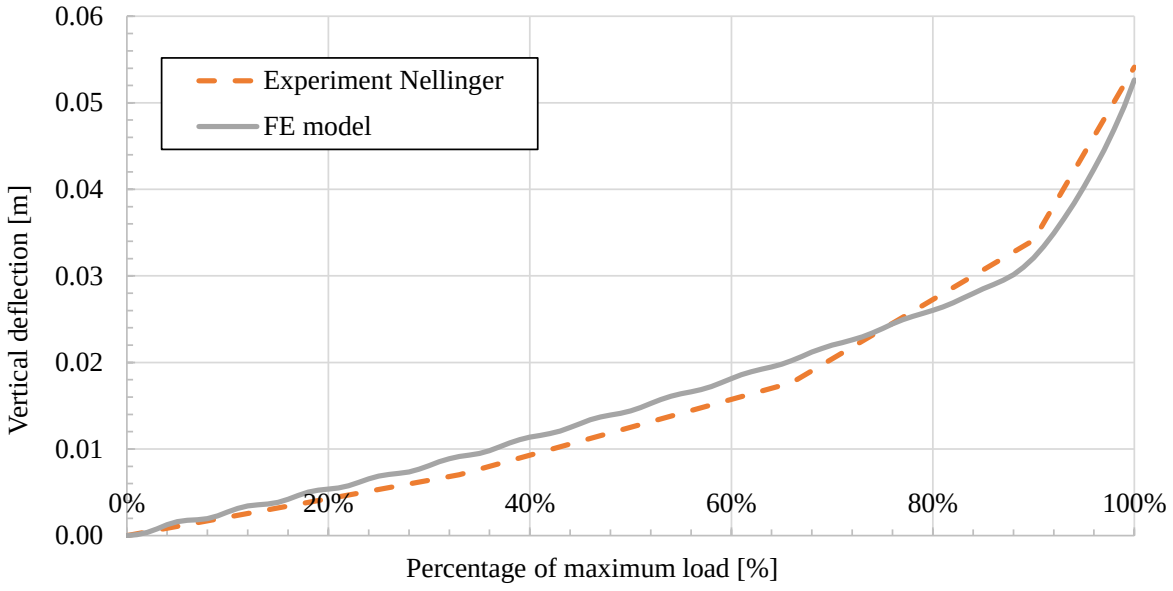

Figure 4.29: Vertical deflection of a composite beam, experimental data by Nellinger [5] and FE model

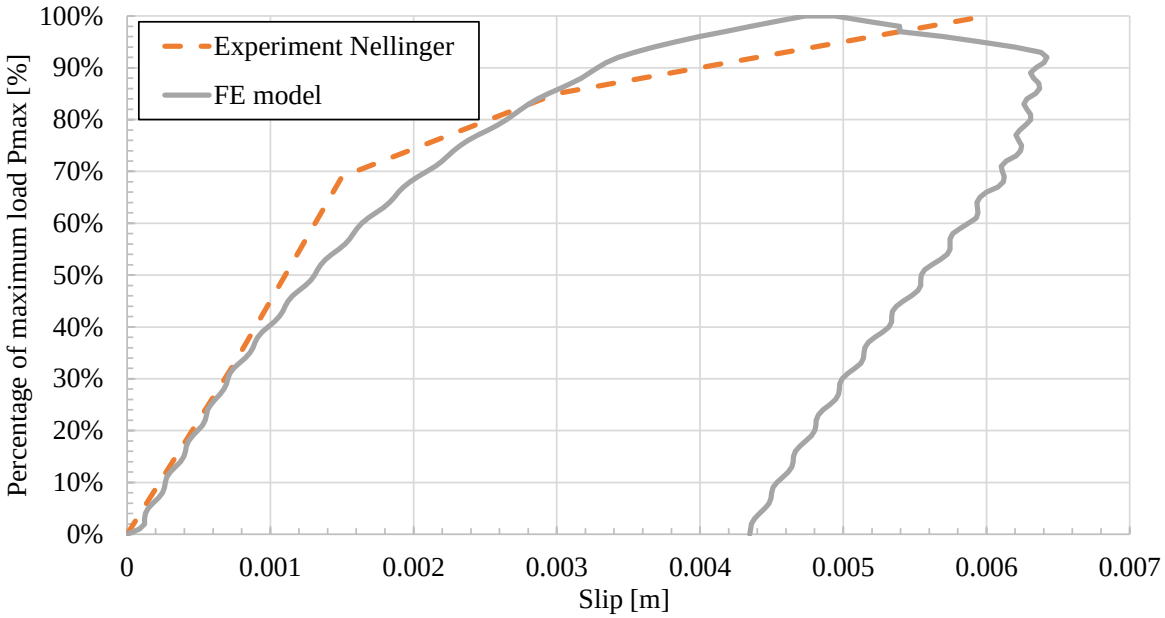

Figure 4.30: Interface slip of a composite beam, experimental data by Nellinger [5] and FE model

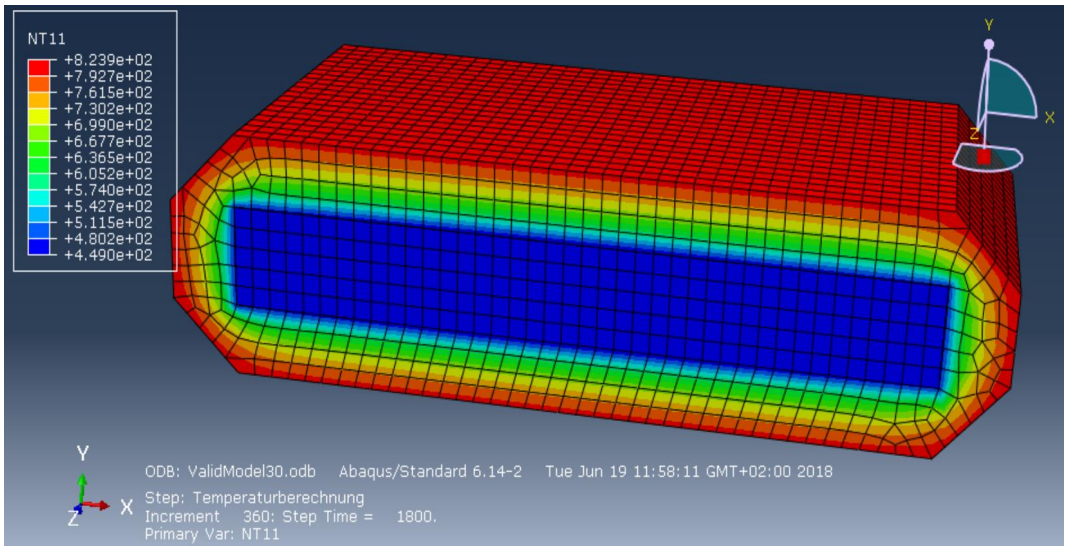

Figure 4.31: Temperature distribution in a steel sheet with 272 µm coating after 30 min ISO 834 fire

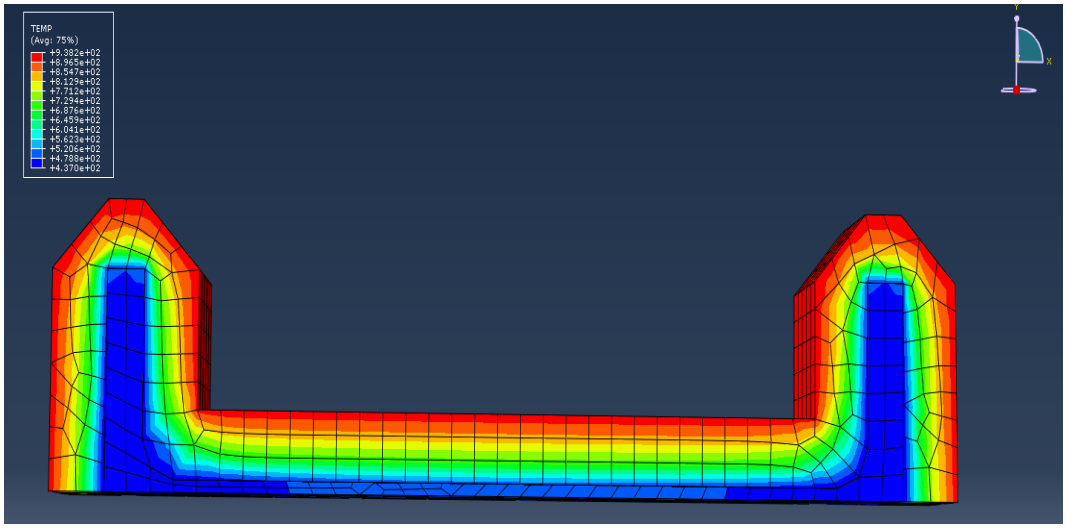

Figure 4.32: Temperature distribution in a HEB 700 profile with 674 µm coating after 60 min ISO 834 fire

4.7 Parametric Studies

4.7.1 Introduction

Within the scope of the parametric studies, the influence of the parameters listed in Table 1.1 on page 18 on the slip of the composite joint were investigated. The results of the parametric studies are presented and discussed in Chapter 6. *Model I*, *Model III*, and *Model V* were used as bases for the parametric studies. The maximum slip over the supports and the deformation at mid-span was the target value for all studies. While the parametric studies with *Model I* and *Model III* focused on the vertical deflection and the load carrying behaviour, the parametric study with *Model V* focused on the behaviour of the composite joint at elevated temperatures.

The following Table 4.3 lists the parameters investigated in each parametric study, the respective FE model used, and the target value.

Table 4.3: Parameters and target values of the parametric studies

Parametric study	**FE model**	**Parameters**	**Target value**
1	*Model I*	Degree of shear connection Span Load	Vertical deflection
2	*Model III*	Degree of shear connection Decking geometry	Vertical deflection
3	*Model V*	Degree of shear connection Span Steel grade Height concrete chord Steel profile Profile type	Slip

4.7.2 Parametric Study 1 - Preliminary Examinations

The objective of the preliminary parametric study was to investigate the influence of various parameters on the load carrying behaviour of composite beams in the fire. Furthermore,

the range of parameters of the following parametric studies was reduced by investigating the influence of the mechanical load and the thermal load on a composite beam in the fire.

The static system of the parametric study is presented in Figure 4.33.

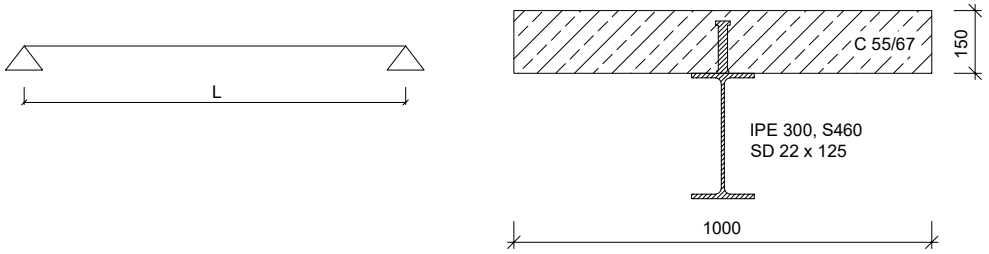

Figure 4.33: Static system and cross section of the composite beam used in Parametric Study 1

Failure criterion

A criterion of failure was defined for the numerical simulation of structures in fire. As described by Zehfuss [54], brittle failure is generally not a concern for structures built with ductile material. As the ductility of both steel and concrete rise further with elevated temperatures, the ductility of the structure also rises and further reduces the probability of brittle failure. Ryan and Robertson [55] propose a failure criterion based on the velocity of the deflection of the structure. However, the numerical simulations as presented in this chapter are independent from time. To compute a velocity, a time-dependent step control would be necessary, which would result in a long computation time and a higher complexity of the numerical model. The convergence of the numerical model cannot be taken as failure criterion, as this is a model dependent criterion [54] and it can be influenced by model dependent details like discretisation, solver, and level of itemization.

To meet the limitations of the model and the computation time, an absolute deflection was introduced as the failure criterion. As in similar experiments and simulations (Zehfuß [54], Kordina [56], and Bihina [57]) the failure criterion was set to:

$$u_{cr} = L/30 \tag{4.21}$$

with L = span of the composite beam.

Procedure of the Parametric Study

For this parametric study, the final mechanical load was put on the composite beam before the start of the flame impingement. Tab 4.4 presents the mechanical loads applied on the composite beam. The load was chosen depending on the span of the composite beam. The single load led to a degree of utilisation of $\mu_0 = 85$ % according to EN 1993-1-2 4.2.4 (3) with η=0.2. The distributed load leads to $\mu_0 = 72$ %, also with η=0.2. Despite the different μ_0, both beams failed at a similar time.

Table 4.4: Mechanical Loads

Span $[m]$	**Distributed load** $[kN/m]$	**Single load** $[kN]$
6.0	221	62.5
7.6	168	37.4
9.0	137	25.5

After the mechanical load, the thermal load was applied according to ISO 834. The temperature of the lower flange of the steel section, the vertical deflection at the mid-span and the slip over the support were monitored.

4.7.3 Parametric Study 2 - Composite Beams with Deep Decking

The objective of the parametric study with deep decking was to investigate the influence steel-concrete composite slabs with deep steel decking have on the load carrying behaviour of a composite beam in a fire situation. The load bearing behaviour of headed studs in the rips of composite slabs with deep decking can be significantly different to the load bearing

behaviour in solid slabs. Based on the work of Nellinger [5] a new method for the calculation of the shear capacity of headed studs in composite slabs was elaborated. The method is presented in Section 4.5. In Parametric Study 2, the geometry of the steel decking and the degree of shear connections were varied. The span of the beam was 9 m, the steel section was an IPE 300 and grade S460, and the concrete grade was C 55/67. Figure 4.34 shows the geometries of the modelled composite slabs. Both geometries were chosen to represent extreme decking geometries that are not covered by the recent code EN 1994-1-1. However, the geometries used in Parametric Study 2 are covered by the proposal of Nellinger [5].

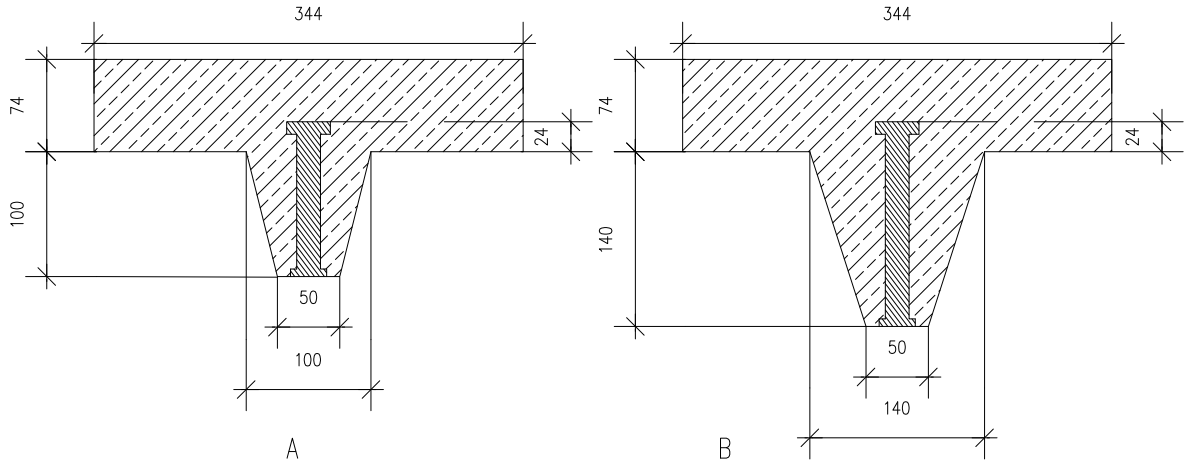

Figure 4.34: Geometry of the deep decking covered in the parametric study.
Left: Geometry A. Right: Geometry B.

Similar to the first parametric study in Section 4.7.2, the composite beam was first loaded with the full mechanical load and then loaded with a thermal load according to ISO 834. The distributed load was the same for all beams in the parametric study: 28.55 kN/m. The failure criterion of the parametric study was set to u_{cr} = L/30 with L = 9 m.

4.7.4 Parametric Study 3 - General Study on Composite Beams with Solid Slabs

The third and largest parametric study was conducted to analyse the influence of various parameters and their combinations on the maximum slip of a composite beam in a fire

situation. As discussed in Section 6.2 the maximum slip in the fire situation can be expected with no mechanical loads on the composite beam. Therefore, the parametric study was conducted only with the weight of the composite beam itself. A fire load according to ISO 834 [14] was used as the thermal load.

The parameters covered in Parametric Study 3 are listed in the following Table 4.5. To cover all possible combinations of parameters 2160 models would have been necessary. To reduce the number of models, some less important parameters were combined with the most influential ones. With this reduction a total of 875 models were built and calculated. The most influential variables that were combined with every possible combination are marked bold in the following Table 4.5. Variables that were only combined with the most influential variables are italicised.

Table 4.5: Parameters of Parametric Study 3

Parameter	**Variation**
Steel grade	**S235**, S355, S460
Beam span	6 m, 8 m, **10 m**, *14 m*
Steel section	**IPE**, HEA, HEM
Height steel section	*200 mm*, **300 mm**, *500 mm*, **600 mm**, 900 mm
Degree of shear connection	**20%**, **40%**, 70%, 100%
Thickness of concrete flange	**140 mm**, 170 mm, 200 mm

The entire simulation, from preprocessing to post-processing, was automatised. Therefore, the number of shear connectors was kept constant for all beams, and only the stiffness and the maximum load carrying of the shear connectors was changed to meet the specific requirements of the shear connection.

The slip of all shear connectors was recorded for the evaluation of the maximal slip of the composite joint in the first 30 minutes of fire exposure. For each beam the absolute maximum slip was taken as the result from all recorded values of slip. All results of Parametric Study 3 appear to be positive, even when *Effect I* led to a negative slip. As always the absolute value of slip was recorded.

In each calculation the self-weight was first imposed on the beam. After the mechanical load the thermal load was imposed for 30 minutes.

5 Investigations into the Bending Moment Resistance of Composite Beams in a Fire Situation

5.1 Development of the Degree of Shear Connection in a Fire Situation

A highly transient temperature field evolves in the composite beam during fire exposure (cf. Chapter 3). Whereas the temperature of the concrete chord stays at or only slightly above ambient conditions, the temperature of the steel section rises steeply. Figure 5.1 shows shows an example of the temperature distribution of a composite beam with an IPE 300 section and a 150 mm concrete chord on top. After 30 minutes of ISO 834 fire from the lower side, large parts of the steel section were at temperatures of over 800 °C. According to EN 1994-1-2 this reduces the steel yield strength to 5 % of its initial value. At the same time, the concrete temperature stayed at under 100 °C up to a distance of 100 mm from the top of the concrete chord. Therefore the material properties of large parts of the concrete section did not change. η rises when fewer shear connectors are needed due to the decreasing strength properties of the steel section, as the degree of shear connection η is the ratio of the number of shear connectors needed for full shear connection to the number of shear connectors provided (cf. 2.13).

Both the simulations conducted in this thesis (cf. Chapter 4.5.4) and fire experiments and calculations conducted by Imagawa [12] and El-Lobody [53] show that there is no significant decrease in the load carrying capacity of a headed stud shear connector up to a temperature of 500 °C within the steel section. However, according to the thermal material properties in

EN 1994-1-2 [2], the steel section experiences a sharp decrease in its load carrying capacity above 200 °C.

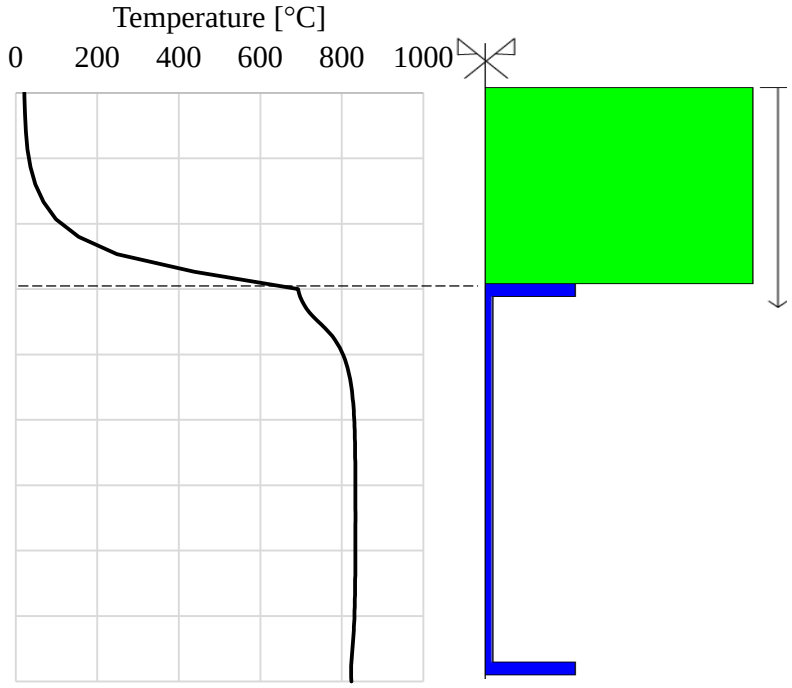

Figure 5.1: Temperature distribution in an exemplary composite beam after 30 minutes of ISO 834 fire

Figure 5.2 shows the development of the degree of shear connection η_θ[I] of a composite beam with an IPE 300 section over the first 30 minutes of fire exposure. The degree of shear connection η is 40 % at ambient conditions. After 10 minutes of fire exposure, η_θ rises to 100 %. At a degree of shear connection $\eta \geq 1$, the shear capacity of the composite joint is greater than the tensile strength of the steel section.

[I] Degree of shear connection in a fire situation

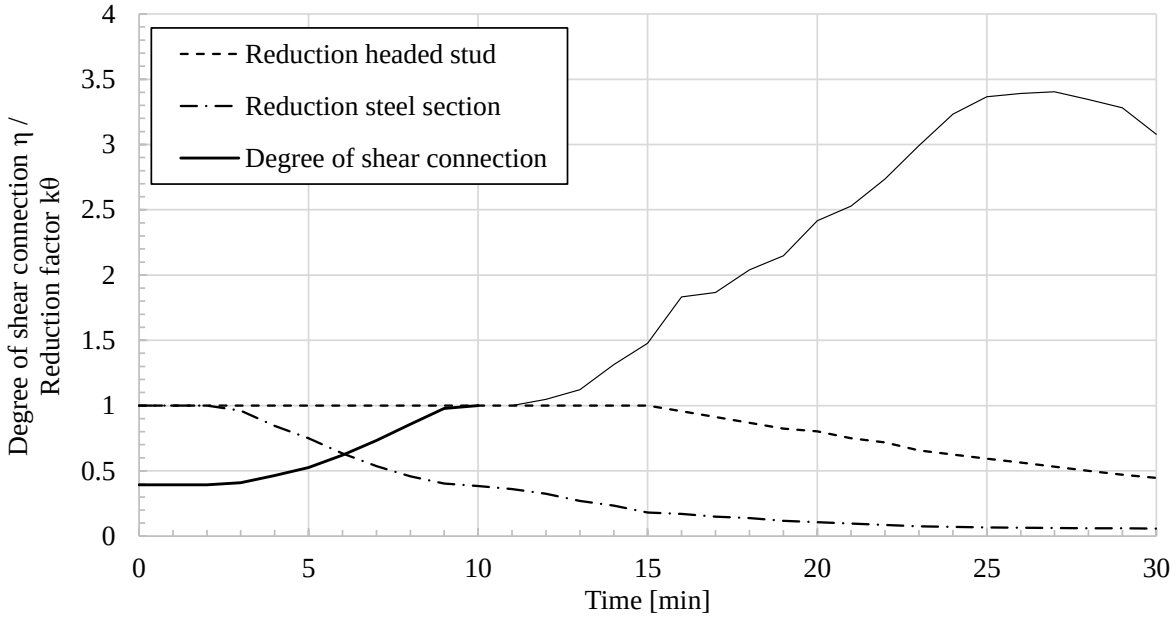

Figure 5.2: Development of the degree of shear connection as well as reduction factors of the headed stud and the steel section with fire exposure according to ISO 834

5.2 Influence of the Stiffness of the Composite Joint on the Deformation Behaviour

Based on Parametric Study 1 in Section 4.7.2, the influence of the degree of shear connection η on the deformation behaviour was investigated. Figure 5.3 and Figure 5.4 show the temperature of failure according to Section 4.7.2 of the composite beams depending on the degree of shear connection η, the span L and the load type. Due to the different μ_0, the failure of the beams with a distributed load and a single load occur at the same temperature.

Between a degree of shear connection $0.4 \leq \eta \leq 1.0$ there is only a slight difference in the critical temperature. Even at $\eta = 0.2$ the critical temperature is only slightly lower than at $\eta = 1.0$. The maximum difference in the temperature of failure between beams with full shear connection and a partial shear connection is 20 °C, or 30 seconds in ISO 834 fire. The behaviour is similar for all spans and both load types.

Figure 5.5 can explain the different deflections at the midspan and therefore the difference of the temperature of failure between η=0.2 and η=1.0. Figure 5.5 also shows the develop-

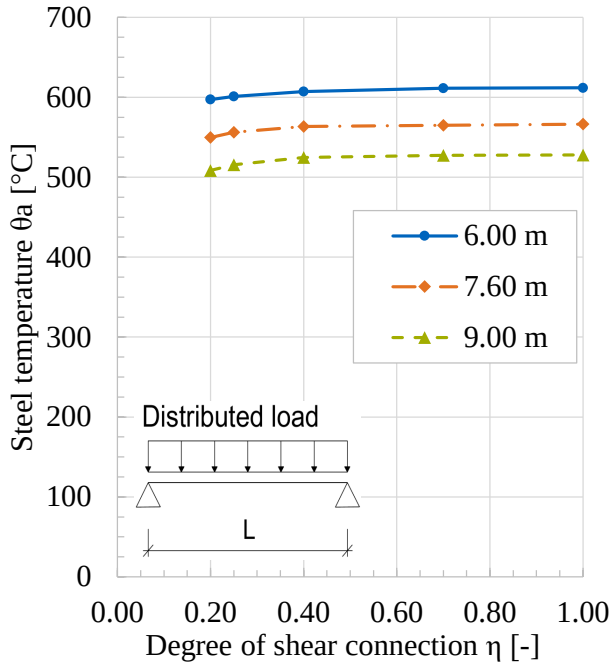

Figure 5.3: Critical temperature with distributed load

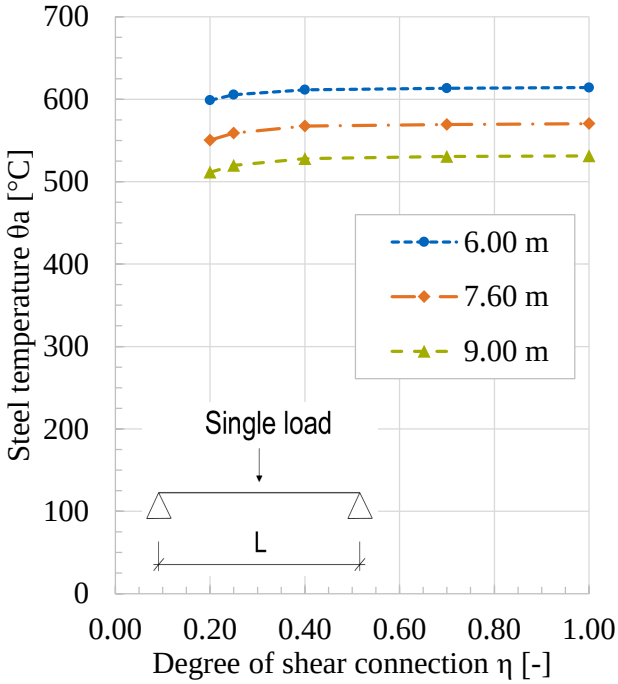

Figure 5.4: Critical temperature with single load

ment of the vertical deflection at the mid-span with rising temperatures for η=0.2, η=0.4 and η=1.0. Additionally, the difference of deflection between the different degrees of shear connection, $\delta u(20\% - 100\%)$ and $\delta u(40\% - 100\%)$ is displayed. The graphs show that the difference of deflection occurred at ambient conditions and barely changed with the rise of temperature.

The results of the parametric study imply that only for a $\eta \leq 0.20$ the deformation behaviour of a composite beam in a fire situation depends on the degree of shear connection.

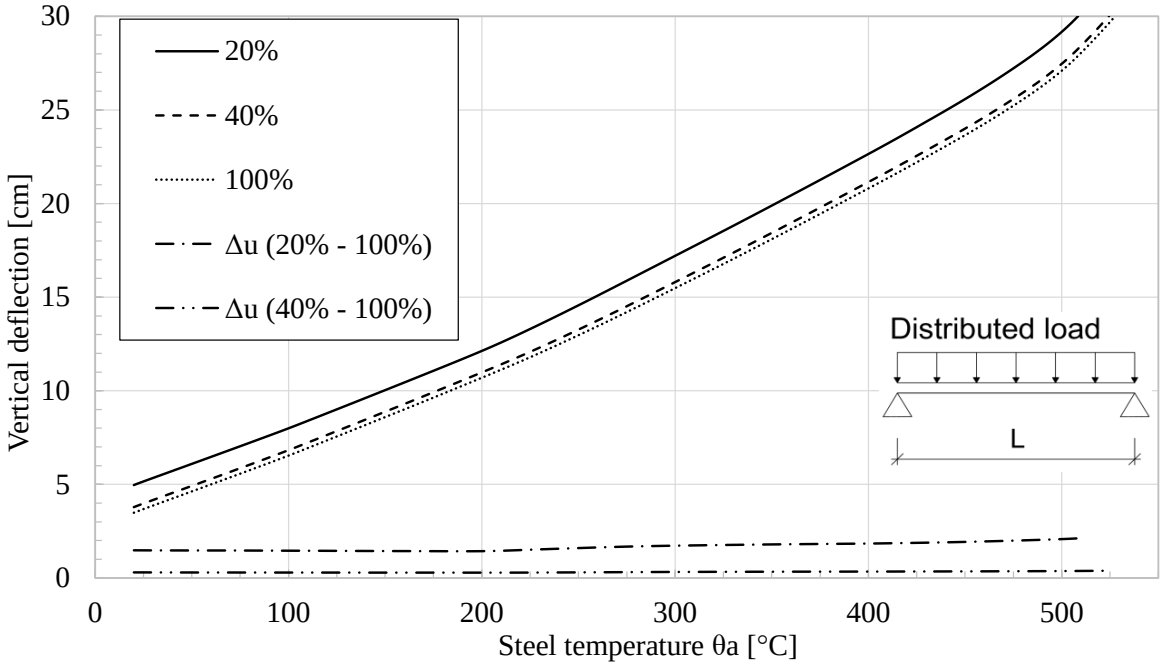

Figure 5.5: Deflection for different degrees of shear connection with L = 9 m

5.3 Influence of the Degree of Shear Connection on the Load Carrying Capacity in Fire

The influence of the degree of shear connection on the load carrying capacity has to be regarded separately for a temperature dependent degree of shear connection $\eta_\theta > 1$ and $\eta_\theta < 1$ at the time of failure. Due to the temperature distribution in a composite beam and as discussed in Section 5.1, the degree of shear connection of a composite beam in fire rises quickly over $\eta_\theta = 1.0$. An IPE 300 section with a solid slab on top and $\eta = 0.4$ at ambient conditions reaches a full shear connection after about 10 minutes of fire exposure. When a full shear connection is reached, the shear capacity of the composite joint is higher than the tensile strength of the degraded steel section. In the ultimate limit state this would lead to a failure of the steel section and not of the composite joint.

The load carrying capacity of a composite beam in fire mainly decreases due to the rising temperature in the steel section; the same rise of temperature leads to a rising degree of

shear connection η_θ. Therefore the influence of the degree of shear connection on the load carrying capacity depends on when the beam fails.

If the beam fails with $\eta_\theta < 1$, there is a significant influence of the degree of shear connection on the load carrying capacity and the degree of shear connection at elevated temperatures η_θ has to be used for the calculation of the ultimate load carrying capacity. If the beam fails with $\eta_\theta > 1$ there is no more influence of the degree of shear connection on the load carrying capacity and the ultimate load carrying capacity can be calculated with a full degree of shear connection.

Both the decay of the load carrying capacity of the composite beam and the increase of the degree of shear connection are dependent on the same variable, the tensile strength of the steel section. The only way to influence the moment of failure with a given degree of shear connection is to influence the degree of utilisation μ_0 of the composite beam. The lower the degree of utilisation at ambient conditions, the longer the beam will maintain integrity in a fire situation before failing.

Hereby η_θ can be calculated as follows:

$$\eta_\theta = \frac{n * min(k_{sc,\theta}; k_{c,\theta})}{n_f * k_{a,\theta}} \tag{5.1}$$

with

$$k_{a,\theta} = k_{y,\theta a} \tag{5.2}$$

$$k_{sc,\theta} = k_{y,\theta v} \tag{5.3}$$

$$k_{c,\theta} = k_{c,\theta c} \tag{5.4}$$

and

θ_a = average temperature of the steel section

θ_v[I] = 0.8 * θ_a

θ_c[II] = 0.4 * θ_a

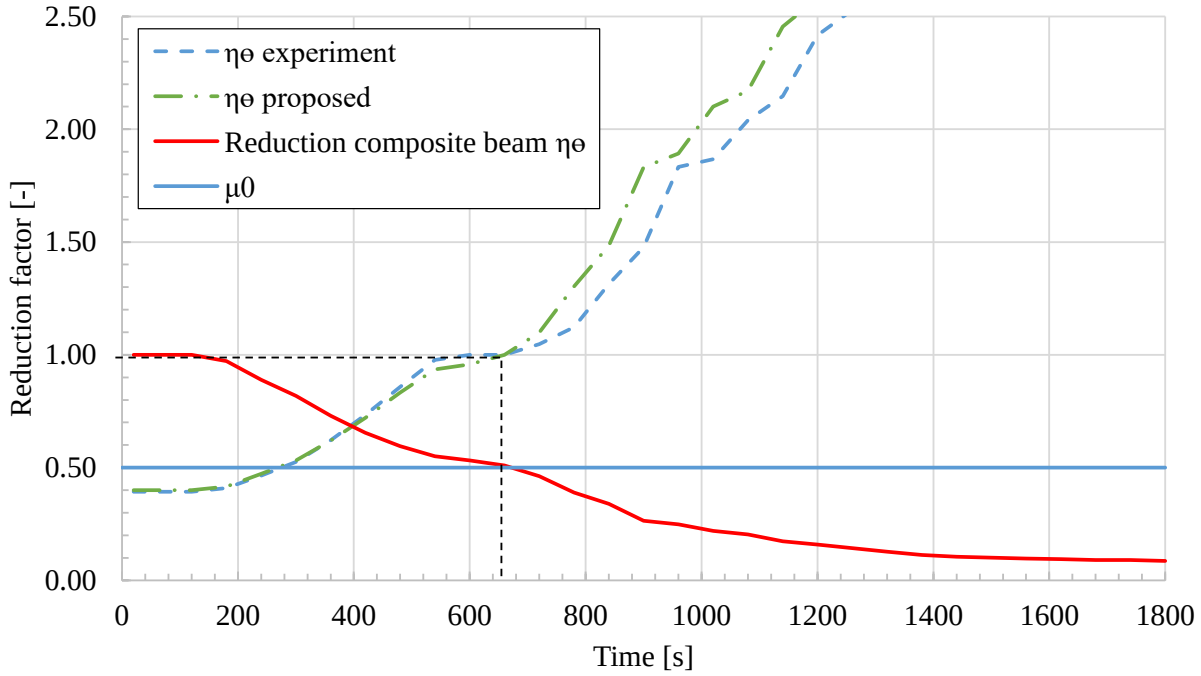

Figure 5.6: Development of the degree of shear connection and the plastic bending resistance of a composite beam in a fire, IPE 300, S 460, 15 cm concrete chord, C40/50

Figure 5.6 shows the development of the degree of shear connection and the reduction factor of the bending resistance of a composite beam in a fire. For the degree of shear connection two calculation methods were used. First it was calculated according to Equation 5.1, and second it was calculated according to measured data in Experiment 1. In both cases, the steel temperature measured in the experiments was used. For reasons of illustration a degree of utilisation $\mu_0 = 0.5$ is also displayed in Figure 5.6. The relevant degree of shear connection is at the point at which the reduction factor of the bending resistance meets μ_0. In this case, with $\mu_0 = 0.5$ and $\eta = 0.4$ at ambient conditions, this would lead to $\eta_\theta = 1.0$ at the point of failure.

[I] Temperature of the stud connector according to EN 1994-1-2 4.3.4.2.5 (2)
[II] Temperature of the concrete according to EN 1994-1-2 4.3.4.2.5 (2)

The development of η_θ and the bending resistance M_{fi,Rd^+}[I] at elevated temperatures are directly proportional to each other as both depend on the reduction of the steel section. In theory, the degradation with the elevated temperatures of the concrete also plays a roll in the calculation of M_{fi,Rd^+} and η_θ. In practice, this influence is small and only comes into action at $\eta_\theta > 1$.

$$M_{fi,Rd^+} \propto \eta_\theta \tag{5.5}$$

Therefore the relation between η_θ and M_{fi,Rd^+} does not depend on the time of failure of a beam in the fire, but only on the degree of shear connection at ambient conditions η and on the location of the plastic neutral axis in the composite beam. Finally, there are two dominant ways to influence η_θ at the time of failure: With the degree of shear connection at ambient conditions η or with the degree of utilisation μ_0.

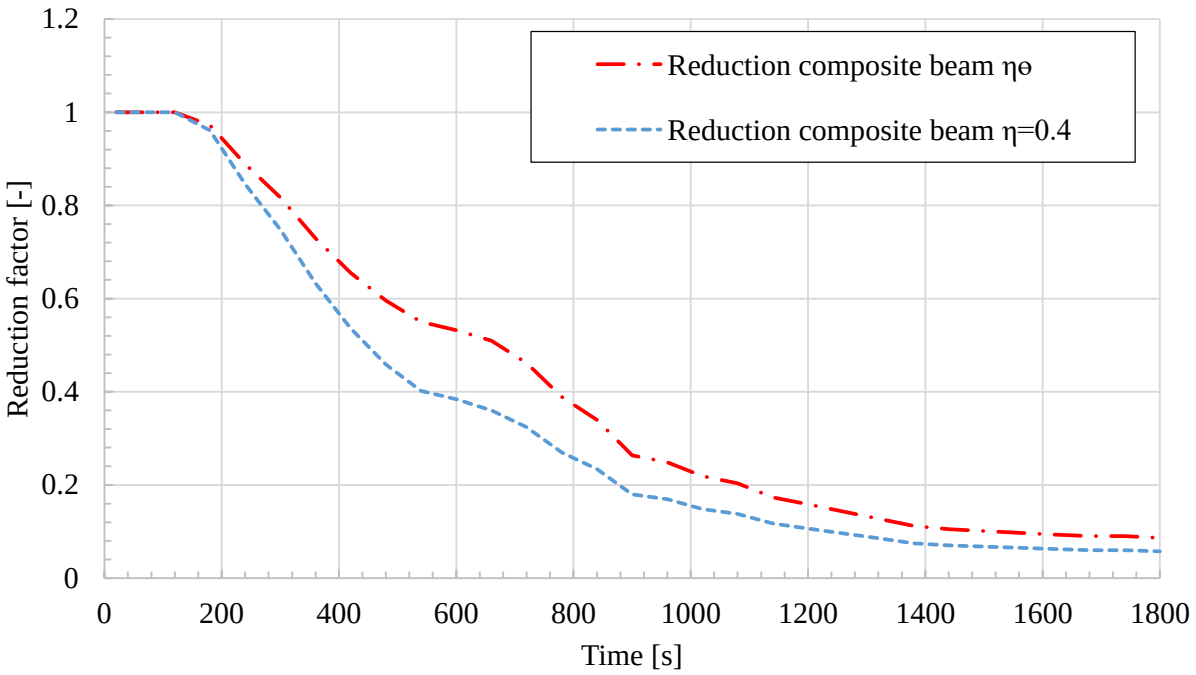

Figure 5.7: Comparison of the reduction of the plastic bending resistance of a composite beam in fire, calculated with a constant η and η_θ. Bending moment calculated for: IPE 300, S 460, 15 cm concrete chord, C40/50, $\eta = 0.4$

[I] Design value of the sagging moment resistance in the fire situation

For the structural design in fire situations, a combination of actions for accidental design situations can be calculated according to EN 1990 [58]. Generally, this leads to a low degree of utilisation for structures in fire and therefore possibly to a high η_θ.

As a conservative approach, the bending resistance of a composite beam in the fire can always be calculated with the lower η and at ambient conditions. The lower η leads to a lower bending resistance of the composite beam. Figure 5.7 shows the comparison between the bending resistance calculated with a constant η and the temperature dependent η_θ. Whereas the course of the reduction of the bending resistance with constant η follows the temperature dependent reduction of the steel section $k_{a,\theta}$[I], the reduction of the composite beam with temperature dependent η_θ is higher due to the rising degree of shear connection.

Figure 5.8 and Figure 5.9 display the development of the degree of shear connection and the plastic bending resistance of composite beams with an HEB 300 and an HEB 600 steel section. Even though the plastic neutral axis, the heating behaviour, and the time of failure of both composite beams are quite different to the composite beam with the IPE 300 steel section, the degree of shear connection at failure, marked with the dashed line in Figure 5.8 , is still around 1.0.

If the degree of utilisation μ_0 were to be changed from $\mu_0 = 0.5$ to $\mu_0 = 0.4$, the temperature dependent η_θ would be well above 1.0 in all cases.

In Figure 5.9 and Figure 5.7 the comparison of the bending resistance calculated with a constant η and a temperature dependent η_θ is shown. For the composite beam with the IPE 300 in Figure 5.7 the difference is quite large, whereas for the composite beam with the HEB 600 in Figure 5.9 Right the difference is quite low. In all cases using a non-temperature dependent η results in a lower bending resistance and can therefore be considered a conservative approach.

[I] Reduction factor of the steel section in a fire situation

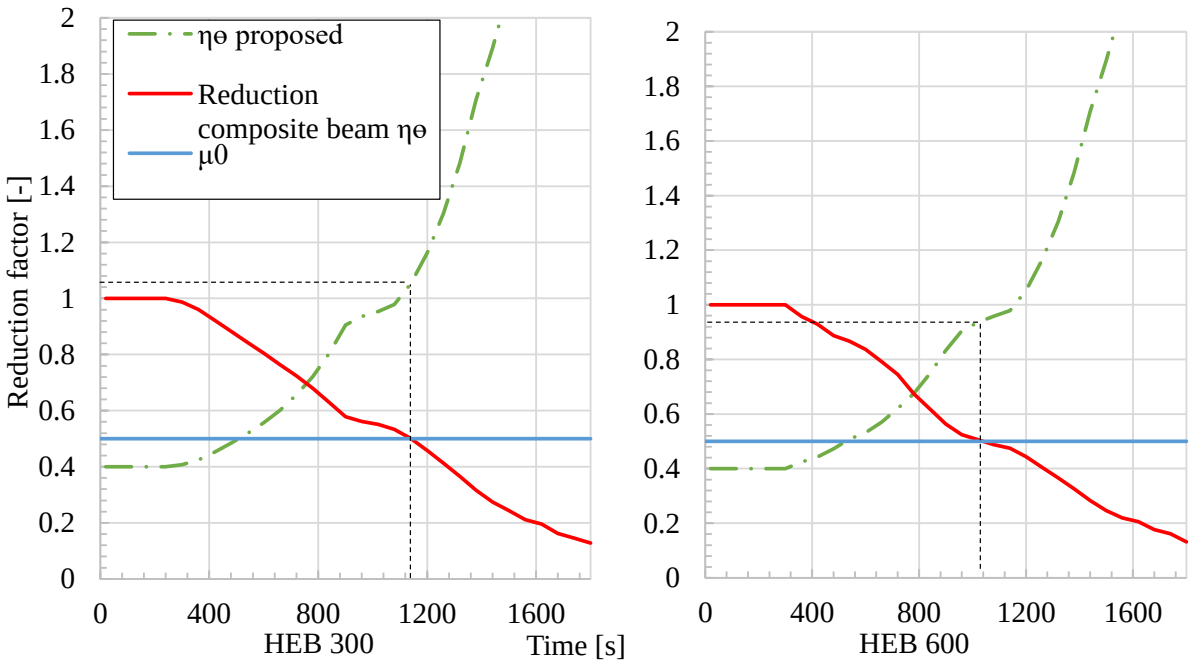

Figure 5.8: Development of the degree of shear connection and the plastic bending resistance of a composite beam in fire. Left: HEB 300, Right: HEB 600. Both S 460, 15 cm concrete chord, C40/50, $\eta = 0.4$

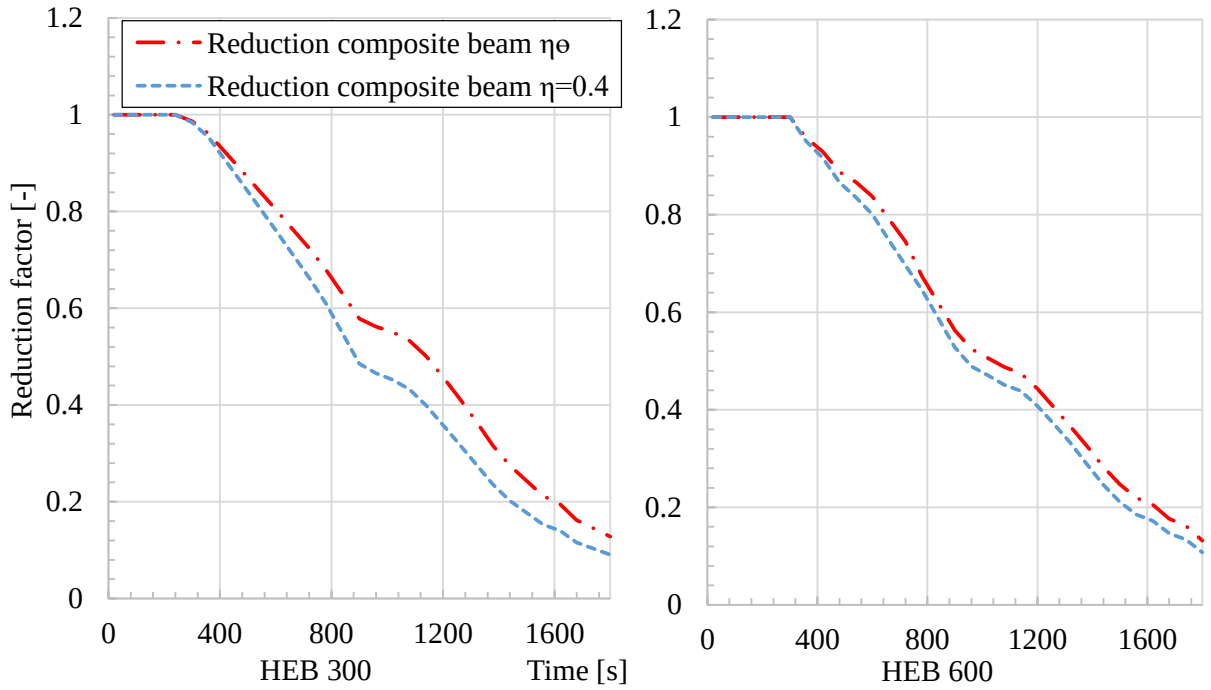

Figure 5.9: Comparison of the reduction of the plastic bending resistance of a composite beam in fire, calculated with a constant η and η_θ. Left: HEB 300, Right: HEB 600. Both S 460, 15 cm concrete chord, C40/50, $\eta = 0.4$

6 Investigations of the Slip in the Composite Joint

6.1 Effects of Elevated Temperatures on the Composite Joint

Three major effects dominate the interface slip in the composite joint between a steel section and a concrete slab in the event of a fire.

1. Negative slip due to thermal elongation of the steel section
2. Positive slip due to the high thermal gradient in the composite beam resulting in bending (thermal curvature)
3. Positive slip due to mechanical load resulting in bending

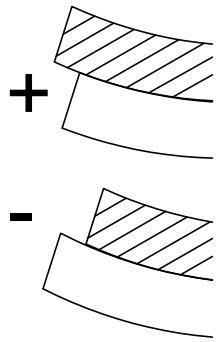

Figure 6.1: Definition of positive and negative slip

6.1.1 Effect I - Thermal Elongation of the Steel Section

The rising steel temperature in the steel section and the concrete slab due to the fire exposure yields high thermal strain. Due to the non-uniform heating, this strain results not only in an elongation of the composite section but also in bending.

As the steel temperature rises much faster than the concrete temperature (see experimental results in Chapter 3.9.1), the steel section becomes longer than the concrete chord. The different thermal elongations of the steel section and the concrete chord lead to negative slip. The impact of this effect increases due to the relatively homogeneous temperature distribution in the steel section. The increase of slip mainly leads to a change in length and only little bending. This negative slip is summarised in *Effect I* (s_I).

Figure 8.7 on page 134 illustrates the impact of this effect with the recorded slip of Beam 7. As the mechanical loads were stopped at minute 33, the vertical displacement and hence the bending both stopped. As the temperature kept rising, *Effect I* led to a steep increase in the slip between minutes 33 and 40.

6.1.2 Effect II - Thermal Curvature of the Composite Beam

Similarly to *Effect I*, *Effect II* also results from the high temperature gradient in the composite beam. The fire facing site of the beam experiences a large rise in temperature, whereas the unexposed side of the concrete slab stays nearly at ambient temperature (cf. Figure 3.18). The high temperature gradient leads to high thermal strain at the fire-exposed side and nearly no thermal strains on the unexposed side of the slab. This predominantly results in a thermal curvature and only a small change in total length. Also, the high temperature changes in the steel section are in contrast to the ambient temperature in the concrete. This positive slip due to the high thermal gradient is named *Effect II* (s_{II}).

Figure 3.24 on page 56 demonstrates the vertical deformation due to the thermal gradient in the composite beam which leads to *Effect II*. The deflection rose by 54 mm at the temperature rose from 20 °C to 100 °C. As the mechanical load did not change during this period, nor did the material properties provoke a change in stiffness of the composite beam, the only explanation that could provoke this deformation is the curvature due to the thermal gradient in the composite beam, namely *Effect II*.

The magnitude of *Effect II* can be controlled by the height of the steel section as well as the inner lever of the composite beam. The change in length of the steel section due to the rising temperature (*Effect I*) is independent of the height of the composite beam. This is in contrast to the resulting rotation α in Figure 6.2, and therefore the deflection, which leads to *Effect II*. The rotation α is set by the height of the lever e from the centre of gravity of the steel section to the point of rotation, which is assumed to be the upper end of the concrete section. Therefore, α and thus *Effect II* is controlled by the heights of both the concrete and the steel section.

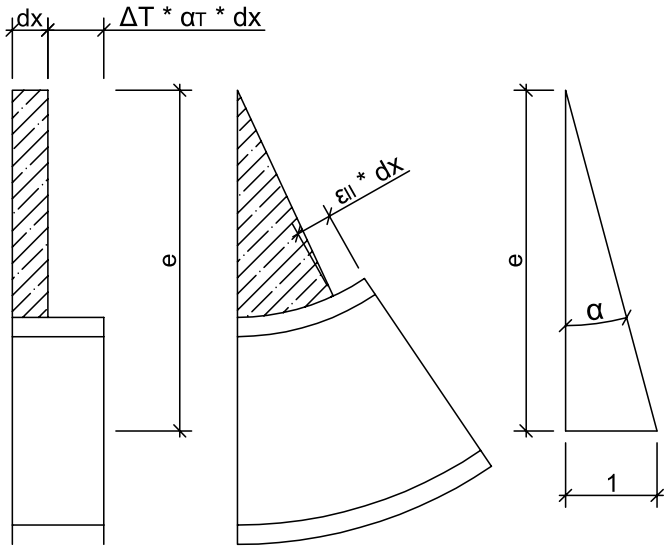

Figure 6.2: Deformation of the composite beam due to the thermal elongation of the steel section. Left: free deformation, Middle: curvature due to bending

6.1.3 Effect III - Bending to Decreasing Stiffness

The third dominating influence on the interface slip is due to the increasing temperatures in the components and therefore the decreasing stiffness of the materials. With decreasing stiffness and constant mechanical load, the vertical deflection increases. The vertical deflection, similar to *Effect II*, leads to an increase in the slip. This positive slip due to the decreasing stiffness is named *Effect III* (s_{III}).

A separate examination of these three effects is provided in Section 6.1.6.

6.1.4 Separate Numerical Examination of the Effects on the Composite Joint

6.1.5 Modelling of the Separate Examination

The effects of the elevated temperature on the composite joint can be reproduced separately. Different mechanical load combinations, material properties, and support conditions have to be applied in the FE model described in Chapter 4. Table 6.1 lists these boundary conditions. Due to the thermally-induced behaviour, *Effect II* cannot be reproduced separately from *Effect I*. Therefore, *Effect II* is simulated together with *Effect I*, and then *Effect I* is subtracted to calculate the result of *Effect II* alone (cf. 6.1).

$$\textit{Effect II} = \textit{Effect I+II} - \textit{Effect I} \tag{6.1}$$

Table 6.1: Boundary conditions for separate consideration of the effects of the composite joint

Effect	**Mechanical load**	**Thermal strain**[1]	**Shear connectors**[2]	**Support**[3]
I	$q_{ed} = g_{ed} = 0$	According to EC4	linear unloading	$w_z = 0$
I + II	$q_{ed} = g_{ed} = 0$	According to EC4	nonlinear unloading	regular
III	25.5 kN/m	$\Delta l/L = 0$	nonlinear unloading	regular

(1) *Thermal strain* describes the thermal elongation of the simulated materials with rising temperatures. 'According to EC4' implies the usage of the material properties according to EN 1994-1-2 [2]. $\Delta l/L = 0$ implies the theoretical approach of no thermal elongation of the materials with rising temperatures.

(2) *Shear connectors* describes the shear behaviour of the springs used in the FE model. For loading, a nonlinear plastic spring characteristic (Equation 4.11) according to Becker

[48] was used, while for unloading, a stiff but linear spring (Equation 4.18) was chosen (see Section 4.5.1).

(3) *Support* describes the way the composite beam is supported. 'Regular' implies a statically determined support of the beam. '$w(z) = 0$' implies a continuous vertical support of the composite beam. The calculation of *Effect I* mainly depends on the support conditions of the beam. A continuous vertical support and an additional horizontal support of the concrete slab at both ends of the composite beam is necessary. The vertical support ensures that the horizontal strain only leads to a change in length of the section, not to a curvature. A horizontal support at both ends of the concrete slab ensures that the concrete section is not loaded with tensile forces and therefore does not change its material behaviour. For this calculation, it is assumed that in case of fire, the concrete slab is always at least partly under pressure. Section 6.2 shows that this assumption is only valid with a mechanical load on the composite beam.

6.1.6 Results of the Separate Examination

Effect III

Figure 6.3 illustrates the slip due to *Effect III*. The first rise in the slip was due to the initial loading of the composite section. After the mechanical load, the ISO 834 fire load was applied. The rising temperature of the steel section mainly led to a falling stiffness of the composite beam and therefore a rising deflection. At a steel temperature of about 480 °C an increasing non-linearity was observed. The stiffness of the steel section experienced a strong decrease at this temperature. To illustrate the impact of the rising temperature on *Effect III*, the slip was also calculated without the degradation of the material properties, named 'Effect III without reduction'. The difference between 'Effect III' and 'Effect III without reduction' was the slip caused by rising temperatures or rather the reduction in the material properties.

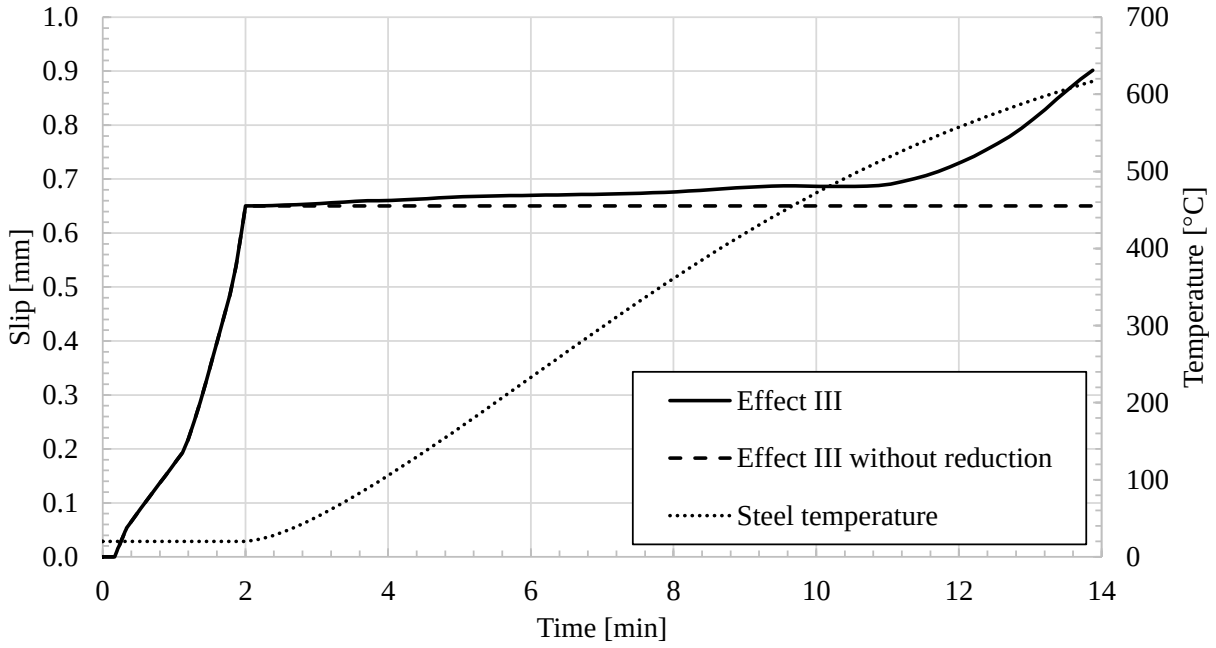

Figure 6.3: Horizontal slip in the composite joint over the support, due to *Effect III* by mechanical and thermal load

Effect I

Effect I describes the change of length in the steel section due to rising temperatures. This effect is massively influenced by the stiffness of the headed stud shear connectors. Therefore, it is of utmost importance to consider the different loading and unloading paths of the headed stud shear connectors (cf. Section 4.5.1). In most situations, the shear connectors are first loaded by the mechanical load in a positive direction. Only with rising temperatures, can negative slip occur. Therefore, the shear connectors have an elastic-plastic load path during loading. For unloading, a comparatively stiff elastic reaction can be expected. If the stiffness of the shear connectors is not adjusted to the stiff unloading path, a slip of over 10 mm at 600 °C was calculated. Thus, *Effect I* has to be seen in combination with the other effects, if not, it is highly overestimated.

Figure 6.4 shows the horizontal slip due to *Effect I*, the combined *Effect I + II*, and *Effect II* calculated with Equation 6.1. The negative slip due to *Effect I* started immediately after the start of the flame impingement and fell steadily with rising temperatures. The rising

temperature of the steel section, and thus the falling compressive strength of it, led to a lower change of slip at higher temperatures. As the steel section was loosing its compressive strength, fewer forces were introduced into the shear connection.

As for the falling compressive strength of the steel section, a failure of the composite joint is only possible at the beginning of the flame impingement (cf. Section 5.1).

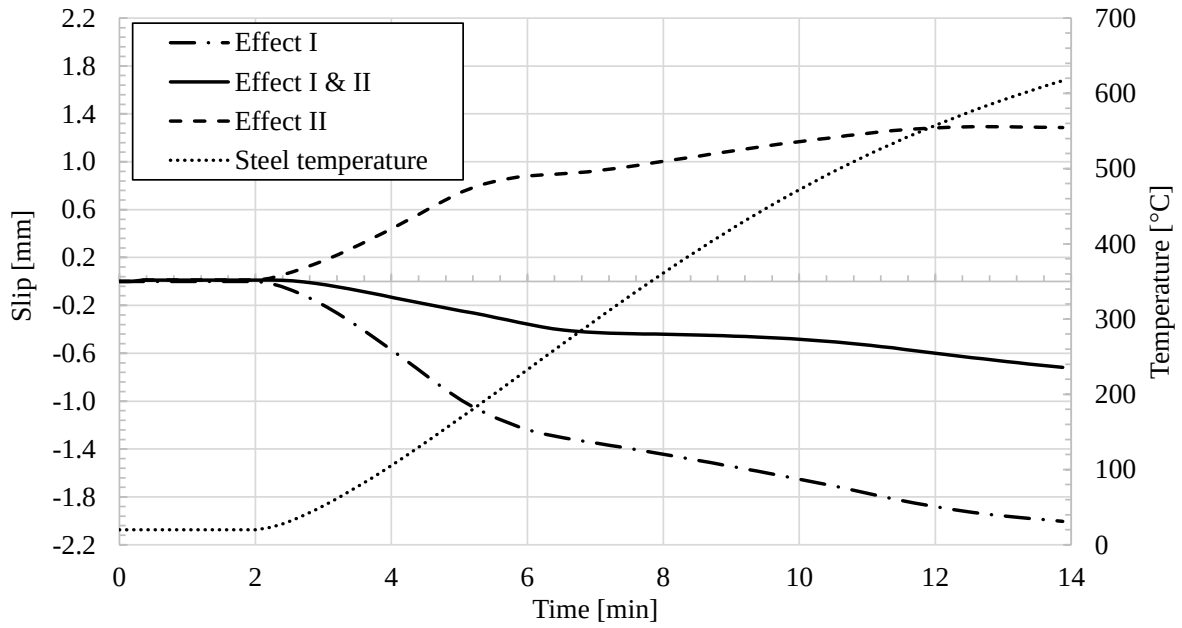

Figure 6.4: Slip due to *Effect I*, *Effect I + II*, and *Effect II*

Effect II

Effect II, slip due to the thermal curvature of the composite beam, causes a positive slip, countervailing the slip due to *Effect I*. Figure 6.4 displays the calculated slip due to *Effect II*. The thermal gradient in a composite beam in fire caused a deflection directly after the beginning of the flame impingement. As a result of this, the maximum influence of *Effect II* was also right at the beginning of the flame impingement. In this exemplary beam, the slip due to *Effect II* did not grow any more after 12 minutes of ISO 834 fire. The time at which *Effect II* has no influence any more correlates to the strong growth of slip due to *Effect III*

shortly before minute 12 in Figure 6.3. It is assumed that the high loss of stiffness of the steel section prevents further slip due to *Effect II*.

6.1.7 Validation of the Separate Calculation

To validate the separate examination of the three effects inside the composite joint, the effects were summarised and compared to the slip of the full validated model presented in Section 4.6. Figure 6.5 illustrates the sum of the three separate effects, and the validated slip of Section 4.6. Up to steel temperatures of just below 600 °C, the separate effects were reproduced precisely. The rising aberrations at steel temperatures of over 600 °C could be explained with the increasing non-linearity of the material properties, which have an impact on the slip. Especially the high non-linearity of *Effect III* (cf. Figure 6.3) prevented a successful superposition of the effects. It can be observed that up to a steel temperature of 600 °C, the separate examination of the three effects was possible and the assumption of the boundary conditions were right. Whereas *Effect II* and *III* led to a rising slip, the thermal elongation of the steel section *Effect I* led to a falling slip. Due to *Effect I*, the longitudinal shear forces inside the composite joint of a composite beam in a fire were gradually unloaded. The highest (positive) slip in the composite joint occurred with the initial mechanical loading. The lowest (negative) slip occurred with rising temperatures due to *Effect I*, just before the slip due to the rising deflection of *Effect III* became dominant.

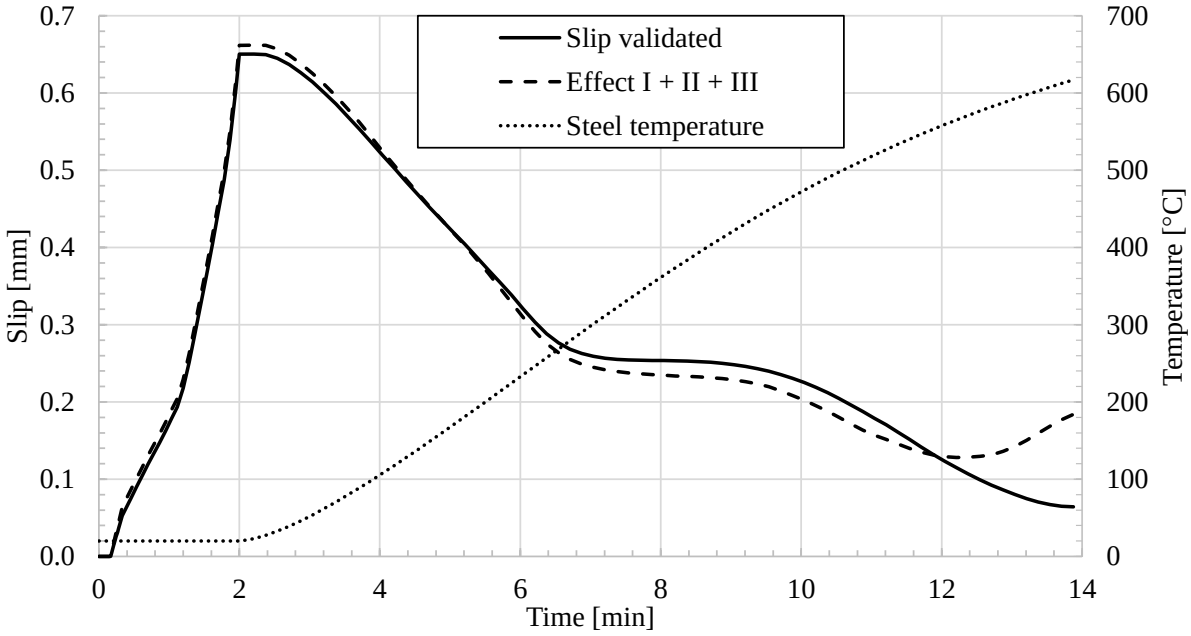

Figure 6.5: Summarized *Effect I, II* and *III*, as well as slip of the validated full model

6.2 Determinant Load Combination for the Slip of the Composite Joint

The course of the interface slip was similar for all experiments and simulations conducted:

1. Vertical mechanical load leads to positive slip
2. A rise in temperatures in the composite beam first leads to negative slip
3. With a large vertical deformation positive slip can occur

For all eight beams in the experiments, the general course of the interface slip over the supports was similar. There was an initial positive slip due to the pre-load. During the flame impingement the slip first fell rapidly and then, with rising steel temperatures, began to fall more slowly.

As the composite joint was stressed with the mechanical loads, the falling slip due to *Effect I* led to a reduction of stress in the composite joint. Figure 6.6 shows the recorded slip of Experiment 1, Beam 1 and Beam 2. The maximum slip was reached only because of the

mechanical load at ambient conditions, whereas after the composite joint was unloaded by the rising temperatures. As the thermal elongation of the steel section led to a continuous negative slip in the composite joint, the lowest slip can occur when no mechanical load led to a positive slip at ambient conditions.

The shear connection of a composite beam had to be designed not to exceed the ductility of 6 mm of the shear connectors given by EN 1994-1-1. The maximum slip is already limited by the application of the minimum degree of shear connection according to EN 1994-1-1 Part 6.6.1.2. However, the minimum slip due to fire exposure is not yet limited. As the negative slip is unique for composite beams in the fire, the controlling load combination is only dead weight and without a live load.

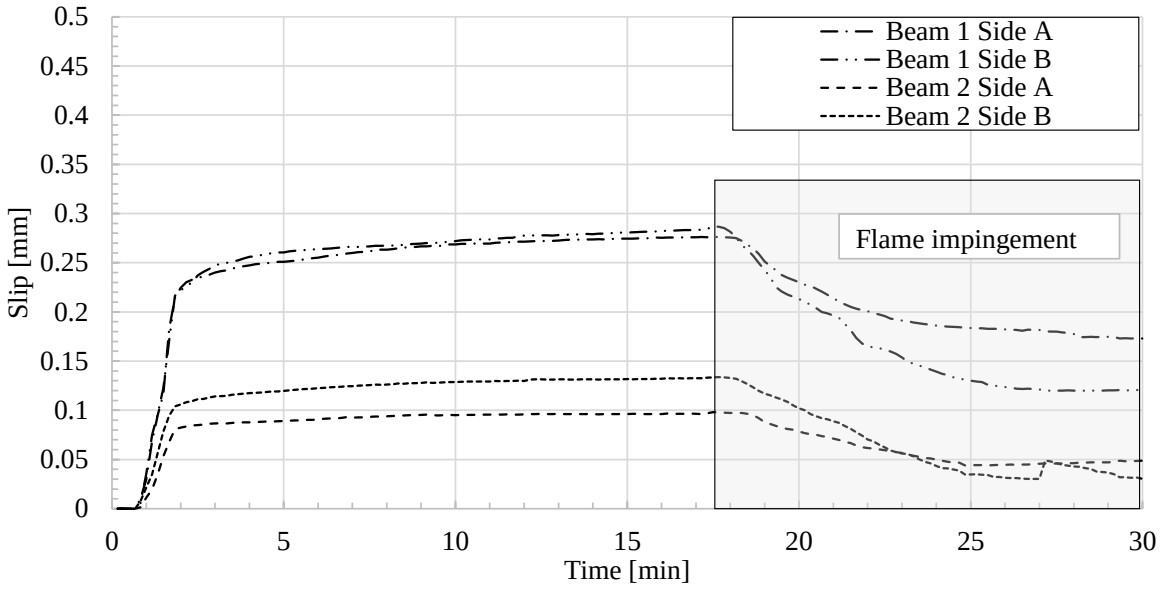

Figure 6.6: Slip over the support in Experiment 1, Beam 1 and Beam 2. Fire load added at minute 16.

7 Analytic Description of the Slip in a Fire Situation

The interface slip of a composite beam can be described by the theory of the elastic composite action (see Section 2.2.1). However, the existing theory does not cover the action of a fire load on the composite beam. Also, the use of the sandwich theory described in Section 2.2.1 is very limited for this application, as it implies a full elastic behaviour of all components.

With the separate examination of the effects of elevated temperatures on the composite joint in Section 6.1 it becomes partly possible to use the theory of the elastic composite action also for composite beams in the fire. As a linear elastic behaviour of the composite beam is implied, the use of the analytic description of the slip of the composite joint in the fire situation is limited to the first few minutes in the fire. Within the scope of this thesis, the analytic description is used for the general understanding of the influences of various parameters on the interface slip, but not for an exact prediction of the slip of a composite joint in the fire situation.

$$s_\theta = s_{\theta,IIa} + s_{\theta,IIb} + s_{\theta,III} - s_{\theta,I} \tag{7.1}$$

7.1 Effect I

For *Effect I*, the thermal elongation of the steel section, the slip at the end of the beam can be described by a continuously supported beam with a thermal load.

For the analytical description of *Effect I* a couple of assumptions and limitations have to be made: A constant temperature is assumed over the entire steel section, linear elastic

behaviour of the composite joint and no limitation of the tensile strength of the concrete chord (cf. Section 8.2.7).

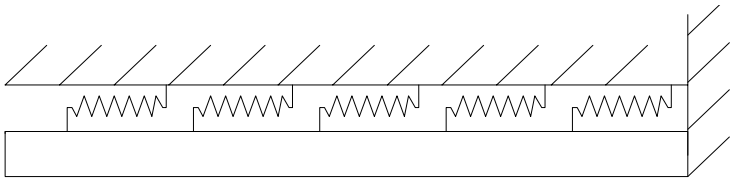

Figure 7.1: Model for the analytical description of *Effect I*

Hereby, the shear connection is considered continuously linear elastic, with the continuous shear support c_v[I] calculated based on C_v[II]:

$$c_v = \frac{C_v * n}{L} \tag{7.2}$$

with n being the number of shear connectors on the composite beam and L being the length of the beam.

The thermal elongation of the steel section without a shear connection would lead to a slip at the end of the beam of:

$$\delta s_T = \alpha_T * \delta T * L \tag{7.3}$$

Due to the restraint of the shear connection the elongation of the steel section can not fully evolve. It can only evolve to the temperature dependent slip $s_{\theta,I}$. The difference between the actual slip $s_{\theta,I}$ and the theoretic slip without shear connection, δs_T, results in a force that equals the spring force in the composite joint:

$$(\delta s_T - s_{\theta,I}) * \frac{EA}{L} = \frac{1}{2} * c_V * L * s_{\theta,I} \tag{7.4}$$

[I] Continuous shear elastic shear connection of a composite joint
[II] Linear elastic spring characteristic of a shear connector

With Equation 7.3 included in Equation 7.4 this leads to:

$$\alpha_T * \delta T * L * \frac{EA}{L} - \frac{s_{\theta,I} * EA}{L} = \frac{1}{2} * c_V * L * s_{\theta,I} \tag{7.5}$$

and

$$s_{\theta,I} = \frac{\alpha_T * \delta T * EA}{\frac{EA}{L} + \frac{1}{2} * c_V * L} \tag{7.6}$$

7.2 Effect II

Effect II describes the positive slip over the supports of a single span composite beam due to the thermal gradient in the beam. For the analytical description *Effect II* is split into parts: *Effect IIa* and *Effect IIb*, with *Effect II* being the sum of both:

$$s_{\theta,II} = s_{\theta,II,a} + s_{\theta,II,b} \tag{7.7}$$

Effect IIa describes the slip due to bending as a result of the temperature difference between the steel section and the concrete chord. Constant temperature distribution in the steel section is assumed for the calculation of this effect. Figure 7.2 displays the temperature distribution of a composite beam with an IPE 300 steel section. The temperature distribution in the concrete chord is approximated to be triangular, in the steel section to be rectangular. The slip due to the high thermal gradient in the concrete chord is calculated in the second part, *Effect IIb*.

7.2.1 Effect IIa

The temperature difference between the steel section and the concrete chord leads to a different length of both components, as already described for *Effect I* with Equation 7.6. The

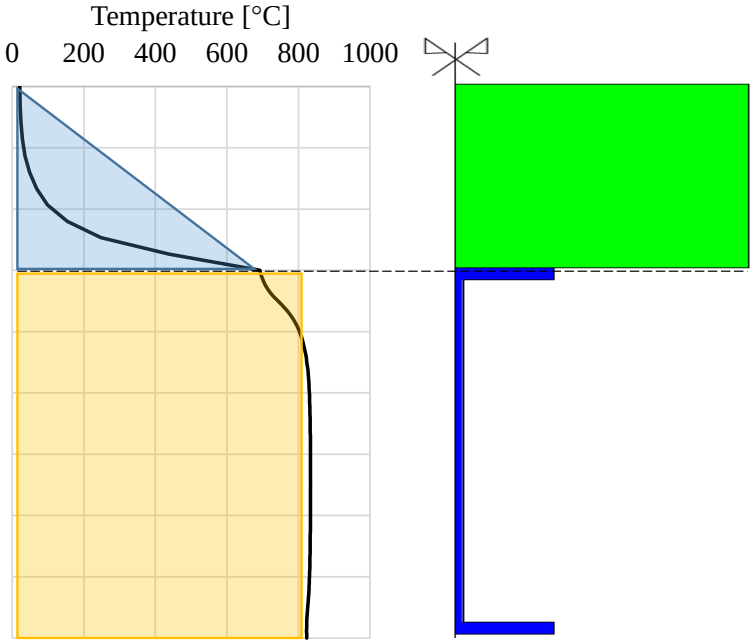

Figure 7.2: Temperature distribution of a composite beam with an IPE 300 steel section after 30 minutes of ISO 834 fire. Blue triangle: Effect IIb, orange rectangle: Effect IIa

temperature gradient in the composite beam leads to a thermal curvature of the composite beam. To calculate this curvature an equivalent load q_{sIIa} is calculated based on the normal forces in the beam that would evolve if the beam could not freely deform. The normal force N_0 in the composite beam is calculated based on an equation of Hoischen [59].

$$N_0 = (\epsilon_{c,\theta} - \epsilon_{a,\theta}) * E_{c,\theta} * A_c * \frac{y_c * (I_c + n * I_a)}{e * n * I_V} \tag{7.8}$$

The force N_0 leads to a moment M_0 in the composite beam:

$$M_0 = N_0 * e \tag{7.9}$$

With M_0 an equivalent load q_{sIIa} can be calculated. Assuming that M_0 has a parabolic distribution over the length of the beam, q_{sIIa} can be calculated as follows:

$$q_{sIIa} = \frac{8 * M_0}{L^2} \tag{7.10}$$

The equivalent load q_{sIIa} can then be used with the closed-form expression of Möhler [16] in Equation 2.4 to calculate $s_{\theta,II,a}$:

$$s_{\theta,II,a} = \frac{q_{sIIa} * L * e}{2\omega^2 * E_c I_V} * \left[1 - 2 * \frac{x}{L} - \frac{2\beta}{\omega * L} * \frac{sinh\left(\frac{\omega}{\beta} * \frac{L}{2} - x\right)}{cosh\left(\frac{\omega * L}{2 * \beta}\right)}\right] \tag{7.11}$$

7.2.2 Effect IIb

The analytical description of *Effect IIb* is done with a equivalent prestressing load P_V (cf. Pirzer [60]). As Möhler [16] does not provide a closed-form expression for a prestressing load, a closed-form expression of Hoischen [17] is used for the description of *Effect IIb*. As a simplification, a linear temperature distribution is assumed between the fire facing side and the far side of the fire. With the temperature of the concrete on the fire facing side of the concrete chord θ_c, the thermal strain of the concrete $\epsilon_{c,l}$ can be calculated.

$$\epsilon_{c,l} = -1.8 * 10^{-4} + 9 * 10^{-6} * \theta_c + 2.3 * 10^{-11} * \theta_c^3 \tag{7.12}$$

From the thermal strain, the stress on the fire facing side of the chord can be calculated. The Young's modulus of the concrete $E_{c,\theta}$ is taken from the middle of the concrete chord.

$$\sigma_{c,l} = E_{c,\theta} * \epsilon_{c,l} \tag{7.13}$$

Assuming a linear temperature, stress, and strain distribution in the concrete chord, the prestressing load P_V can be calculated:

$$P_V = 0.5 * \sigma_{c,l} * A_c \tag{7.14}$$

The normal force in the concrete chord is calculated according to Hoischen [59]:

$$N_0 = P_V * \frac{y_c * (I_c + nI_a)}{e * nI_V} \tag{7.15}$$

I_c, I_a, I_V, and y_c are defined in Figure 2.3. n is defined in Equation 2.8.

The shear force due to *Effect IIb* T_{IIb} is then calculated with the normal force in the steel section and the concrete chord N_0.

$$T_{IIb}(x) = N_0 * \xi * \frac{sinh(\omega * (\frac{L}{2} - x))}{cosh(\omega * \frac{L}{2})} \tag{7.16}$$

with ξ being an abbreviation:

$$\xi^2 = \frac{c_V * e * n * I_V}{y_c E_c A_c * (I_c + n * I_a)} \tag{7.17}$$

With the shear force $T_{IIb}(x)$ and the elastic spring constant of the shear connection c_v, the slip at any given point of a simply supported beam can be calculated.

$$s_{\theta,II,b}(x) = \frac{T_{IIb}(x)}{c_V} \tag{7.18}$$

7.3 Effect III

Effect III, the positive slip due to bending of the composite beam with degradation of the material properties, can be similar to the slip at ambient conditions with the theory of the elastic composite action. With this, the description of the slip of Möhler [16] (cf. Equation 2.4) is changed to incorporate temperature dependent material behaviour.

$$s_{\theta,III}(x) = \frac{q * L * e}{2\omega_\theta^2 * E_{\theta c} I_V} * \left[1 - 2 * \frac{x}{L} - \frac{2\beta}{\omega_\theta * L} * \frac{sinh\left(\frac{\omega_\theta}{\beta} * \frac{L}{2} - x\right)}{cosh\left(\frac{\omega_\theta * L}{2 * \beta}\right)}\right] \tag{7.19}$$

With ω_θ, E_θ, and n_θ being temperature dependent:

$$\omega_\theta^2 = \frac{\overline{C} * b(1 + \frac{A_c}{n_\theta A_a})}{E_{\theta c} * A_c} \tag{7.20}$$

and

$$n_\theta = \frac{E_{\theta a}}{E_{\theta c}} \tag{7.21}$$

8 Influences on the Maximum Slip of the Composite Joint in a Fire

8.1 Parameters with Little to No Influence on the Maximum Slip

8.1.1 Intumescent Coating

Model IV was used to investigate the influence of intumescent coating on the maximum slip of a composite beam in a fire. Within the scope of the research, the material properties of the intumescent coating Sika Unitherm Platinum [45] were used. Each beam was calculated with various protection levels:

- Without protection
- With intumescent coating to reach a steel temperature of 500 °C after 30 minutes of fire, called 'R30'
- With intumescent coating to reach a steel temperature of 500 °C after 60 minutes of fire, called 'R60'
- With planking to reach a temperature of 500 °C after 30 minutes of fire, called 'B'

All beams were loaded with self weight at ambient conditions. After the application of the mechanical load, an ISO 834 thermal load was applied.

The expansion of the intumescent coating starts at a temperature of 300 °C and reaches its maximum at 530 °C (cf. Figure 4.7). Therefore, the protection of the intumescent coating also starts only at a temperature of 300 °C. Before this temperature, the steel section is not

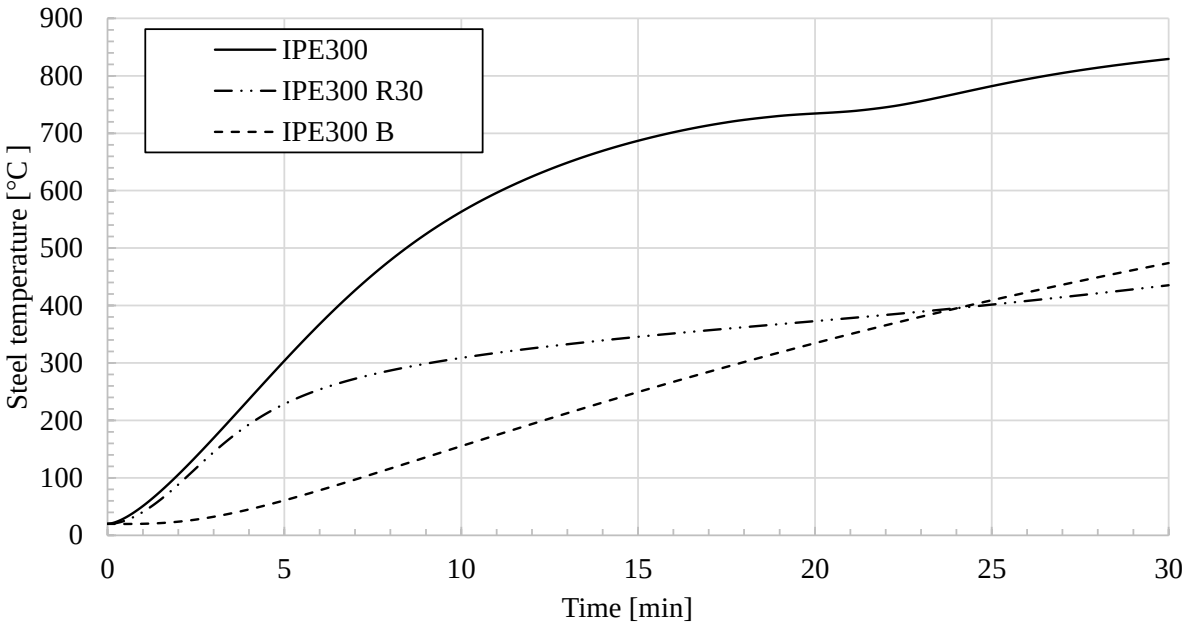

Figure 8.1: Heating of the steel section of a composite beam:
An unprotected IPE 300, called 'IPE300',
an IPE 300 protected with intumescent coating, called 'IPE300 R30',
and an IPE 300 protected with planking, called 'IPE300 B'.

protected, and the behaviour of the composite beam is similar to an unprotected composite beam. Figure 8.1 shows the temperature development within a steel section of a composite beam. The setup of all three beams was similar, with the difference that the first beam was unprotected, the second beam was protected with an intumescent coating, and the third beam was protected with planking. The temperature developments of the beam protected with intumescent coating and the unprotected beam were similar for the first few minutes. Only after five minutes of fire exposure was there a significant difference in the temperature development.

Figure 8.2 shows the development of the slip over the supports of composite beams protected with an intumescent coating in the first five minutes of fire exposure according to ISO 834. The setup of the composite beam was similar to Beam 1 described in Section 3.2 on page 33. The thickness of the protection was chosen to fullfill different fire resistance durations according to EN 13501-2 [61].

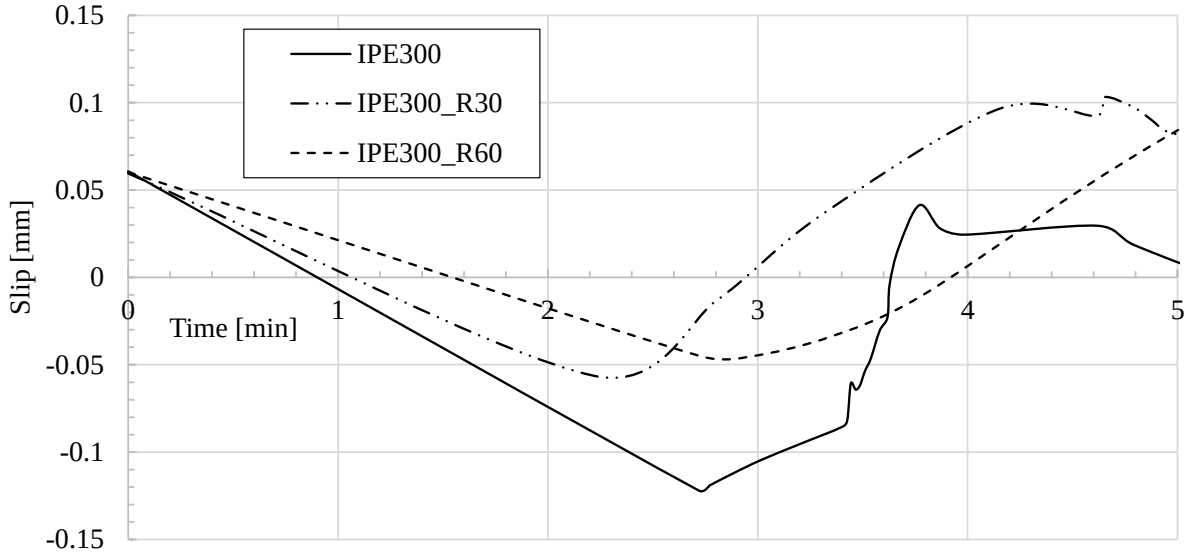

Figure 8.2: Slip over the support of composite beams exposed to ISO 834 fire:
An unprotected IPE 300, called 'IPE300',
an IPE 300 protected with intumescent coating, called 'IPE300 R30',
and an IPE 300 protected with planking, called 'IPE300 B'.

There was little difference in the gradient of the initial slip decrease due to *Effect I*. Due to the different gradient, there was a variation of the minimum slip before *Effect II* came into action and the slip over the supports started to rise again. The difference in the gradient of the slip can be explained by the insulation of the steel with dry, unexpanded coating.

Figure 8.3 shows the development of the slip and the expansion factor of the intumescent coating of the same composite beam as presented in Figure 8.1 and Figure 8.2, but with a coating to fulfill the R30 criterion. The initial drop of the slip and the start of the subsequent rise of the slip both happened when the coating was still not expanded and there was still only the protection of the dry, unexpanded coating.

To conclude, the expansion of the covered intumescent coating starts only when the coating reaches a temperature of 300 °C. The slip of the composite joint however is controlling for the maximal slip for the first few minutes of fire exposure, before a temperature of 300 °C is reached. Therefore, the only influence of intumescent coating on the maximum slip of a composite beam in fire is the little insulation of the unexpanded coating.

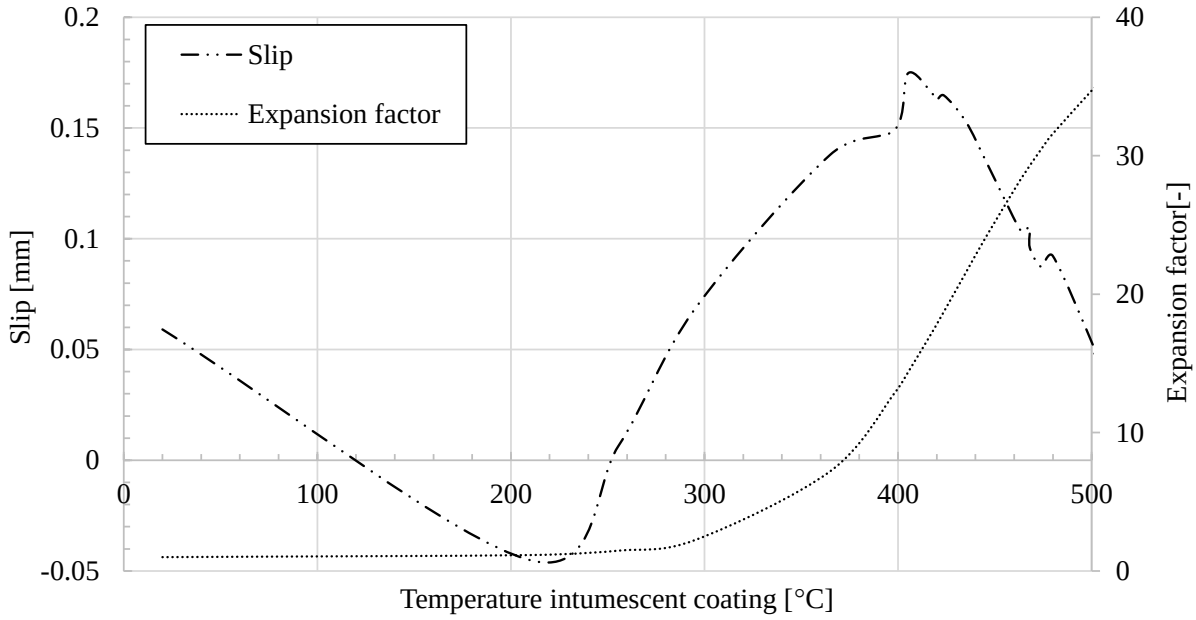

Figure 8.3: Slip over the support and expansion factor of the intumescent coating for the composite beam with the protected IPE 300 steel section.

8.1.2 Way of Load Application

As described in Chapter 7, the development of *Effect I* and *Effect II* is only dependent on the temperature distribution and the geometry of the composite beam. Mechanical loads on the composite beam only influence the slip due to the increase in bending with *Effect III*. Nevertheless, mechanical loads lead to a slip contrary to the dominant slip due to thermal loads. Therefore the determinant load chase is only self-weight and thermal loads, as discussed in Section 6.2. Any vertical load on a single span composite beam, distributed load or single load, leads to a reduction of the interface slip in the composite joint in the fire situation.

8.1.3 Influence of the Heating Rate

Besides the ISO 834 fire curve, the influence of a natural fire curve was investigated within the experiments. The controlling difference between the two fire curves is the delayed rise of temperature for the natural fire curve. The temperature of the natural fire curve stays at

200 °C in the first 15 minutes of the fire impingement, and after 40 minutes it nearly reaches the temperature of the ISO 834 fire.

The natural fire curve was applied to Beams 7 and 8. The resulting temperatures were very similar to the temperatures measured in the experiments with the ISO 834 fire load, only the development was delayed. See Figure 8.4 for the temperature development in Beams 7 and 8 due to the natural fire curve.

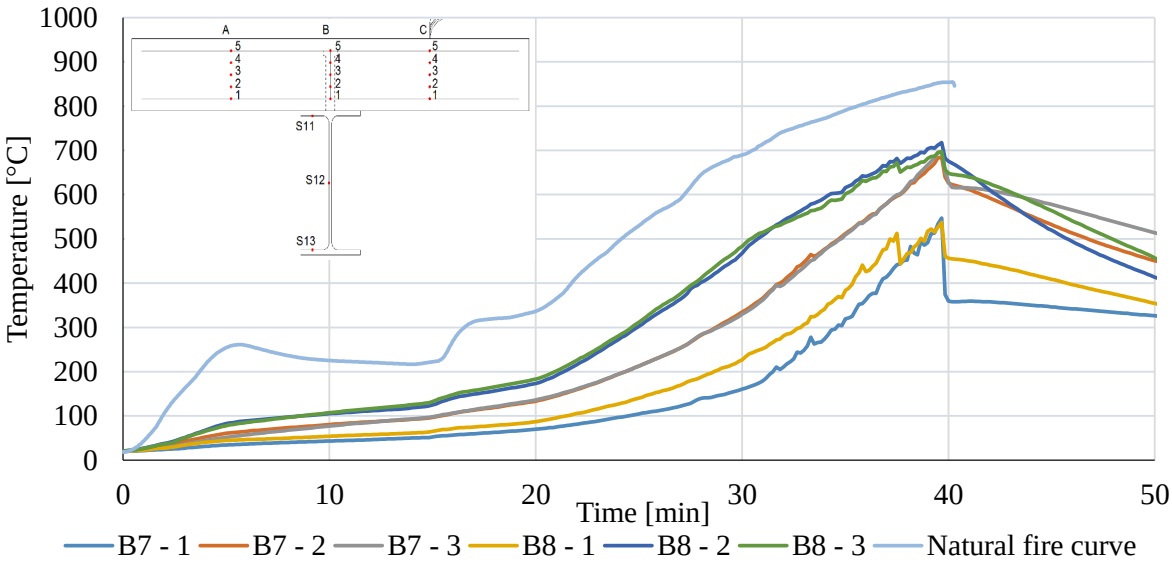

Figure 8.4: Evolution of the steel temperature in Beam 7 and 8 due to a natural fire curve

Even though the temperature developments of Beam 6 and Beam 8 were different due to the different fire loads, the final temperature distribution of the beams was similar, as can be seen in Figure 8.5.

As the temperature distribution heavily influences both slip and vertical displacement, a similar development can be seen for the deformations of the composite beam. Two beams with different fire loads, Beam 5 and Beam 7, both IPE 300 beams with a steel grade S355, reached the 400 mm abortion criterion already during the fire impingement. The vertical displacement of these two beams can be seen in Figure 8.6. Beam 5 was loaded with ISO 834 fire. Therefore the thermal load, as well as the vertical deflection, rose steeply. Beam 7 was loaded with the natural fire curve, which had a delayed temperature evolution and therefore

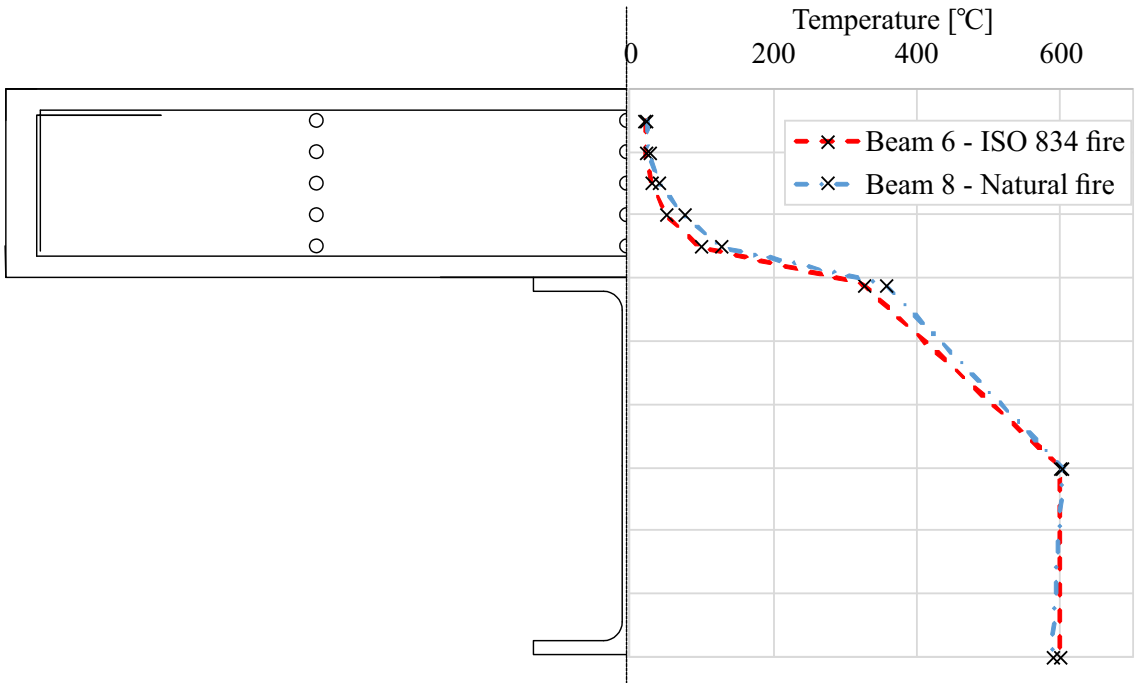

Figure 8.5: Temperature distribution in Beam 6 and Beam 8 at a maximum steel temperature of 600 °C

the vertical deflection was also delayed. At the vertical blue and green line, the respective beam reached the test abortion criterion of 400 mm vertical deflection. At this point the mechanical load was taken off the beams.

The same point is also marked in Figure 8.7, which displays the slip of the composite joint of Beams 5 and 7. It can be seen that after the mechanical load was removed there is a strong decline of slip.

Also, the slip of Beam 5 decreased much earlier than the slip of Beam 7, causing the moment of test abortion, marked with the blue and green line, to be much earlier for Beam 5 than for Beam 7.

The slip of Beam 7 did not decrease as much as the slip of Beam 5. The difference in decrease can be explained by the different temperature distribution. While there was nearly no temperature difference for the tested HEB sections (see Figure 8.5), there was a slight temperature difference in the concrete chord and the upper flange for the tested IPE sections,

as displayed in Figure 8.5. As especially the temperatures of the upper flange and the adjacent concrete chord are important for the stiffness of the headed stud shear connectors, the lower stiffness of the shear connectors in Beam 5 led to a higher slip.

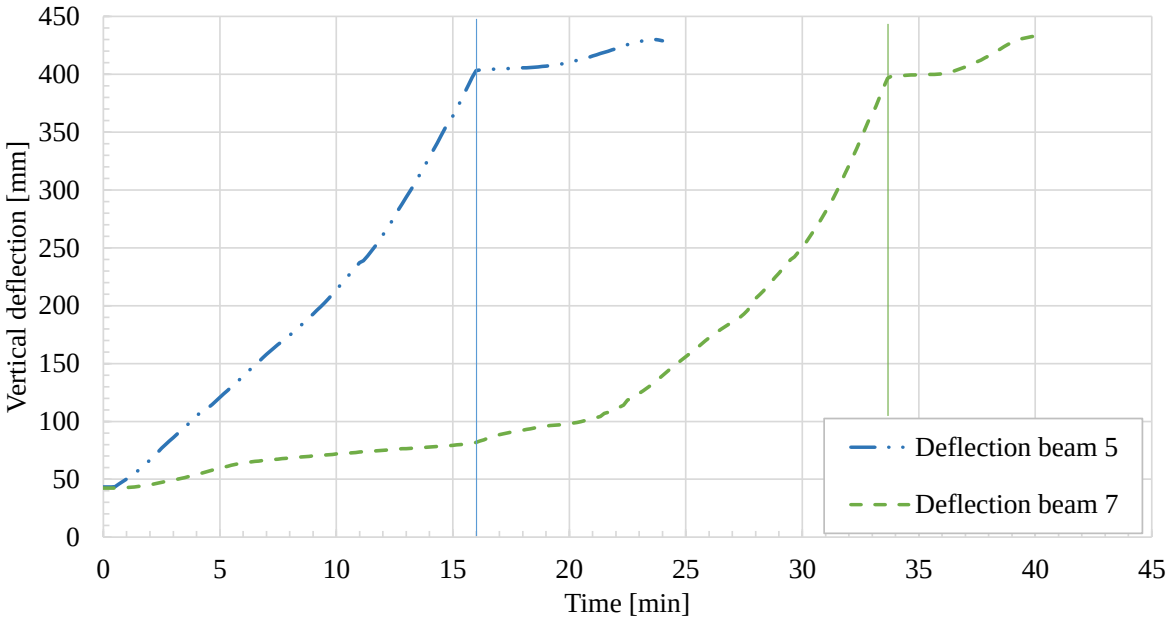

Figure 8.6: Vertical deformation of Beams 5 and 7 during fire impingement

It can be concluded that the different fire loads have nearly no influence on the average steel temperature and therefore on the ultimate load carrying capacity of a composite beam in a fire situation. Some influence of the fire load on the temperature of the composite joint was recorded. Nevertheless, the temperatures of the composite joint and the shear connectors were still below a critical temperature that would make a reduction of the shear capacity necessary.

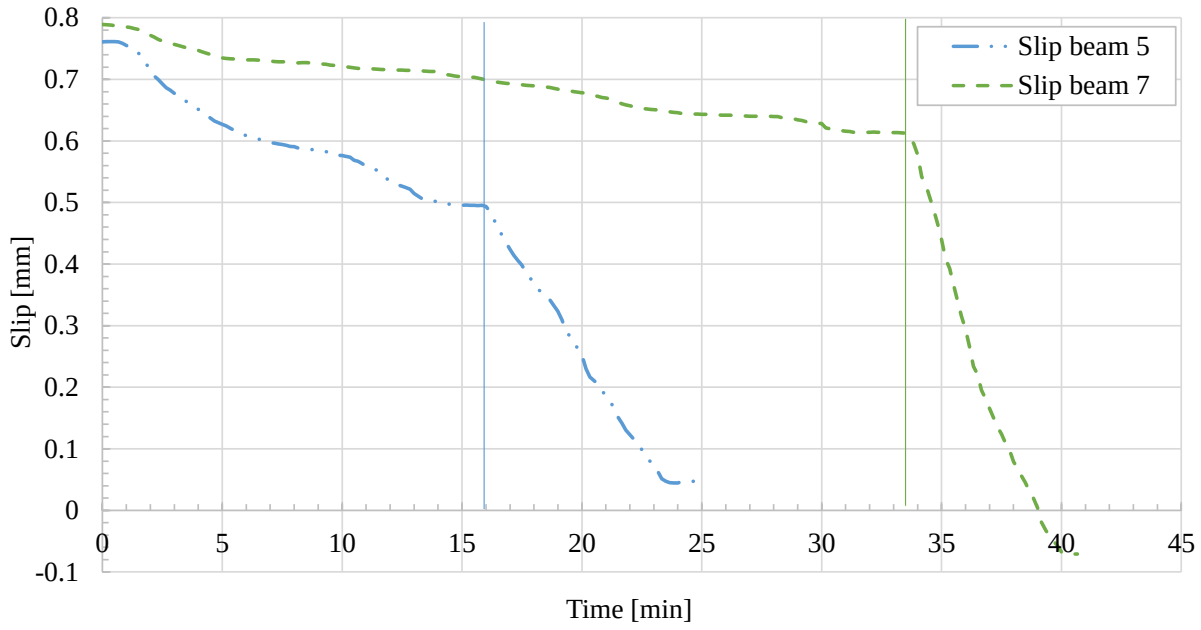

Figure 8.7: Interface slip of Beams 5 and 7 during fire impingement

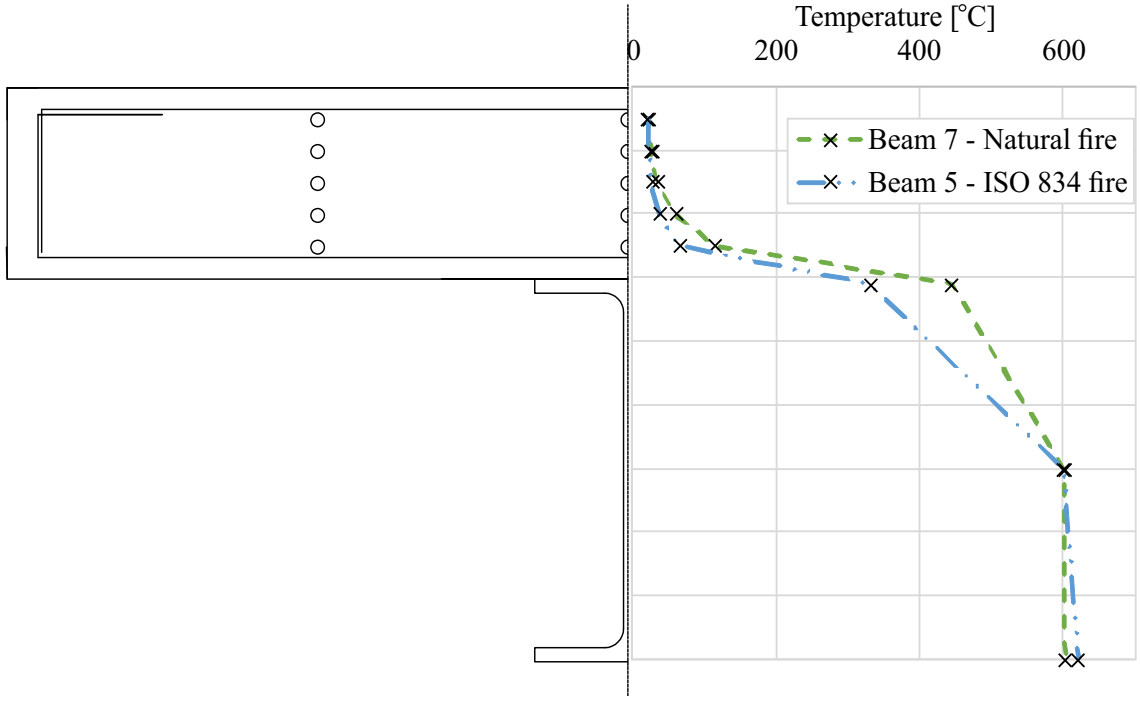

Figure 8.8: Temperature distribution in Beam 5 and Beam 7 at a maximum steel temperature of 600 °C

8.1.4 Influence of the Production Process

There are two different ways to produce a composite beam, and both lead to particular residual stresses in the composite beam. Whereas Beams 1 to 4 were produced to include the dead load in the elastic composite action, for Beams 5 to 6 the elastic composite action was only effective for the live load. Due to plastic stress redistribution, the ultimate load carrying capacity is generally not affected by these residual stresses.

Beam 3 was produced with full support of the steel section to include the dead load of the composite beam. Beam 6 was produced with only both ends of the steel beam supported. Therefore, the entire self-weight of the composite beam was taken by the steel section, and the elastic composite action only worked for the live load.

Figure 8.9 displays the vertical displacement of Beams 3 and 6, both of which were HEB 300, S355 and $\eta = 0.4$. The deformation of the composite beams during flame impingement can be divided into three phases. In the first phase, from minute 0 to 7, the deformation rose linearly and similar for both beams, and therefore for this phase, a similar stiffness of the composite beams can be assumed. In the second phase from minute 7 to 21 a non-linear load carrying behaviour evolved due to load redistribution within the composite beams. In the third phase, the vertical deflection rose steeply for both beams due to the additional external load. As the plastic load carrying capacity of the beams was reached in the third phase, the deflection rose similarly for both beams, which indicates a similar stiffness of the composite beams in this phase.

The behaviour of the composite beams within the first phase is controlling, as for the composite joint in a fire situation, only the first 5 to 10 minutes of the flame impingement are relevant (see Chapter 5.1). The results suggest that there is no difference in behaviour for the two production methods covered. Therefore it can be assumed that there is no influence of the production method on the composite joint.

As also the stiffness of the beams is similar in phase three, it can be assumed that there is no influence of the construction method on the ultimate load carrying capacity.

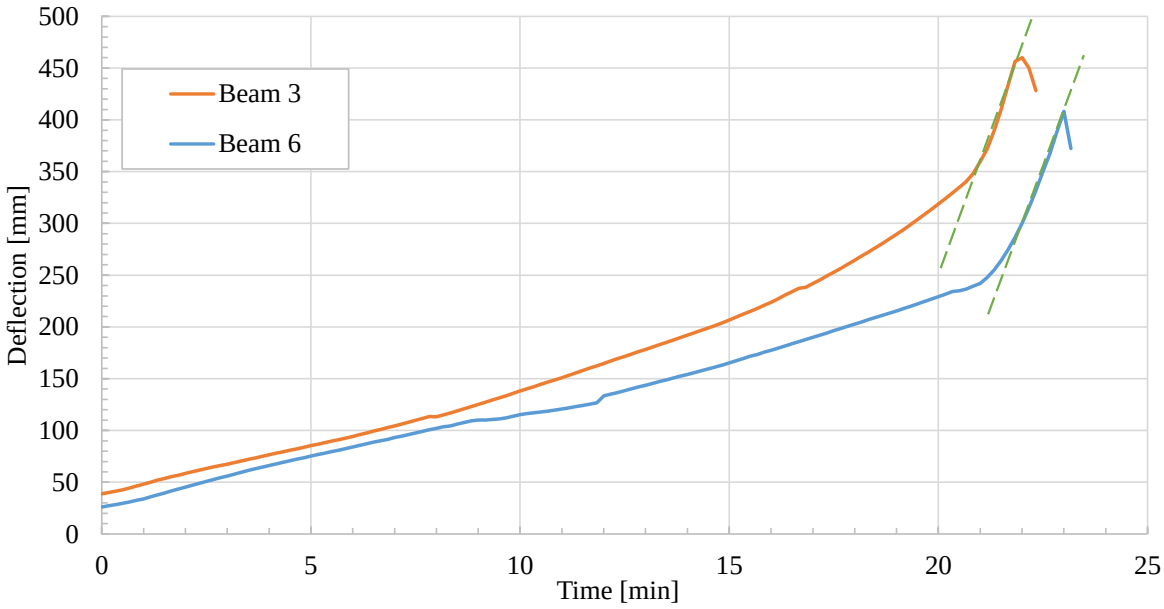

Figure 8.9: Vertical deflection of Beam 3 and Beam 6 at the midspan during flame impingement

8.2 Parameters with Large Influence on the Maximum Slip

8.2.1 Influence of the Stiffness of the Composite Joint

The stiffness of the composite joint is the dominant influence on the maximum slip of a composite beam in a fire situation. Figure 8.10 shows the maximum computed slip of the parametric study with the stiffness of the composite joint. Hereby the stiffness c_v is calculated with Equation 7.2 and represents the initial stiffness of a shear connection C_v multiplied with the number of shear connectors per meter.

The results of the parametric study clearly show the high influence of the maximal slip on c_v. As the stiffness is calculated by the relation of P_{max}, s_y, and the number of shear connectors per meter, there is a variety of influence factors on the stiffness of the shear connectors:

- degree of shear connector η

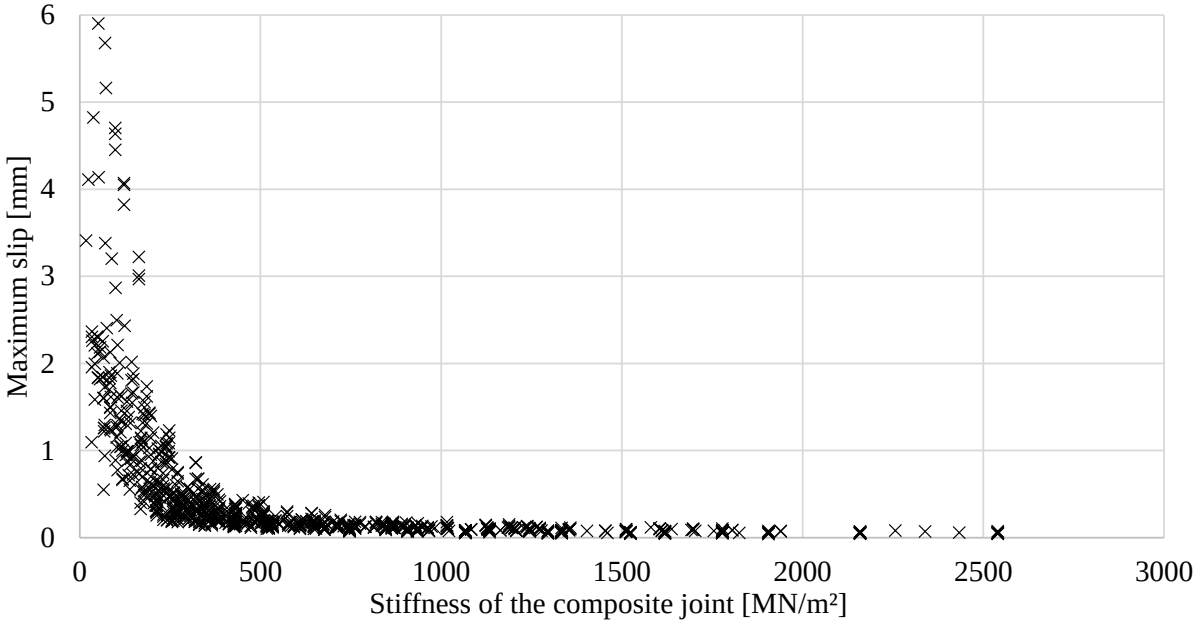

Figure 8.10: Maximum slip of computed composite beams in the fire situation with the respective stiffness of the composite joint c_v

- f_{ay} and A_a[I]
- $f_{cm,\theta}$ and A_c[II]
- length of the composite beam L
- geometry of the headed stud shear connectors
- tensile capacity $f_{c,\theta}$ of the concrete
- position of the headed studs during the placement of the concrete

With a large number of influential factors on the stiffness, it is challenging to predict or calculate it. Given the significant influence of only a small change of stiffness and the difficult calculation, the influence of the shear connection does not seem to be an appropriate way of limiting the maximum slip of the composite joint in a fire situation. Instead of describing

[I] Cross-sectional area of structural steel section
[II] Cross-sectional area of concrete

the stiffness of the composite joint itself, important values on the stiffness are used and evaluated.

8.2.2 Influence of the Degree of Shear Connection

Experimental Results

In the experiments, three different degrees of shear connection were tested: $\eta = 0.4$, $\eta = 0.52$, and $\eta = 0.6$. Due to the different preloading procedures only Beams 1 & 2 and 3 & 4 are comparable. Therefore the slip of Beam 1 ($\eta = 0.4$) is compared to Beam 2 ($\eta = 0.6$) in Figure 3.21 and the slip of Beam 3 ($\eta = 0.4$) is compared to Beam 4 ($\eta = 0.6$) in the following Figure 8.11.

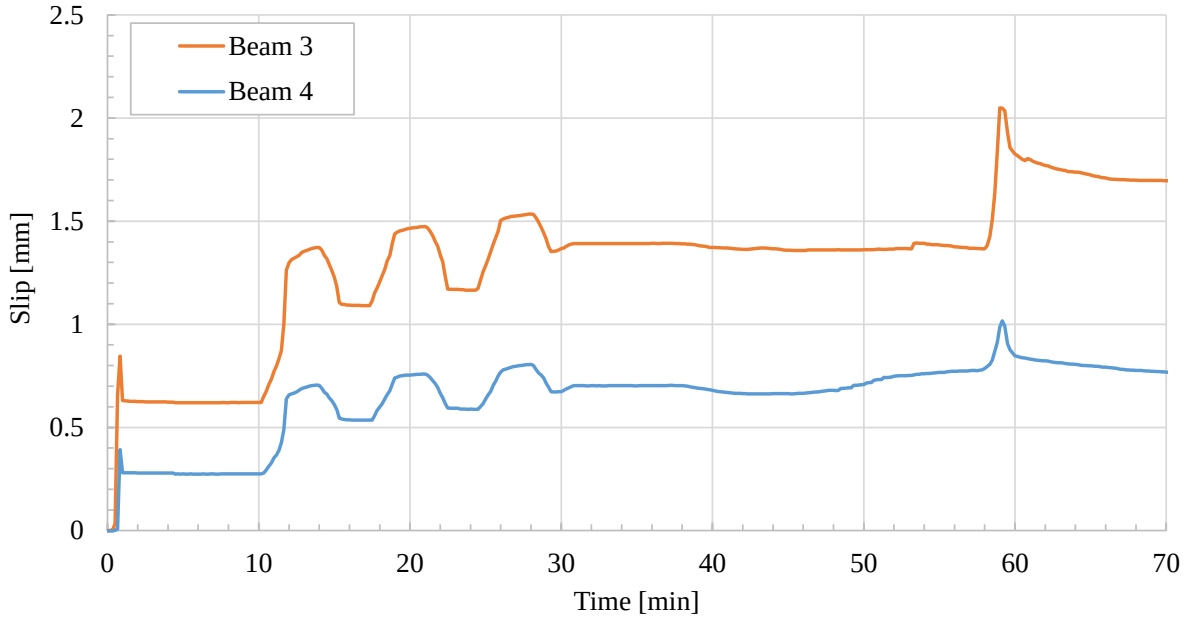

Figure 8.11: Average interface slip of Beam 3 ($\eta = 0.4$) and Beam 4 ($\eta = 0.6$)

In both cases, the lower degree of shear connection leads to a higher initial deformation of the composite joint, but also a higher negative slip due to the flame impingement. As the negative slip due to the lower degree of shear connection is much higher, negative slip can become the leading variable action. A high degree of shear connection can effectively prevent slip in the composite joint, also in fire situations.

Numerical Results

A degree of shear connection between $\eta = 0.2$ and $\eta = 1.0$ was considered in the parametric study. Figure 8.12 shows the maximum slip of the composite beams in the first 30 minutes of fire exposure. Whereas the slip at $\eta = 1.0$ is always low with an average of 0.11 mm, the maximum slip at $\eta = 0.2$ is considerably higher with an average of 1.11 mm, with a much higher standard deviation of 1.10 mm and a maximum of 5.9 mm.

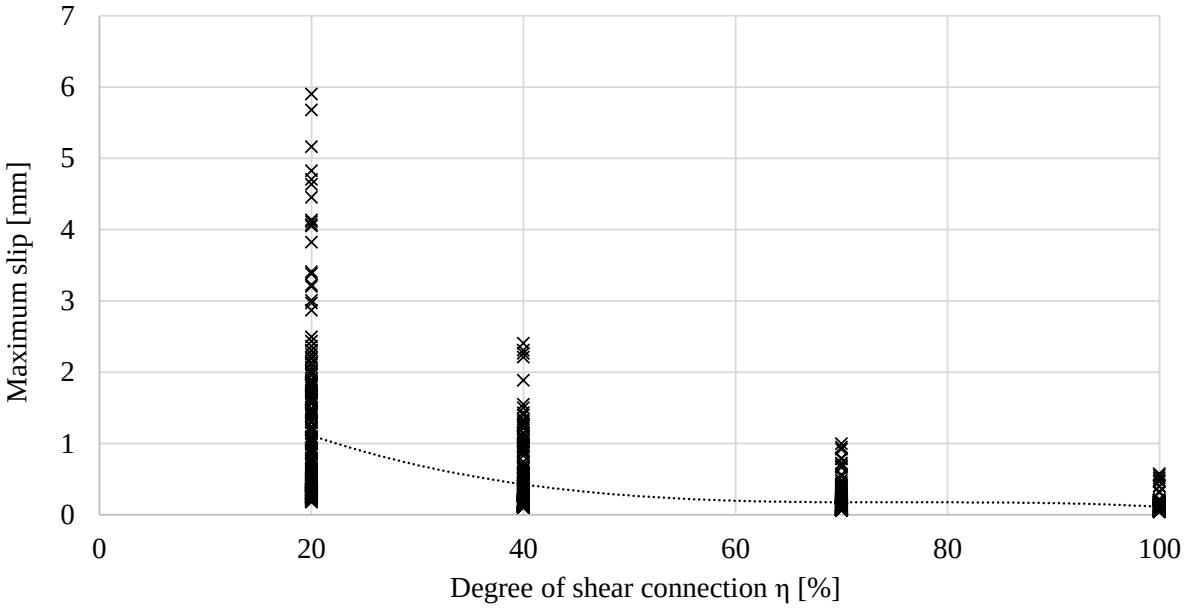

Figure 8.12: Maximum slip of computed composite beams in the fire situation with a degree of shear connection between $\eta = 0.2$ and $\eta = 1.0$

Analytic Results

In the analytic description of the slip, the degree of shear connection was used to calculate the stiffness of the composite joint c_v. Especially for *Effect I* which is modelled as a continuously supported beam, the stiffness of the composite joint highly influences the maximum slip of the composite joint.

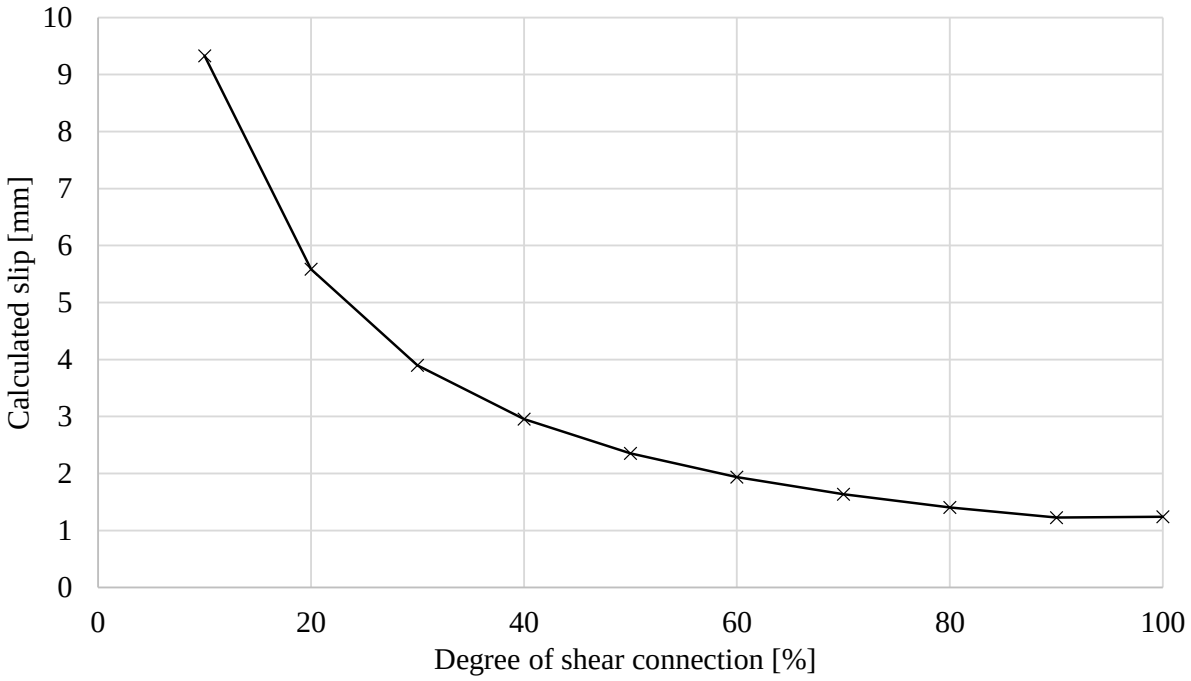

Figure 8.13: Maximum slip of calculated composite beams in the fire situation with a degree of shear connection between $\eta = 0.1$ and $\eta = 1.0$

Conclusion

The degree of shear connection η directly influences the stiffness of a composite joint. Therefore a high influence of the degree of shear connection on the maximum slip in the fire situation was observed in the experiment and in the numerical and analytic examinations. Only a small non-linearity can be observed for a degree of shear connection $\eta \leq 0.4$, while the behaviour at $\eta > 0.4$ is highly non-linear.

8.2.3 Influence of the Steel Grade

As the steel grade has a significant influence on the stiffness of the shear connection, there is a noticeable influence of the steel grade on the maximum slip of a composite beam in a fire situation. As discussed in Chapter 7, the stiffness of the shear connection c_v is calculated with the number of shear connectors per meter multiplied by the initial stiffness of a shear connector C_v. As a result of this the number of shear connectors per meter is determined with

η and the minimal normal force carrying capacity of the steel section and the concrete chord. For most composite beams covered within the scope of this thesis the characteristic normal force carrying capacity of the steel section is lower than of the concrete chord. A higher steel grade and therefore a higher load carrying capacity leads to more shear connectors and thus to a stiffer shear connection.

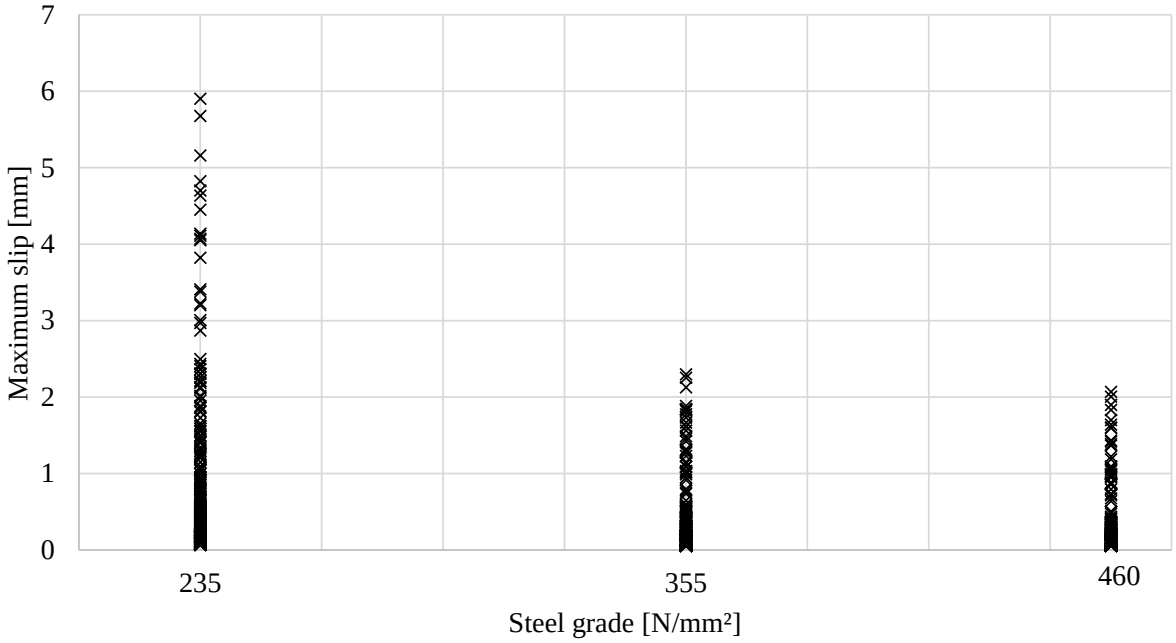

Figure 8.14: Influence of the steel grade on the maximal slip of a composite beam in a fire situation for $6m \leq L \leq 12m$

8.2.4 Influence of the Beam Length

The maximum slip of a composite beam in a fire situation is highly dependent on the initial slip due to *Effect I*. As described in Equation 7.6 in Chapter 7, there is a direct correlation between the maximum slip due to *Effect I* and the beam length. A longer beam leads to a higher thermal elongation and therefore to a higher slip over the supports of a single span beam. Figure 8.15 shows the maximum slip of a composite beam in a fire situation of a composite beam with a degree of shear connection $\eta = 0.2$ at a steel temperature of 220 °C

for a beam length between 0 m and 14 m. The dominating *Effect I* leads to the steep rise of slip between 0 m and 8 m and a steady rise of slip over 8 m.

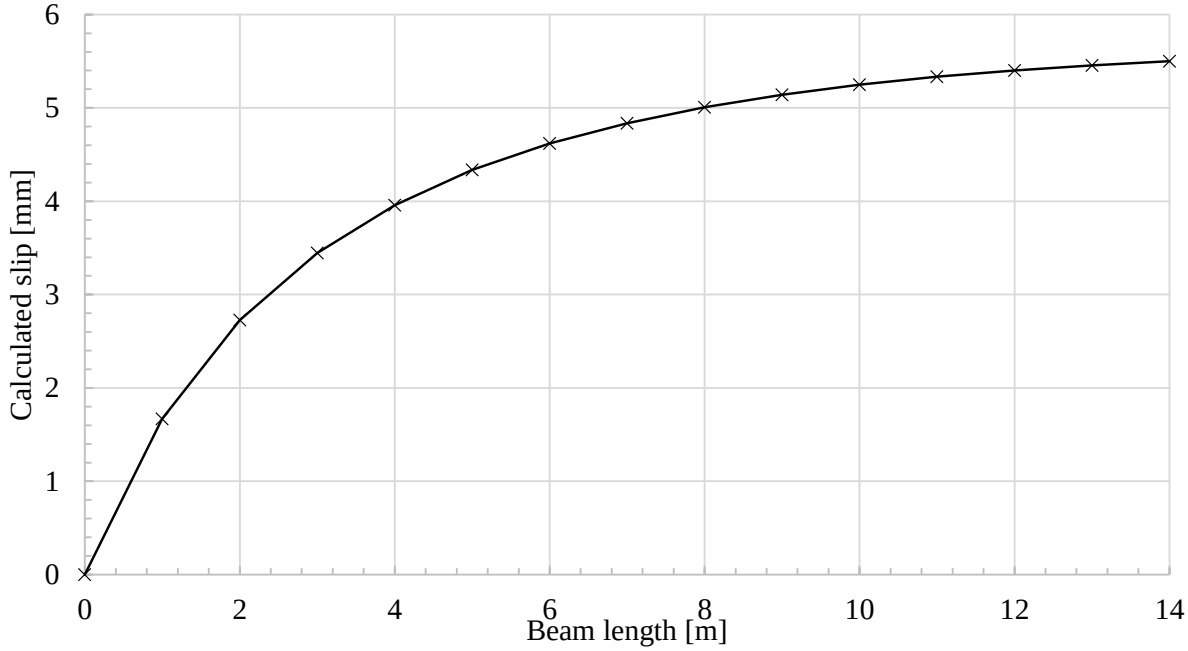

Figure 8.15: Slip calculated with Equation 7.1 of a single span beam with a uncracked concrete chord at $\theta_a = 220$ °C with $\eta = 0.2$. Geometry similar to experimental Beam 1 described in Chapter 3, without mechanical load

Figure 8.15 shows that the influence of the beam length due to *Effect I* becomes smaller with a larger beam length.

In the scope of the parametric study, an effective length of the composite beam of 6 m, 8 m, 10 m, and 14 m was considered. The results clearly show a high influence of the beam length on the maximum values of slip computed. Figure 8.16 shows the relation between the beam length and the maximum slip computed in the parametric study. A closer look on the values of maximum slip shows that the high slip due to *Effect I* only becomes dominant in a few cases, whereas for a vast majority of specimens the slip stays far below the theoretical slip of the theory of the elastic composite action. The difference can be explained with the tensile failure of the concrete chord: For most specimens, the concrete chord failed on tension, and the maximum slip stayed lower than the theoretical value due to *Effect I*.

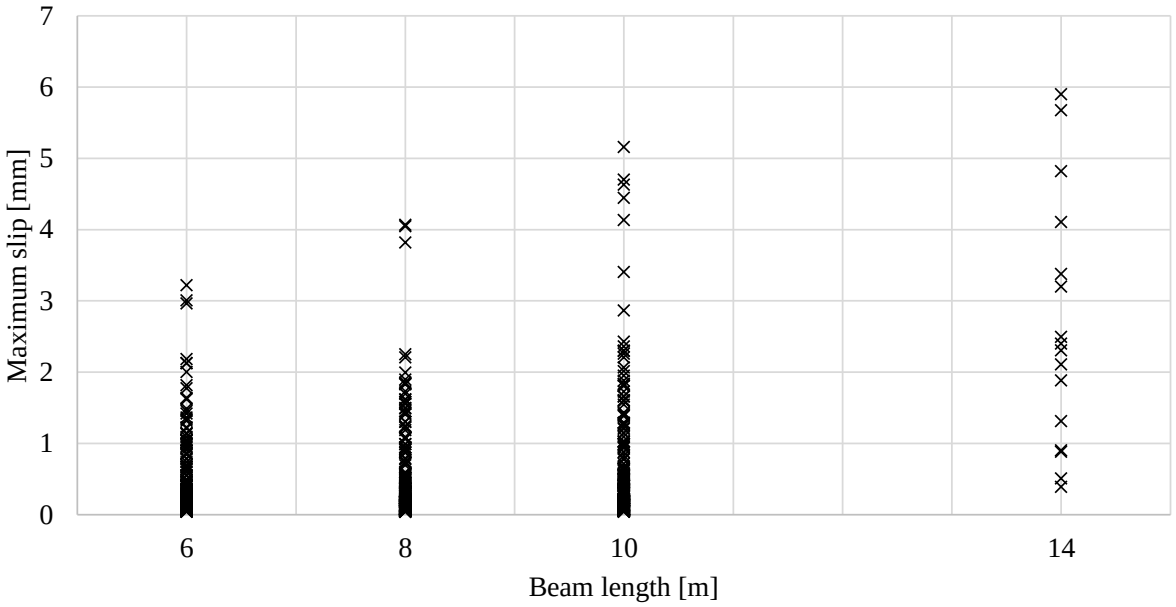

Figure 8.16: Results of the parametric study: Influence of the beam length on the maximum slip in the fire situation

To conclude, the maximum slip of a single span composite beam in the fire situation does depend on the length of the beam. *Effect I* leads to a dependency which decreases with a growing length of the composite beam.

8.2.5 Influence of the Decking Geometry on the Maximal Slip

Figure 8.17 shows the time of failure of the two examined geometries as a function of the degree of shear connection. Whereas the time of failure is relatively constant for both geometries between $\eta = 0.4$ and $\eta = 1.0$, there is a strong decrease in the time of failure for $\eta < 0.2$. Generally, the influence of the degree of shear connection is similar for deep decking and solid slabs and at low degrees of shear connection an increasing nonlinearity can be observed.

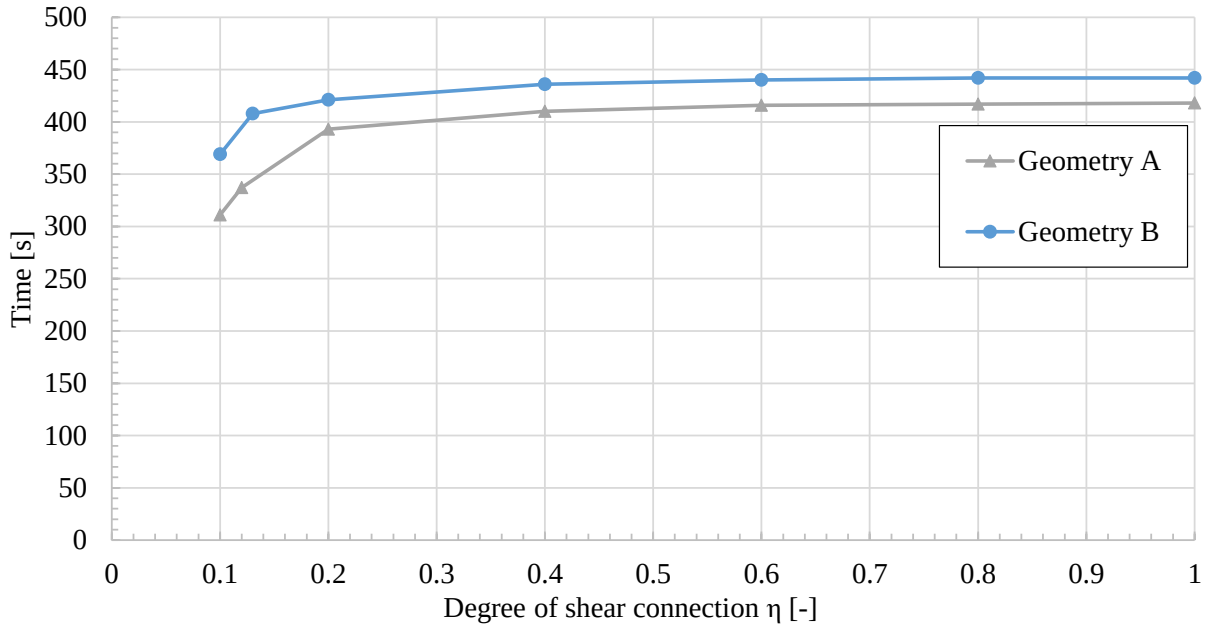

Figure 8.17: Critical temperature for the examined beams with deep decking. Geometries A and B can be found in Figure 4.34 on page 97.

There is a different behaviour in the development of the degree of shear connection at elevated temperatures for composite beams with deep decking and for composite beams with solid slabs. While for solid slabs the temperature development in the headed stud shear connectors is much slower than in the steel section (cf. Section 5.1 on page 100), the temperature development in the headed studs is faster for deep decking. Therefore the degree of shear connection generally rises slower with deep decking, and the point of failure of the composite beam is likely to be reached before reaching a full shear connection. Figure 8.18 shows the development of the degree of shear connection with exposure to ISO 834 fire

for Geometry A and Geometry B, as introduced in Figure 4.34. Both geometries reach the failure criterion of $u_{cr} = L/30$ at a degree of shear connection well below $\eta = 1$. In Figure 8.18 the failure is marked with a vertical line. As shown in Figure 8.19, the failure with $\eta<1$ does not necessarily lead to a failure of the composite joint, but rather to a lower stiffness of the shear connection in comparison to the stiffness of the steel section.

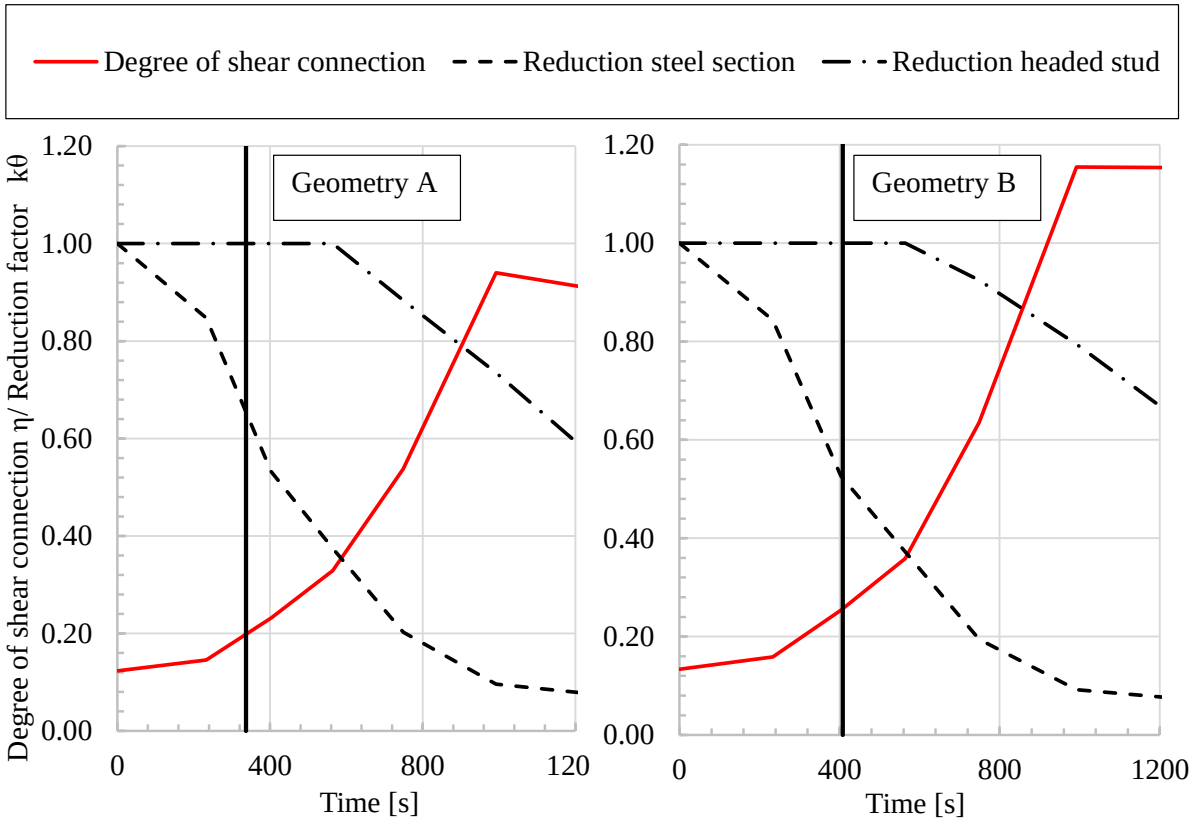

Figure 8.18: Development of the degree of shear connection for the examined beams with deep decking.
Time of failure Geometry A: 337 s.
Time of failure Geometry B: 408 s.

Figure 8.19 depicts the slip of the composite joint over the support at ambient conditions and at the moment of failure. It can be observed that the calculated slip of Geometry B is higher than the ductility criterion u_{cr} of 6 mm according to EN 1994-1-1 already at ambient conditions. When the computed composite beams reached the failure criterion, the maximum slip of the composite joint was lower than at ambient conditions. Due to the high

slip the use of a geometry with a stiffness as low as Geometry B would not be possible. The low stiffness of the shear connection also leads to high slip in the fire situation.

Based on the current calculation model of the ultimate load carrying capacity of headed studs in deep decking, a reduced degree of shear connection would lead to a violation of the ductility criterion u_{cr}.

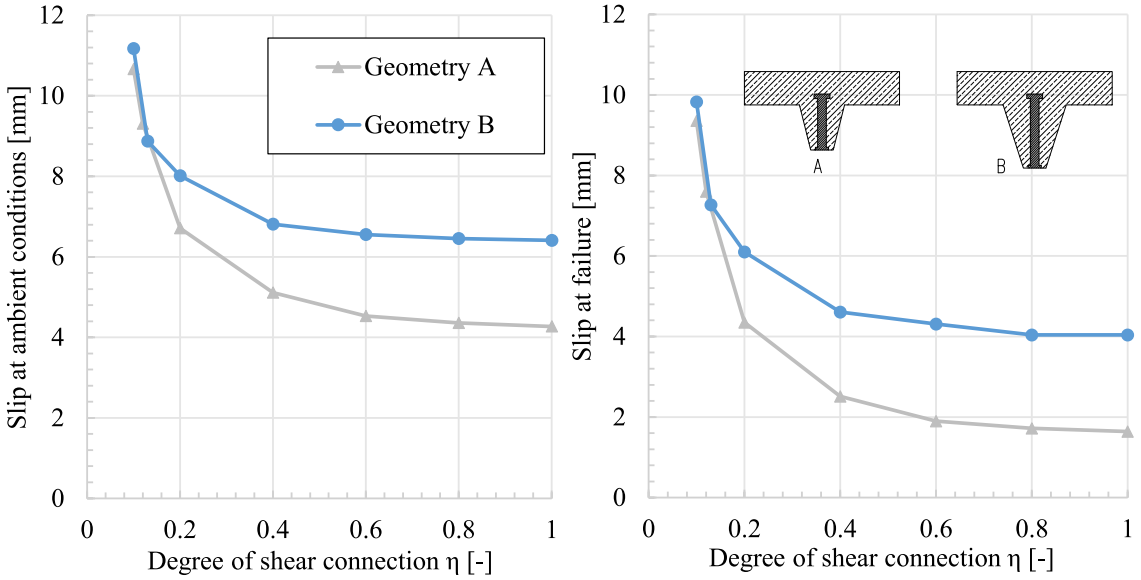

Figure 8.19: Slip of the headed stud shear connectors over the supports at ambient conditions and at failure

8.2.6 Influence of the Inner Lever Arm

The change of length of the steel section with rising temperatures is independent of the height of the composite beam. Therefore *Effect I* is independent of the height of both the steel and concrete sections. However the curvature of the composite beam due to rising temperatures, and therefore *Effect II*, highly depends on the distance between the rotational axis and the centre of the thermal elongation. In the following Figure 8.20, the constant thermal elongation of the steel section is dimensioned with $\overline{1}$, and the inner lever is called e.

As the thermal elongation $\overline{1}$ is constant, the angle α which highly influences the curvature κ is only dependent on the height of the inner lever arm e.

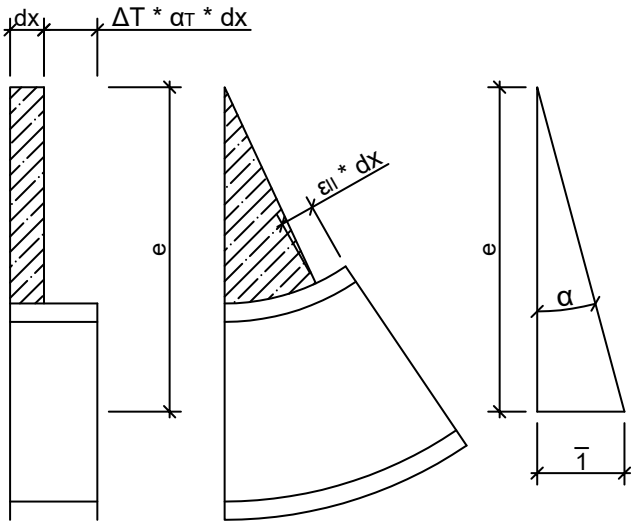

Figure 8.20: Deformation of the composite beam due to the thermal elongation of the steel section. Left: free deformation, Middle: bending due to thermal curvature

With a growing height of the steel section and the concrete chord, the inner lever arm e becomes larger and the slip due to the thermal curvature, *Effect II*, becomes smaller. As *Effect II* leads to a slip contrary to *Effect I*, the maximum total slip increases. In Figure 8.21 the influence of the height of the steel section on the maximum slip in the first 30 minutes of fire exposure is shown. Between the steel section height of 200 mm and 500 mm there is a continuous rise of slip; after the maximum of slip at a steel height of 500 mm, the maximal slip drops again. The decrease of slip after the maximum of slip at 500 mm can be explained with the higher shear capacity of the composite joint that comes along with the larger surface of the steel section and a constant degree of shear connection. The higher shear capacity leads to a tensile failure of the concrete chord and limits therefore the maximum slip.

The influence of the height of the concrete chord, on the other hand, is rather small. A higher concrete chord even leads to a decrease of the maximum slip.

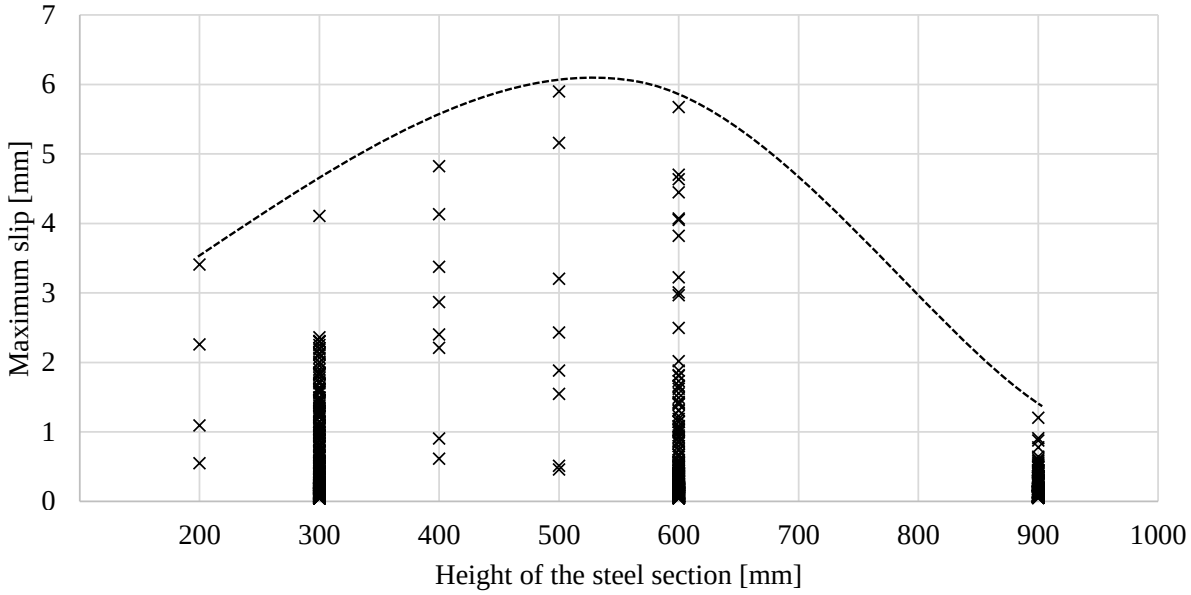

Figure 8.21: Influence of the height of the steel section on the maximum slip

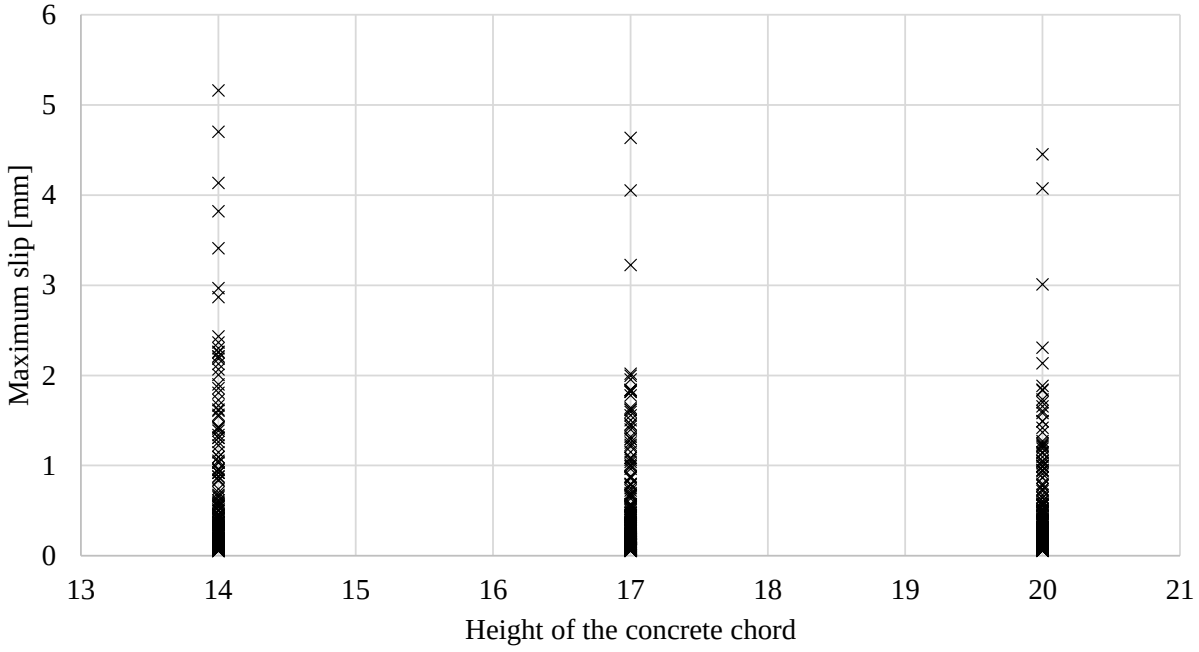

Figure 8.22: Influence of the height of the concrete chord on the maximum slip for L = 6 m to L = 12 m

8.2.7 Influence of the Relation of the Tensile Capacity of the Concrete Chord to the Shear Capacity of the Composite Joint

With rising temperatures and rising thermal strains in the composite beam, the negative slip due to *Effect I* becomes larger. The increasing difference in length between the steel and the concrete section is accompanied by growing normal forces in the steel and the concrete. In a composite beam, the tensile force in the concrete chord and the compressive force in the steel section are transmitted by the shear connection. As a result of this the maximum shear forces are limited by the composite joint, the respective degree of shear connection η, the compressive capacity of the steel section and the tensile capacity of the concrete chord. If the shear forces become higher than the tensile capacity of the concrete ($V_{P,Rk}$[I]$>N_{ct}$[II]), cracking of the concrete chord occurs. Given the limit of the crack width of w_{max}[III] $= 0.5$ mm for the typical exposure class X0 and XC1 in high rise buildings according to EN 1992-1-1 7.3 [26], the cracking of the concrete can lead to a significant elongation of the concrete chord and therefore to the reduction of the maximum slip. Figure 8.23 shows the crack formation in a simulated composite beam.

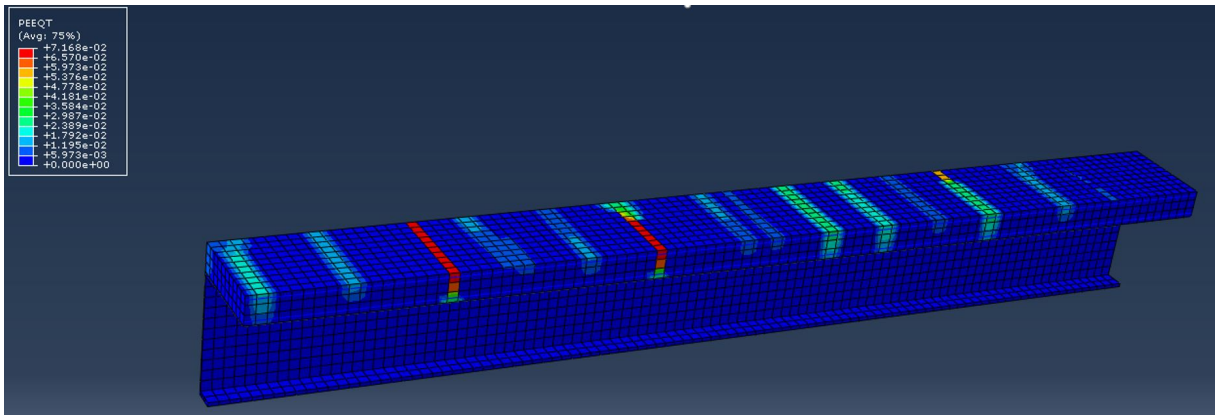

Figure 8.23: Formation of cracks in the concrete chord of a composite beam with an IPE 600 S460, $\eta = 20$ % and $N_{ct}/V_{P,Rk} = 0.55$.

[I] Characteristic shear capacity of the composite joint
[II] Tensile capacity of the uncracked concrete chord
[III] Limit for the calculated crack width according to EN 1992-1-1 [26]

Figure 8.24 displays the maximum slip of the computed composite beams in the first 30 minutes of fire exposure. The results suggest that with the relation of $N_{ct}/V_{P,Rk} > 1$ there is no cracking of the concrete chord, and the resulting slip is significantly higher than with a relation $N_{ct}/V_{P,Rk} < 1$. As in an uncracked concrete section, the tensile stiffness of the reinforcement of the concrete chord is significantly lower than the tensile stiffness of concrete section, the reinforcement ration ρ_l[I] does not influence the initial cracking of the concrete.

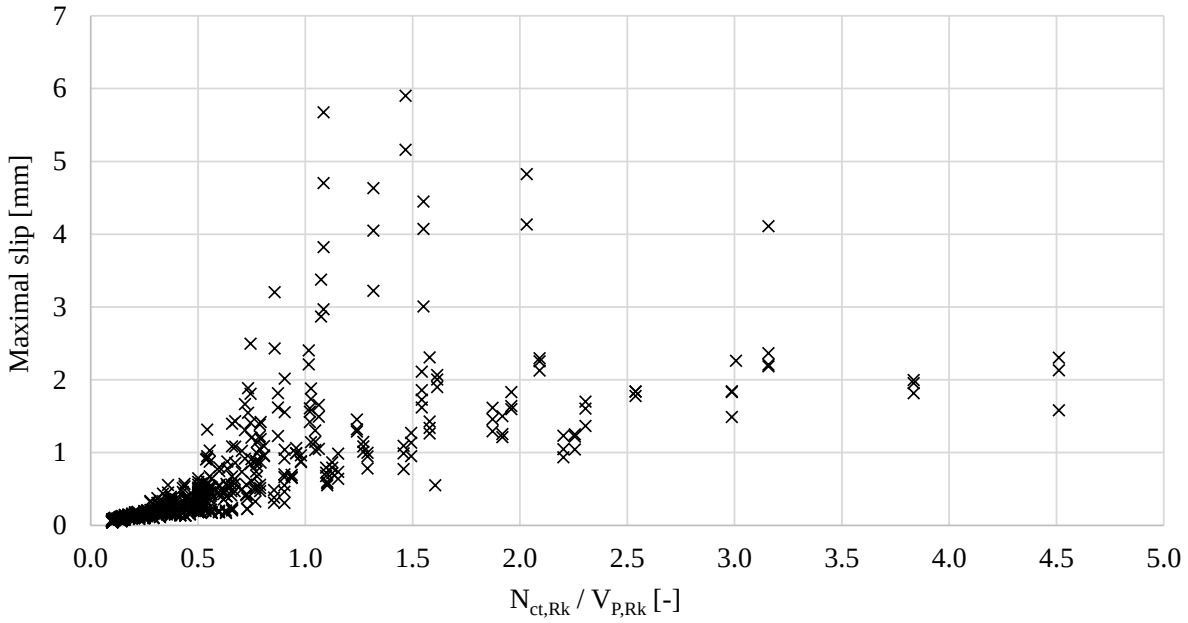

Figure 8.24: Relation of the tensile capacity of the concrete chord N_{ct} to the shear capacity of the composite joint $V_{P,Rk}$

The course of slip over the support for two computed composite beams in the fire situation is shown in Figure 8.25 and Figure 8.26. Whereas Figure 8.25 shows a composite beam with $N_{ct}/V_{P,Rk} > 1$, Figure 8.26 shows a similar beam with $N_{ct}/V_{P,Rk} < 1$. Both composite beams consist of an IPE 600 steel section and a 14 cm concrete chord with $\eta = 0.2$ for both beams. The steel grade of the beam in the first graph is S235, in the second graph S460. With the same degree of shear connection, the different steel grades lead to a significantly higher shear capacity of the composite joint.

[I] Reinforcement ratio for longitudinal reinforcement

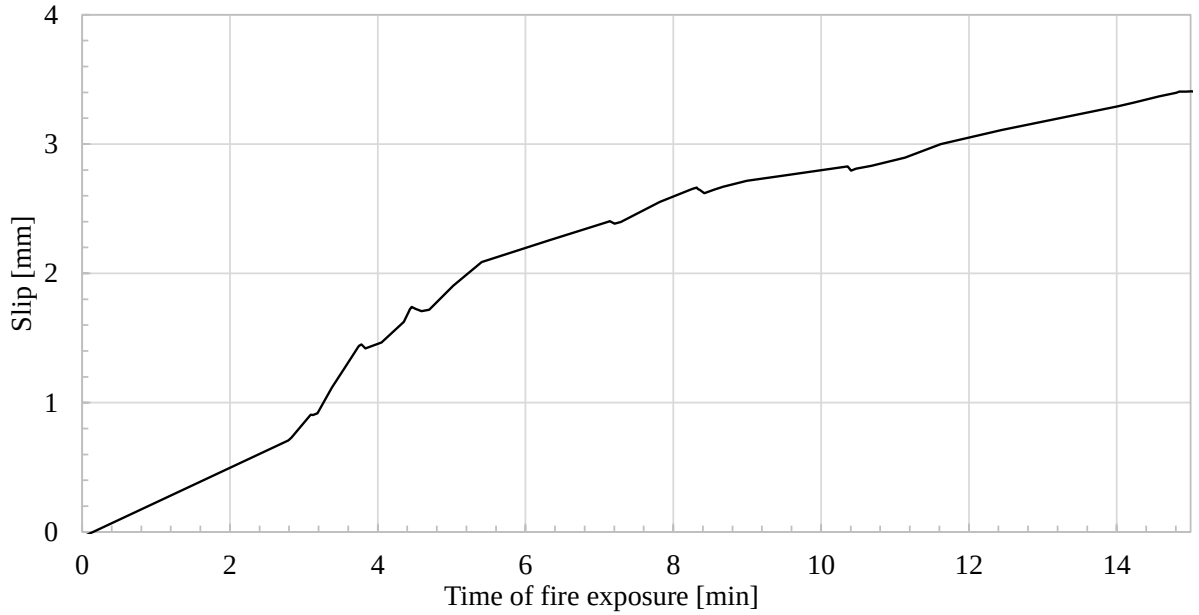

Figure 8.25: Maximum slip of a IPE 600 S235 with a 14 cm concrete chord and $\eta = 20$ %, $N_{ct}/V_{P,Rk} = 1.08$

Whereas the slip of the beam with $N_{ct}/V_{P,Rk} > 1$ kept rising steeply during the entire time of fire exposure, the slip of the beam with $N_{ct}/V_{P,Rk} < 1$ stopped rising at a certain slip. In the simulations the peaks in slip in Figure 8.26 occurred at the same time as the cracking of the concrete chord, as shown in Figure 8.23.

The tensile failure of the concrete chord is feasible as long as there is only a little or no vertical load on a single span composite beam. Higher vertical loads would lead to a compressive zone in the concrete chord which would prevent the tensile failure. However, as discussed in Section 6.2, the rising temperatures due to a fire situation generally leads to a decreasing slip with vertical loads on the composite beam. The limitation of the maximum slip in the fire situation is only necessary with little or no vertical load. The tensile failure of the concrete section of a composite beam can therefore be used for an effective control of the maximum slip with no vertical loads on the composite beam.

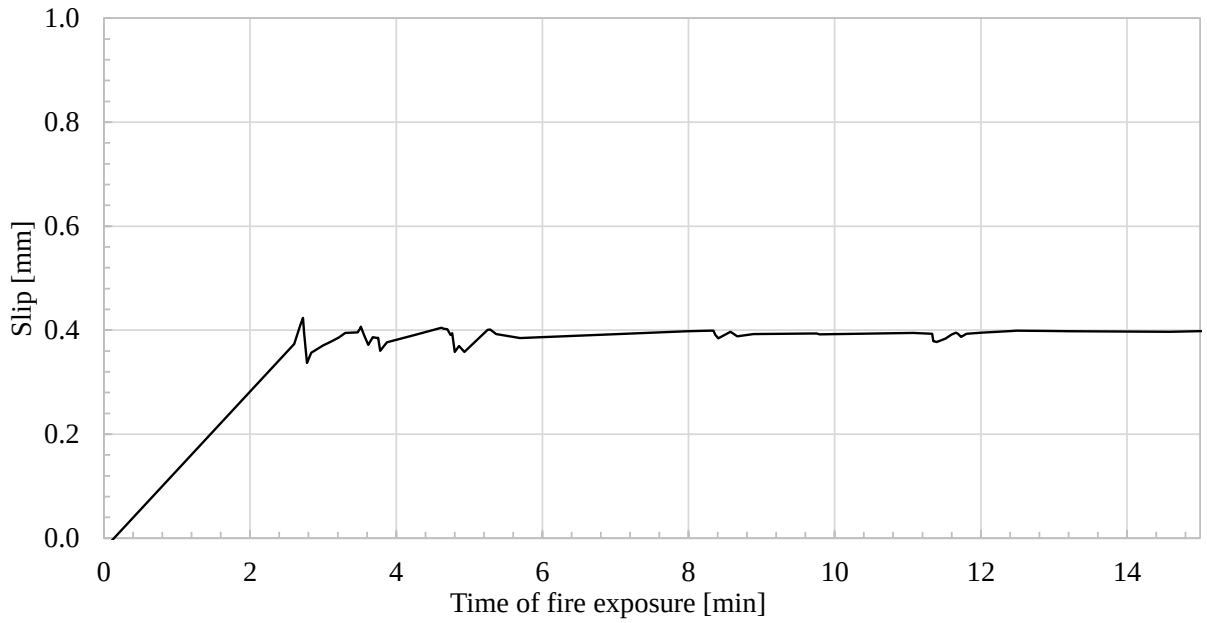

Figure 8.26: Maximum slip of a IPE 600 S460 with a 14 cm concrete chord and $\eta = 20$ %, $N_{ct}/V_{P,Rk} = 0.55$

9 Proposal for the Use of the Partial Connection Theory

9.1 General

As presented in Chapter 1, there are two questions that need to be answered to permit the safe use of composite beams with a partial shear connection in a fire situation:

1. How is the bending resistance of a composite beam with a partial shear connection calculated in a fire situation?
2. How is the compliance of the deformation of the composite joint with the deformation capacity of the shear connectors ensured?

Both proposals, for the calculation of the bending resistance and the assurance of the compliance, are built with two options. The first option represents a simplification, which can be used as a conservative approach. It is proposed to improve the ease of use of a partial shear connection in fire situations. The second option represents a more accurate design approach, but entails slightly more complicated calculations.

9.2 Proposal for the Calculation of the Plastic Resistance Moment

As a simplified design, the plastic resistance moment of a composite beam in the fire situation M_{fi,Rd^+} may be calculated according to EN 1994-1-1 6.2.1.3 [1], with η being the degree of shear connection under ambient conditions. $N_{c,f}$ shall be determined by plastic theory.

If a higher plastic resistance moment of the composite beam is desired, the temperature dependent degree of shear connection η_θ can be calculated.

$$\eta_\theta = \frac{n * min(k_{sc,\theta}; k_{c,\theta})}{n_f * k_{a,\theta}} \tag{9.1}$$

n and n_f are calculated according to EN 1994-1-1 6.6.1 and

$k_{a,\theta} = k_{y,\theta a}$

$k_{sc,\theta} = k_{y,\theta v}$

$k_{c,\theta} = k_{c,\theta c}$

The temperature of the shear stud θ_v and the temperature of the concrete θ_c can be taken from EN 1994-1-1 4.3.4.2.5 (2).

9.3 Proposals for the Assurance of the Compliance of Deformation Behaviour

In the simplified design, the minimum degree of shear connection η according to EN 1994-1-1 6.6.1.1 (1) shall be set to:

$$\eta \geq 0.4 \tag{9.2}$$

Alternatively, if a degree of shear connection lower than $\eta = 0.4$ is desired, further calculations can be done:

The minimum shear capacity of the composite joint shall be determined similar to the calculation of the minimum reinforcement areas for crack control according to EN 1992-1-1

7.3.2 [26]. With this the minimum shear capacity needs to be equal to or greater than the tensile force of the concrete chord just before cracking:

$$\eta * n_f * P_{Rk} \geq b_{eff} * f_{ct,eff} * h_c \tag{9.3}$$

Hereby, P_{rk} can be determined according to EN 1994-1-1 6.6.3.1.

$f_{ct,eff}$ is the mean value of the tensile strength of the concrete at the time when the cracks may first be expected to occur. Generally $f_{ct,eff} = f_{c,\theta}$, assuming there is no reduction due to rising temperatures.

9.4 Explanation for the Minimum Degree of Shear Connection

The maximum slip of a single span composite beam in a fire situation is dominated by the shear stiffness of the composite joint. While the stiffness of the shear connection is difficult to determine, the degree of shear connection is easy to calculate and has a high influence on the stiffness. Section 8.2.2 shows that between $\eta = 1.0$ and $\eta = 0.4$ there is only a moderate growth of slip, while between $\eta = 0.4$ and $\eta = 0.1$ the slip grows steeply. By restricting the degree of shear connection to $\eta = 0.4$ it is assumed that even with an unusually low stiffness of the shear connectors the maximum slip of the composite joint is under 6 mm and in the linear and low region of Figure 9.1.

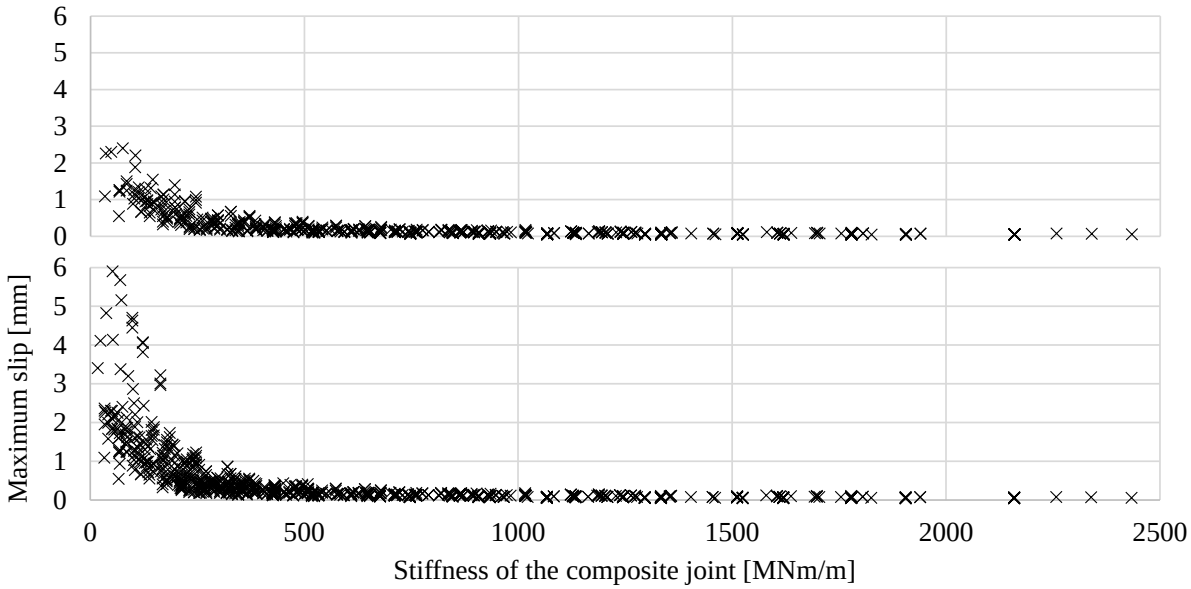

Figure 9.1: Influence of the stiffness of the composite joint on the maximum slip in the fire situation.
Top: $0.4 \leq \eta \leq 1.0$
Bottom: $0.2 \leq \eta \leq 1.0$

9.5 Explanation of the Determination of a Minimum Shear Capacity

The limitation of the minimum shear capacity of the composite joint on the tensile capacity of the concrete chord ensures local cracking of the concrete chord with high negative slip. The thermal elongation of the steel section leads to a compressive force in the steel section and a tensile force in the concrete chord. If the shear capacity is higher than the tensile capacity of the concrete chord, the excessive slip is effectively reduced by concrete cracking.

In the parametric study, the average slip of a composite beam with a relation of $N_{ct}/V_{P,Rk} < 1$ is at 0.27 mm, and with $N_{ct}/V_{P,Rk} > 1$ the average slip is at 1.89 mm. The maximum computed slip of composite beams with $N_{ct}/V_{P,Rk} < 1$ is 3.20 mm, whereas the maximum slip of a composite beam with $N_{ct}/V_{P,Rk} > 1$ is 5.90 mm.

As the maximum slip of a composite beam in a fire situation is highly dependent on the load-slip-curve of the shear connectors a lower stiffness of the shear connectors would lead

to an even higher slip. By limiting the shear capacity to $\eta * n_f * P_{Rk} \geq b_{eff} * f_{ct,eff} * h_c$ the maximal slip of a composite beam in a fire situation is effectively limited to not exceed the ductility criterion. This regulation also allows a possible lower stiffness of the shear connectors.

10 Conclusion

This thesis aimed to develop rules for the safe application of a reduced degree of shear connection at elevated temperatures.

Two obstacles were identified for the safe use of a reduced degree of shear connection in a fire situation: First, the maximum slip of the composite joint, which has to be limited to the deformation capacity of the shear connectors. Second, the calculation of the bending moment resistance at elevated temperatures with a reduced degree of shear connection. The rules focus on single span composite beams according to EN 1994-1-1 with ductile shear connectors and a positive bending moment.

To develop rules for limiting the maximum slip, the behaviour of the shear connection was analysed from three different perspectives: Large scale fire experiments were conducted, a detailed finite element model was elaborated, and an analytic model of the slip in a fire situation was developed.

For a more detailed description, the slip in the composite joint was split into three controlling effects of elevated temperatures: *Effect I* describes the negative slip due to the different thermal elongation of the steel section and the concrete chord. *Effect II* describes the positive slip due to the thermal curvature and the resulting bending of the composite beam. *Effect III* describes the positive slip due to the bending of the composite beam with decreasing stiffness of the components. The three effects were computed separately with the numerical models and validated against the results of the experiments. The linearised analytic description was also based on these three effects.

An important finding was that the mechanical loads on a single span composite beam led to positive slip due to *Effect III*, whereas temperature loads mainly led to negative slip due to *Effect I*. Therefore, the decisive load case is without mechanical load, i.e. only with self-weight.

Significant influences of elevated temperatures on the maximum slip were discussed to elaborate rules for the limitation of the maximum slip. The stiffness of the composite joint was identified to be the controlling variable on the maximum slip of the composite beam in a fire situation. Only with low stiffness can high slip occur. However, the stiffness of the composite joint can be challenging to determine. As the degree of shear connection has a direct influence on the stiffness of the composite beam, it can be used to control the stiffness. With a degree of shear connection $\eta \geq 0.4$, the slip is constantly low. At $\eta \leq 0.4$ there is a nonlinear rise of slip. Tensile failure of the concrete chord can lead to a significant reduction of the maximum slip. With rising temperatures, tensile forces evolve in the concrete chord. If the shear capacity of the composite joint is higher than the tensile capacity of the concrete chord, the concrete chord eventually fails and the slip is depleted. The results of the parametric study show a significant influence of the relation $N_{ct}/V_{P,Rk}$: at $N_{ct}/V_{P,Rk} < 1$ the maximum slip is constantly low.

A model was developed for calculating the load carrying capacity of headed stud shear connectors in deep decking at elevated temperatures. From this, it appears the geometry of the decking has a large influence on the stiffness of the composite joint. However, the developed model still needs further validation. With the current code a reduced degree of shear connection is not possible for headed stud shear connectors in deep decking in a fire situation.

Two options are proposed to limit the maximum slip to the deformation capacity of the shear connectors. First, the minimum degree of shear connection can be set to: $\eta = 0.4$. Alternatively, if a lower degree of shear connection is desired, the relation between the tensile capacity of the concrete and the shear capacity of the composite joint is limited to: $\eta * n_f * P_{Rk} \geq b_{eff} * f_{ct,eff} * h_c$.

For calculating the bending moment resistance of a composite beam in a fire situation, the plastic theory is applied. The degree of shear connection η of a composite beam increases in a fire situation due to the loss of stiffness in the steel section. For the calculation of the bending moment capacity, a temperature dependent degree of shear connection η_θ can

be calculated. To determine η_θ, an FE-model can be used to calculate the corresponding temperatures of the steel section, the concrete chord, and the headed stud shear connectors. Alternatively temperature assumptions can be made for the concrete and headed stud shear connectors based on the steel temperature. For a simplified calculation, the degree of shear connection at ambient conditions η can be used for the calculation of the bending moment capacity.

With the given rules a safe and economic use of the partial connection theory in a fire situation is enabled. Both the maximum slip of the composite joint and the bending moment resistance can be controlled either by a simplified approach or a more detailed calculation.

11 Perspective

The behaviour of the composite joint is highly dependent on the behaviour of the shear connectors at elevated temperatures. The behaviour of headed stud shear connectors in solid slabs and composite slabs that are covered by the EN 1994-1-1 at elevated temperatures is well known. However, the behaviour of headed stud shear connectors in composite slabs with deep decking at elevated temperatures is still hard to determine.

While there is a lot of research available for composite beams with deep decking at ambient conditions (e.g. Nellinger [5], Lawson [4] and Konrad [6]), there is barely any research available at elevated temperatures. In fact, results of the experiments of the DISCCO-project [4] with high (CF80) and slim (CP60) composite decking indicate that the shear capacity for headed studs in deep decking is overestimated by the EN 1994-1-1 even at ambient conditions [62].

Section 8.2.5 shows that there is a significant influence of the geometry of the composite decking on the maximum slip. A new design method *NL500* [49] for the shear capacity of composite beams in deep decking is introduced in Section 4.5.5. However, there are still high uncertainties in the new method that make further investigations inevitable.

As there is currently only very little research available on the load carrying behaviour of headed stud shear connectors in deep decking at elevated temperatures, it is right now practically impossible to use a reduced degree of shear connection for composite beams with deep decking and requirements towards the fire resistance. Therefore, is it imperative to conduct further research on composite beams with deep decking in fire situations.

12 Bibliography

[1] EN 1994-1-1:2004, Eurocode 4: Design of composite steel and concrete structures Part 1-1: General rules and rules for buildings.

[2] EN 1994-1-2:2005, Eurocode 4 — Design of composite steel and concrete structures - Part 1-2: General rules - Structural fire design.

[3] Henning Lungershausen. Zur Schubtragfähigkeit von Kopfbolzendübeln: Dissertation, 1988.

[4] R. M. Lawson, R. Obiala, C. Odenbreit, F. Eggert, F. Hanus, Eleftherios Aggelopoulos, T. Sheehan, X. Dai, D. Lam, U. Kuhlmann, and S. Nellinger. *Development of improved shear connection rules in composite beams (DISCCO): Final report*, volume 28457 of *EUR. Research Fund for Coal and Steel*. Publications Office, Luxembourg, 2017.

[5] Nellinger. On the behaviour of shear stud connections in composite beams with deep decking: Dissertation, 13.11.2015.

[6] Matthias Konrad. Tragverhalten von Kopfbolzen in Verbundträgern bei senkrecht spannenden Trapezprofilblechen: Dissertation.

[7] Andreas Jähring. *Zum Tragverhalten von Kopfbolzendübln in Hochfestem Beton*. Dissertation, Technical University of Munich, 2008.

[8] L Chen, S Jiang, G Li, and W Wang. Experimental studies on behavior of headed stud shear connectors at elevated temperatures, 2012.

[9] O. Mirza, B. Uy, and S. Krezo. Experimental Studies on the Behaviour of Headed Stud Shear Connectors for Composite Steel Concrete Beams under Elevated Temperatures. In Lau Hieng Ho, editor, *Steel and Aluminium Structures*, pages 467–473, Singapore, 13.06.2011 - 15.06.2011. Research Publishing Services.

[10] Choi, Han, and Kim. Performance of Shear Studs in Fire. In *Applications of Structural Fire Engineering*, pages 490–494. Technical University in Prague, Prague, 2009.

[11] Bin Zhao and Joel Kruppa. Experimental and numerical investigation of fire behavior of steel and concrete composite beams. *Proceedings of An Engineering Foundation Conference*, pages 129–142, 1997.

[12] Yusuke Imagawa, Osamu Ohyama, and Akimitsu Kurita. Mechanical Properties of Shear Stud during and after Fire. *Structural Engineering International*, 22(4):487–492, 2012.

[13] B. Zhao. *Fire resistance of composite slabs with profiled steel sheet and of composite steel concrete beams, part 2: Composite beams: Final report*, volume 16822 of *Technical steel research Properties and service performance*. Off. for Official Publ. of the Europ. Communities, Luxembourg, 1997.

[14] ISO 834-1: 1999-09: Fire-resistance tests - Elements of building construction - Part 1: General requirements.

[15] Lingzhu Chen, Guoqiang Li, and Shouchao Jiang. The Structural Behaviour of Headed Stud Shear Connectors at Elevated Temperatures. In Liew J Y Richard and Chin Lee Siew, editors, *Proceedings of the 10th International Conference on Advances in Steel Concrete Composite and Hybrid Structures*, pages 942–949, Singapore, 02.07.2012 - 04.07.2012. Research Publishing Services.

[16] Karl Möhler. *Über das Tragverhalten von Biegeträgern und Druckstäben mit zusammengesetzten Querschnitten und nachgiebigen Verbindungsmitteln*. Dissertation, Technische Universität Karlsruhe, 1956.

[17] A Hoischen. Beitrag zur Berechnung zusammengesetzter Vollwandträger mit elastischen Verbindungsmitteln: Dissertation, 1952.

[18] J. Schanzenbach. *Zum Einfluss von Dübelnachgiebigkeit und Unterverdübelung auf das Tragverhalten von Verbunddurchlaufträgern im Hoch- und Industriebau: Dissertation*. na, Kaiserslautern, 1989.

[19] Roland Bärtschi. *Load-bearing behaviour of composite beams in low degrees of partial shear connection*. Dissertation, ETH Zürich, 2005.

[20] Vasif Atilla Oven. *The behaviour of composite beams with partial interaction at elevated temperatures*. Dissertation, University of Sheffield, 1996.

[21] Wei-yong Wang, Michael D. Engelhardt, Guo-Qiang Li, and Guo-sheng Huang. Behavior of Steel–Concrete Partially Composite Beams Subjected to Fire—Part 1: Experimental Study. *Fire Technology*, 53(3):1039–1058, 2017.

[22] Weiyong Wang, Kang Wang, Michael D. Engelhardt, and Guoqiang Li. Behavior of Steel–Concrete Partially Composite Beams Subjected to Fire—Part 2: Analytical Study. *Fire Technology*, 53(3):1147–1170, 2017.

[23] Ling-Zhu Chen, Shou-Chao Jiang, Guo-Qiang Li, and Gianluca Ranzi. The Performance of Composite Beams with Steel Bar Truss Floor Slabs Exposed to Fire. In *8th International Conference on Structures in Fire*, 11-13.6.2014.

[24] Martin Mensinger, Jochen Zehfuß, Sven Brunkhorst, and Samuel Pfenning. Mindestverdübelung von Verbundträgern im Brand: IGF-Vorhaben 19105 N, 2018.

[25] DIN EN ISO 13918:2008-10. Schweißen - Bolzen und Keramikringe für das Lichtbogenbolzenschweißen.

[26] EN 1992-1-1:2004, Eurocode 2: Design of concrete structures —Part 1-1: General rules and rules for buildings.

[27] DIN 488-1:2009-08, Betonstahl - Teil 1: Stahlsorten, Eigenschaften und Kennzeichnung, 2009.

[28] EN 206:2014-07, Concrete - Specification, performance, production and conformity.

[29] EN 12390-2:2009, Testing hardened concrete - Part 2: Making and curing specimens for strength tests.

[30] EN 10027-1:2017-01, Designation systems for steels - Part 1: Steel names.

[31] EN ISO 6892-1:2017-02, Metallic materials - Tensile testing - Part 1: Method of test at room temperature (ISO 6892-1:2016).

[32] DIN 50125:2016-12; Prüfung metallischer Werkstoffe - Zugproben.

[33] Sven Brunkhorst, Samuel Pfenning, Jochen Zehfuß, and Martin Mensinger. Influence of elevated temperatures on the composite joint of a composite beam in fire, 2018.

[34] EN 1992-1-2:2004-12, Eurocode 2: Design of concrete structures — Part 1-2: General rules — Structural fire design.

[35] EN 1993-1-2:2005, Eurocode 3: Design of steel strucutures-Part 1-2: General rules-Structural fire design.

[36] Abaqus /CAE Users Guide, editor. *CAE Users Guide*. 2016.

[37] EN 1991-1-2:2002, Eurocode 1: Action on structures-Part1-2: General actions-Actions on structures exposed to fire.

[38] Jens Dr.-Ing Minnert and Gerd Dr.-Ing Wagenknecht. *Verbundbau-Praxis: Berechnung und Konstruktion nach Eurocode 4 Bauwerk-Basis-Bibliothek*. Bauwerk. Beuth, Berlin, 2nd ed. edition, 2013.

[39] Reinhard Bergmann. Zur Geschichte der Biegesteifigkeit bei Verbundstützen. *Stahlbau*, 73(9):656–660, 2004.

[40] Thorsten Rolf Mannsfeld. *Tragverhalten von Stahlbetonflächentragwerken unter Berücksichtigung der temperaturbedingten Nichtlinearitäten im Brandfall*. Dissertation, Wuppertal, 2011.

[41] Martin Mensinger, Peter Schaumann, Peter Kraus, and Florian Tabeling. Optimierter Einsatz intumeszierender Anstriche im Stahlbau, 2014.

[42] Florian Tabeling. Zum Hochtemperaturverhalten dämmschichtbildender Brandschutzsysteme auf Stahlbauteilen: Dissertation, 2014.

[43] Jörg Sothmann. Zur Modellierung geschützer und ungeschützter Verbunddeckenträgersysteme im Brandfall: Dissertation, 2013.

[44] O. Molochnikova and Jörg Sothmann. Vereinfachte numerische Simulation von Dämmschichtbildenden Brandschutzsystemen: 4th Symposium Structural Fire Engineering. Braunschweig, 2017.

[45] Warrington Certification Limited. European Technical Approval ETA - 11/0014, Sika Unitherm Platimum, 31.05.2013 - 07.09.2016.

[46] Martin Claßen and Martin Herbrand. Mindestverdübelung von Verbundträgern mit kleinskaligen Verbundmitteln- Herleitung des Mindestverdübelungsgrades durch systematischen Einsatz nicht-linearer Finite-Elemente-Berechnungen. *Bauingenieur*, 91(RWTH-2016-04916), 2016.

[47] Rudolf Röß. Tragverhalten von Verbundträgern mit Profilblechen unter Brandbelastung: master's thesis, 2017.

[48] Jürgen Becker. Beitrag zur Auslegung der Verdübelung von Verbundträgern des Hochbaus unter ruhender und nichtruhender Belastung, 1997.

[49] Martin Mensinger, Samuel Pfenning, and Rudolf Röß. Tragverhalten von Kopfbolzendübeln mit Profilblechen unter Brandbelastung. In *Festschrift Jörg Lange*. Universitäts- und Landesbibliothek Darmstadt, Darmstadt, 2018.

[50] Ling-Zhu Chen, Gianluca Ranzi, Shou-Chao Jiang, Faham Tahmasebinia, and Guo-Qiang Li. Behaviour and design of shear connectors in composite slabs at elevated temperatures. *Journal of Constructional Steel Research*, 115:387–397, 2015.

[51] N. Gattesco and E. Giuriani. Experimental study on stud shear connectors subjected to cyclic loading. *Journal of Constructional Steel Research*, 38(1):1–21, 1996.

[52] Jürgen Tresch. Einfluss des Verdübelungsgrades auf die Tragfähigkeit eines Verbundträgers im Brand: master's thesis, 2017.

[53] Ehab and El-lobody. Finite element modelling of shear connection for steel-concrete composite girders: Dissertation, 2002.

[54] Jochen Zehfuß. Bemessung von Tragsystemen mehrgeschossiger Gebäude in Stahlbauweise für realistische Brandbeanspruchung: Dissertation, 2004.

[55] J.V. Ryan and A. F. Robertson. Proposed Criteria für Defining Load Failure of Beams, Floors, and Roof Constructions During Fire Tests, 1959.

[56] Karl Kordina, Falk Herschelmann, and Ekkehard Richter. Parameterstudie für Verbundträger der Feuerwiderstandsklasse F 90 (Versuche zum Erwärmungsverhalten): Schlußbericht, 1984.

[57] Gisèle Bihina, Bin Zhao, and Abdelhamid Bouchaïr. Investigation on the Behaviour of a Composite Floor Made of Cellular Beams in Fire Situation. *Journal of Structural Fire Engineering*, 5(2):175–188, 2014.

[58] EN 1990:2002, Eurocode: Basis of structural design.

[59] A Hoischen. Verbundträger mit elastischer und unterbrochener Verdübelung. In *Der Bauingenieur 1954 volume 7*, pages 241–244.

[60] Thomas Pirzer. *Untersuchung des Schlupfverhaltens von Verbundträgern im Brand: Master thesis.* München, 2018.

[61] EN 13501-2:2016 Fire classification of construction products and building elements - Part 2: Classification using data from fire resistance tests, excluding ventilation services.

[62] C. Odenbreit. Presentation SC4.T3, 11.07.2017.

13 Glossary

List of abbreviations

ETA European Technical Approval

FE-model Finite element model

ISO 834 Temperature load according to heating curve in ISO 834-1 6.1.1 [14]

Latin lower case letters

b_{eff}	m	Total effective width of flanges for shear lag
c_v	$\frac{\text{kNm}}{\text{m}}$	Continuous shear elastic shear connection of a composite joint
$c_p(\theta)$	J/(kg K)	Specific heat capacity, temperature dependent
c_{sc}	N/mm	Stiffness of the headed stud shear connection on tension
d_{sc}	mm	Diameter of headed stud shear connector
f_{ay}	N/mm^2	Nominal value for the yield strength of structural steel at ambient conditions
$f_{ay,\theta}$	N/mm^2	Nominal value for the yield strength of structural steel in fire situations
f_{ap}	N/mm^2	Nominal value for the proportional limit of structural steel at ambient conditions
$f_{ap,\theta}$	N/mm^2	Nominal value for the proportional limit of structural steel in fire situations

$f_{c,\theta}$	N/mm^2	Characteristic value for the compressive cylinder strength of concrete in the fire situation
$f_{ck,\theta}$	N/mm^2	Characteristic value of the cylinder compressive strength of concrete at 28 days, temperature dependent
$f_{cm,\theta}$	N/mm^2	Mean value of concrete cylinder compressive strength
$f_{c,\theta}$	N/mm^2	Mean value of axial tensile strength of concrete, temperature dependent
f_{sy}	N/mm^2	Nominal value of the yield strength of reinforcing steel
f_u	N/mm^2	Specified ultimate tensile strength
h_s	mm	Height of the centroidal axis of the concrete failure surface over the steel section according to Equation 4.17
h_{sc}	mm	Nominal height of a stud connector
h_c	mm	Thickness of the concrete slab
$k_{a,\theta}$	−	Reduction factor of the steel section in a fire situation
$k_{Ec,\theta}$	−	Temperature dependent reduction factor of the tangent modulus E_{cm}
$k_{u,\theta}$	−	Reduction factor for the yield strength of structural steel at elevated temperature
n_f	−	Number of shear connectors needed for full shear connection according to EN 1994-1-1 6.6.1.2 (1)
n	−	Number of shear connectors, or relation between the Young's modulus of steel and concrete
n_y	−	Number of possible yield hinges in the headed stud
s	mm	Slip of a composite joint

s_0	mm	Slip of a headed stud shear connector at end of linear elastic load-slip path
s_{max}	mm	Slip of a headed stud shear connector at failure
s_{p1}	mm	Slip of a headed stud shear connector at maximum load carrying capacity, as implemented in Abaqus, similar to s_y
s_{p2}	mm	Slip of a headed stud shear connector at end of the linear elastic load-slip path, as implemented in Abaqus, similar to s_0
s_y	mm	Slip of a headed stud shear connector when reaching maximum load carrying capacity
u_{cr}	mm	Deflection failure criterion
w_{max}	mm	Limit for the calculated crack width according to EN 1992-1-1 [26]

Latin upper case letters

A_a	mm^2	Cross-sectional area of structural steel section
A_c	mm^2	Cross-sectional area of concrete
A_{sc}	mm^2	Cross-sectional area of headed stud shear connector
C_v	$\frac{kN}{m}$	Linear elastic spring characteristic of a shear connector
E_a	N/mm^2	Characteristic value for the modulus of elasticity of structural steel at ambient conditions
$E_{a\theta}$	N/mm^2	Characteristic value for the modulus of elasticity of structural steel in the fire situation
$E_{cm\theta}$	N/mm^2	Secant modulus of elasticity of concrete, temperature dependent
E_{cm}	N/mm^2	Secant modulus of elasticity of concrete

$E_{c\theta}$	N/mm^2	Tangent modulus of elasticity of concrete, temperature dependent
F_0	kN	Load of a headed stud shear connector at end of the linear elastic load-slip path, as implemented in Abaqus
I_a	cm^4	Second moment of area of the steel section
I_c	cm^4	Second moment of area of the concrete chord
I_V	cm^4	Second moment of area of the composite section
$I_{y,fi}$	mm^4	Second moment of area of the concrete cone
K_c	$-$	Ratio of the second stress invariant on the tensile meridian to that on the compressive meridian in Abaqus material model
L	m	Span of a composite beam
$M_{fi,Rd+}$	kNm	Design value of the sagging moment resistance in the fire situation
N_{ct}	kN	Design value of the compressive normal force in the concrete flange
$N_{c,f}$	kN	Design value of the compressive normal force in the concrete flange with full shear connection
N_{ct}	kN	Tensile capacity of the uncracked concrete chord
P_{max}	kN	Maximum shear capacity of a headed stud shear connector at ambient conditions
P_{Rd}	kN	Design value of the shear resistance of a single connector
Q_{inf}	kN	Load of a headed stud shear connector between end of the linear elastic load-slip path and P_{max}, as implemented in Abaqus
$V_{P,Rk}$	kN	Characteristic shear capacity of the composite joint

Greek letters

$\alpha_{i,(\theta)}$	–	Expansion factor intumecent coating
α_{c1}	–	Factor for long-term concrete strength
α_{θ}	–	Coefficient of thermal expansion, temperature dependent
γ_V	–	Partial factor for design shear resistance of a headed stud
δ_{uk}	mm	Characteristic value of slip capacity
$\epsilon_{c,\theta}$	–	Concrete strain in the fire situation
$\epsilon_{ay,\theta}$	–	Yield strain in the fire situation
$\epsilon_{ap,\theta}$	–	Strain at the proportional limit in the fire situation
ε_{aba}	–	Eccentricity in Abaqus material model
ϵ_{uk}	–	Characteristic strain of reinforcement or prestressing steel at maximum load
η	–	Degree of shear connection at ambient conditions
η_{θ}	–	Degree of shear connection in a fire situation
$\theta_{sc,a}$	°C	Temperature of a headed stud over the weld in fire situation
$\theta_{sc,c}$	°C	Temperature of the concrete around the weld of a headed stud shear connector in fire situation
θ_v	°C	Temperature of the stud connector according to EN 1994-1-2 4.3.4.2.5 (2)
θ_c	°C	Temperature of the concrete according to EN 1994-1-2 4.3.4.2.5 (2)
$\lambda(\theta)$	$\mathrm{m\,W/(m*K)}$	Conductivity, temperature dependent
λ_{eq}	$\mathrm{m\,W/(m*K)}$	Equivalent conductivity intumecent coating
μ_0	–	Degree of utilization at time t=0 according to EN 1993-1-2 4.2.4

μ_{ca}	–	Coefficient of friction between steel and concrete
ν_a	–	Poisson's ratio for structural steel
$\rho(\theta)$	kg/m^3	Density, temperature dependent
ρ_l	–	Reinforcement ratio for longitudinal reinforcement
σ_{b0}/σ_{c0}	–	Ratio of initial equibiaxial compressive yield stress to initial uni-axial compressive yield stress in Abaqus material model
Ψ_{aba}	–	Dilatation angle in Abaqus material model

14 List of Figures

15 List of Tables

16 Appendix

Anhang 1: Eidesstattliche Erklärung

Anhang I

Eidesstattliche Erklärung

Ich erkläre an Eides statt, dass ich die bei der promotionsführenden Einrichtung
Ingenieurfakultät Bau Geo Umwelt

---

der TUM zur Promotionsprüfung vorgelegte Arbeit mit dem Titel:
The Application of the Partial Connection Theory on Composite Beams in Fire Situations

---

in Lehrstuhl für Metallbau
Fakultät, Institut, Lehrstuhl, Klinik, Krankenhaus, Abteilung

unter der Anleitung und Betreuung durch: Prof. Dr.-Ing. Martin Mensinger ohne sonstige Hilfe erstellt und bei der Abfassung nur die gemäß § 6 Ab. 6 und 7 Satz 2 angebotenen Hilfsmittel benutzt habe.

☒ Ich habe keine Organisation eingeschaltet, die gegen Entgelt Betreuerinnen und Betreuer für die Anfertigung von Dissertationen sucht, oder die mir obliegenden Pflichten hinsichtlich der Prüfungsleistungen für mich ganz oder teilweise erledigt.

☒ Ich habe die Dissertation in dieser oder ähnlicher Form in keinem anderen Prüfungsverfahren als Prüfungsleistung vorgelegt.

☐ Die vollständige Dissertation wurde in _____ veröffentlicht. Die promotionsführende Einrichtung

_____

hat der Veröffentlichung zugestimmt.

☒ Ich habe den angestrebten Doktorgrad noch nicht erworben und bin nicht in einem früheren Promotionsverfahren für den angestrebten Doktorgrad endgültig gescheitert.

☐ Ich habe bereits am _____ bei der Fakultät für _____

_____

der Hochschule _____
unter Vorlage einer Dissertation mit dem Thema _____

_____

die Zulassung zur Promotion beantragt mit dem Ergebnis: _____

_____

Die öffentlich zugängliche Promotionsordnung der TUM ist mir bekannt, insbesondere habe ich die Bedeutung von § 28 (Nichtigkeit der Promotion) und § 29 (Entzug des Doktorgrades) zur Kenntnis genommen. Ich bin mir der Konsequenzen einer falschen Eidesstattlichen Erklärung bewusst.

Mit der Aufnahme meiner personenbezogenen Daten in die Alumni-Datei bei der TUM bin ich

☒ einverstanden, ☐ nicht einverstanden.

Ort, Datum, Unterschrift